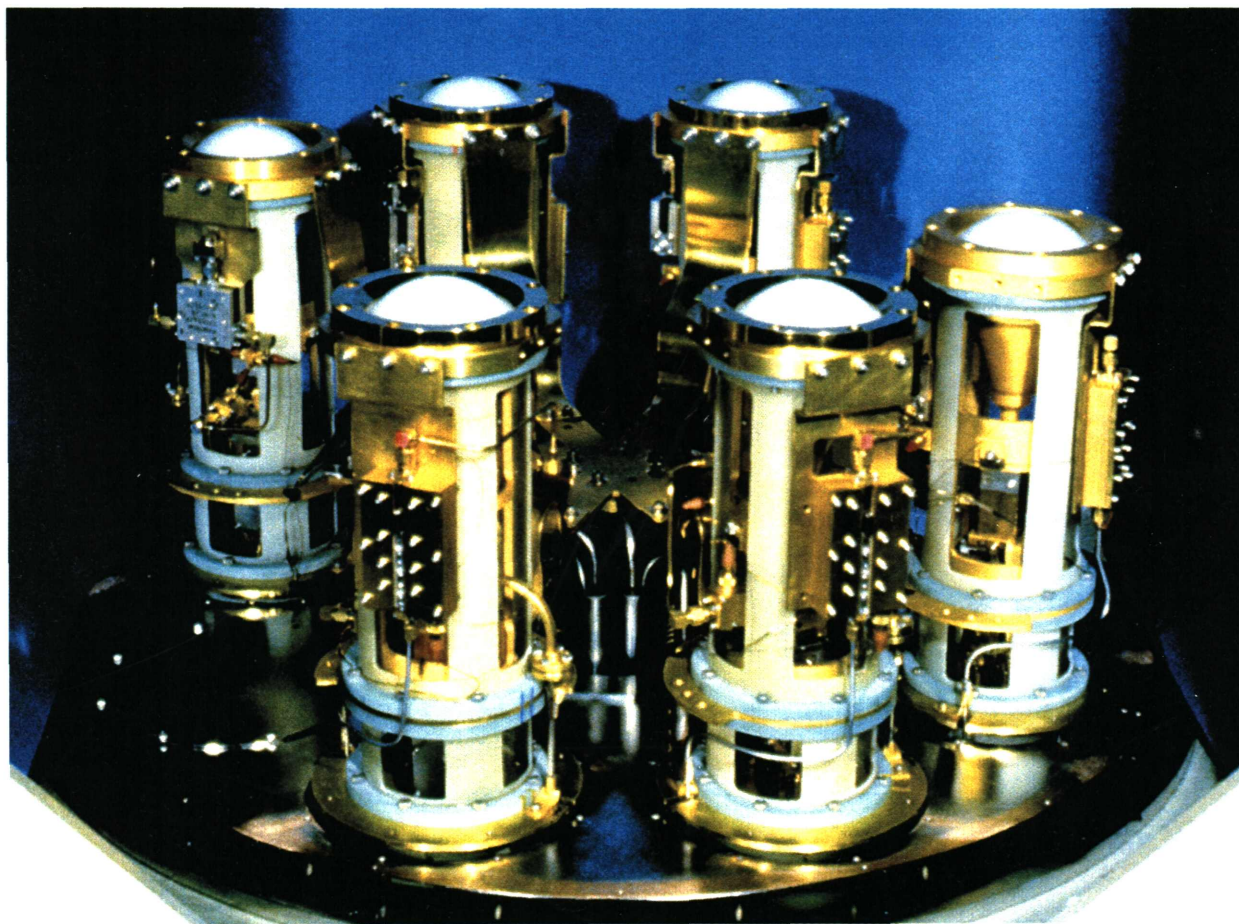


# MILLIMETER ARRAY PROGRAM PLAN



## Design and Development Volume 2

January 1998



**NATIONAL RADIO ASTRONOMY OBSERVATORY**

A facility of the National Science Foundation operated under  
cooperative agreement by Associated Universities, Inc.

**Cover:** A photograph of the multiband receiver which is currently in use on the NRAO 12 Meter Telescope and which will serve as a fiducial design for the packaging of the Millimeter Array receivers. In a single 4K cryogenic dewar as many as eight receiver inserts can be permanently mounted (six are shown here). Each receiver insert is complete with a focusing lens, feed horn, local-oscillator-injection coupler, mixer, isolator, and intermediate-frequency amplifier. The mixer uses a superconductor-insulator-superconductor (SIS) junction, and the amplifier uses a heterostructure field-effect transistor (HFET) developed at the NRAO.

**MILLIMETER ARRAY**  
**PROGRAM PLAN**  
**DESIGN AND DEVELOPMENT VOLUME II**

**JANUARY 1998**

**ASSOCIATED UNIVERSITIES, INC.**  
***NATIONAL RADIO ASTRONOMY OBSERVATORY***



## TABLE OF CONTENTS

I. INTRODUCTION .....	1
II. OVERVIEW OF THE MILLIMETER ARRAY DESIGN AND DEVELOPMENT PLAN .....	2
2.1 Project Requirements .....	2
2.2 Science Requirements for the MMA Design and Development Phase .....	2
2.3 NSF Expectations for the MMA Design and Development Phase .....	4
2.4 NRAO Principles for the MMA Design and Development Phase .....	4
2.5 Project Goals .....	4
III. ORGANIZATION OF THE MMA PROJECT .....	6
IV. INSTRUMENTATION DEVELOPMENT FOR THE MMA .....	8
Table 4.1 Overview and Comparison of MMA Instrumentation Goals .....	8
4.1 Antenna .....	9
Table 4.2 Antenna Specifications .....	9
4.2 System .....	10
4.3 Receivers .....	10
4.4 Local Oscillator .....	11
4.5 Correlator .....	12
4.6 Computing .....	13
V. IMPLICATIONS OF A REMOTE SITE FOR THE MMA: ROLE OF THE TEST INTERFEROMETER .....	14
VI. WORK BREAKDOWN STRUCTURE .....	16
Table 6.1 D&D Gantt Chart .....	17
Table 6.2 Milestones and Deliverables by Task .....	21
Table 6.3 Milestones and Deliverables: Chronological .....	23
6.4 Personnel Projections .....	24
6.5 Budget .....	24
Table 6.4 Personnel Projections by Calendar Year .....	25
Table 6.5 Personnel Projections by Task: Calendar Year 1999 .....	25
Table 6.6 MMA Design and Development: Total Cost .....	26
VII. DESIGN AND DEVELOPMENT IN THE MMA PROJECT CONTEXT .....	27
7.1 Operations .....	27
7.2 Construction: Role of MMA Partnerships .....	27
Table 7.1 Project Overview Gantt Chart .....	29
APPENDIX A – T. J. Cornwell, M. A. Holdaway, and J. M. Uson – “Radio Interferometric Imaging of Very Large Objects: Implications for Array Design”	
APPENDIX B – AUI/NRAO Organization Chart	
APPENDIX C – MMA Organization Chart	
APPENDIX D – Millimeter Array Memos	
APPENDIX E – MMA Memo 145: Antennas for the Millimeter Wave Array	
APPENDIX F – MMA Memo 190: A System Design for the MMA	
APPENDIX G – MMA Memo 151: Design of Planar Image Separating and Balanced Mixers	
APPENDIX H – MMA Memo 166: The MMA Correlator	
APPENDIX I – MMA Memo 164: MMA Computing Working Group Report	



## I. INTRODUCTION

The Millimeter Array is a revolutionary instrument, a direct result of the revolution in astronomy achieved in the twentieth century. While the present century will surely be remembered for the discovery that the universe was evolving from a discrete beginning, we have been slow to appreciate the corollary requirement that everything *in* the universe also must be evolving from its own beginning. This simple conclusion is now leading to a profound reassessment of the priorities for instruments necessary for astronomical research. Since cosmic sources evolve from matter that is cold to matter that is hot, if we hope to observe cosmic objects as they form, tools are needed to permit astronomers to see cold matter in the universe with the same clarity of detail that the Hubble Space Telescope, for example, allows us to see warm matter. The Millimeter Array is that tool.

The purpose of the Millimeter Array Program Plan, Design and Development Volume II, is to outline the steps to be taken to make the Millimeter Array a reality. The overall project is divided into three overlapping and interdependent stages: Design and Development, Construction, and Operations. This volume addresses the initial phase, a three-year design and development phase that leads to prototype hardware from which performance and cost parameters for the array may be assessed. It is the second synopsis of the Millimeter Array Design and Development Plan; the first was presented by Associated Universities, Inc., to the National Science Foundation at their request in September 1992. The present volume supplements and supersedes the former in all respects.

The Millimeter Array Design and Development Plan, outlined in the sections below, includes a description of the requirements for the design and prototyping activities and the manner in which the tasks defined to meet these requirements will be carried out. A complete work breakdown structure along with staffing and budgetary tables is included. Finally, a skeleton outline is given so as to place the design and development activities in the larger context of the entire MMA project.



## II. OVERVIEW OF THE MILLIMETER ARRAY DESIGN AND DEVELOPMENT PLAN

### 2.1 Project Requirements

The requirements for the Millimeter Array (MMA) Design and Development (D&D) phase have come from the astronomers who wish to optimize the MMA for their scientific research, within the stewardship of the National Science Foundation (NSF) which has the ultimate responsibility for the project, as organized by the National Radio Astronomy Observatory (NRAO) in its role as a National Observatory charged with fostering radio astronomy in the United States. There is universal agreement on the central requirement for the MMA, namely:

*The Millimeter Array will provide sensitive, high-precision astronomical imaging at sub-arcsecond, 0".1, resolution at millimeter and submillimeter wavelengths.*

### 2.2 Science Requirements for the MMA Design and Development Phase

The scientific requirements for the MMA have been established and revised through a series of MMA science workshops held from 1985 to 1995. The proceedings of these workshops are published and have been made available in electronic form on the World Wide Web. In the MMA astronomers are seeking an instrument that will allow them to make spectroscopic images of the gas, and continuum images of the dust, in normal galaxies such as the Milky Way very early in the history of the universe. They want to observe the details of the formation of individual stars throughout the Galaxy. They want to measure the isotopic composition of the ejecta from giant stars that are progressively shedding nearly all their mass in the final throes of stellar evolution. And they want to observe energetic events on the Sun, to establish the chemical composition of comets, monitor volcanic outbursts on Io, and assess the abundance of icy asteroids beyond the orbits of Jupiter and Neptune. These representative observational programs, and many others that could be mentioned, lead to three principal requirements for the MMA:

- Precision Imaging
- Sensitivity to Detect Faint Objects
- Ease of Access for a Wide Range of Scientific Research

These requirements lead to some clear specifications for the MMA. In particular, a large number of antennas is needed to give the good Fourier (uv-plane) coverage that produces precision synthesis imaging; the antenna array must have a physical extent of approximately 3 km to achieve 0".1 at one of its prime millimeter frequencies, 230 GHz, and the antennas must be transportable to achieve precision imaging on all spatial scales up to 0".1. However, these same considerations lead to some practical consequences that define the work to be done in the MMA D&D phase. For example, the angular size of objects astronomers wish to image—forming groups of galaxies, interacting galaxies, regions of star formation—may be smaller than approximately 3 arcseconds or they may be as large as 3 arcminutes. If astronomers want to make an image

of an object as large as  $3\lambda$ , and they want that object to fit in the primary beam of the individual antennas, then the diameter of the antenna can be no more than about 1000 times the wavelength at which the observations are made. For observations done at 1 mm wavelength this means the individual antennas making up the array should have a diameter of less than one meter. An enormous number of such small antennas are needed to get enough collecting area to realize much sensitivity: 150 such antennas is needed just to achieve the same collecting area as the present NRAO 12 Meter Telescope. The cost of equipping such an array with cryogenic receivers, and of cross-correlating the data, makes such a solution impractical.

In order to preserve the scientific capability to image large objects, and satisfy the practical requirement that the antennas be of diameter large enough that a reasonable number of them will provide the needed sensitivity, means that the array must be capable of producing not just precision images, but precision *mosaic* images. Making such images requires observing with multiple, precision antenna pointings. In a seminal work Cornwell, Holdaway, and Uson (included here as Appendix A) showed that this can indeed be done if the deviation from perfection of the antenna figure is no more than three percent of the observing wavelength and if the pointing error of the antennas does not exceed five percent of the primary beamwidth. These severe technical requirements, deriving from a science requirement, are the engineering specifications for the antennas. Meeting such specifications in the antenna design is a major task to be accomplished in the MMA D&D program.

The need for sensitivity sufficient for the study of faint objects with the MMA implies a requirement for (1) development of broadband, quantum-limited receivers; (2) design of antennas of very low blockage so that the *warm spillover* is minimized; and (3) choice of a site for the array where the background emission and absorption from atmospheric water is minimal. The first two points are the focus of the D&D instrumentation development described below. The site issue is resolved by noting that since atmospheric water vapor is concentrated low in the Earth's atmosphere, the necessary site for the MMA is at high elevation. Two site options have been studied: Mauna Kea at 12,500 feet above sea level and Llano de Chajnantor in the Chilean Altiplano at 16,500 feet elevation.

The combination of requirements for a high-tech instrument to be located in a remote site means that great care must be taken in the design of the array. The MMA instrumentation will need to be reliable to minimize the failure rate and modular so that it can easily be removed when necessary for repair at a laboratory located at a lower altitude. Together, these considerations mean that the MMA design requires attention to maintenance issues. The three-year MMA Design and Development program is structured to make this possible.

The final astronomical requirement for the MMA to be addressed in the MMA D&D phase concerns ease of scientific access. Recognizing that the MMA will be extremely fast—images of small fields can be done in minutes—and suitable for a wide range of scientific investigation, astronomers seek to receive *images* as one of the data products from the array. This goal should not remove the ability of the sophisticated synthesis astronomer to refine his or her image through subsequent processing, but it should allow non-expert astronomers to use the instrument easily and effectively. It involves development of instrumentation and software not presently part of operating radio synthesis instruments. Fortunately, some of the ideas that will

go into this task for the MMA can be tried and refined on existing instruments; that is the thrust of the MMA D&D effort in the area of data processing.

### 2.3 NSF Expectations for the MMA Design and Development Phase

Structure of the MMA project as three overlapping phases—Design and Development, Construction, and Operations—is a construct suggested by the NSF Astronomy Advisory Committee in 1992. It recognized that paper studies alone are not sufficient and prototyping must accompany design. With built prototypes one can realistically assess the cost and performance of the array to be constructed. The fact that a synthesis array such as the MMA is composed of multiple copies and variations of fundamental pieces means that with the construction of a few prototypes one can forecast the as-built cost and performance of the complete instrument with considerable confidence. This is a prudent approach for a synthesis telescope project.

The *deliverables* to the NSF of the MMA D&D program are these:

- a firm, *auditable*, cost estimate for construction of the MMA based on instrumentation and software prototypes;
- a site for construction of the MMA with all use permits in place;
- negotiated partnership agreements with international partners and/or U.S. agencies other than the NSF.

The requirement for partnership in the MMA speaks to issues that transcend the task of designing and prototyping a forefront scientific instrument. Nevertheless, the interests shown in the MMA by potential partners have the potential to enhance the scientific capabilities of the instrument significantly and, as such, this requirement may be both beneficial and achievable.

### 2.4 NRAO Principles for the MMA Design and Development Phase

An instrument as capable as the Millimeter Array will have a profound effect on astronomical research in the U.S. and it will have a profound effect on the NRAO. A major goal of the MMA D&D phase is to develop an organization for the project such that the MMA enhances all of the research infrastructure of radio astronomy in the U.S. To this end two specific principles have been established:

- Full involvement in the MMA D&D program of the university groups that are involved in millimeter wavelength synthesis astronomy.
- Fostering of the long-term vitality of the strong millimeter-wave research and technical development groups at U.S. universities.

### 2.5 Project Goals

The MMA D&D project requirements outlined above result in the following goals for this initial three-year phase of the project:

- Definition and implementation of an organizational and management structure, including oversight mechanisms and review processes, that will serve the entire MMA project.

- **A comprehensive proof-of-concept for the MMA instrumentation through construction of prototype hardware.**
- **A plan for integration of prototype hardware on a test interferometer.**
- **Establishment of a firm cost basis for the MMA by means of the prototyping.**
- **Involvement of interested MMA international partners early in the instrumentation design and prototyping work.**
- **Appointment of the key instrumentation design teams and assurance that they are working effectively.**
- **Selection of an optimal site for the MMA and delivery of all required permits.**
- **Partnership arrangements with foreign countries or other non-NSF U.S. governmental agencies.**
- **The continuing involvement of the U.S. community in development of the MMA and fostering of the long-term vitality of U.S. university-based millimeter-wave research and development groups.**

### III. ORGANIZATION OF THE MMA PROJECT

The Millimeter Array project is an integral part of the NRAO, organized as a construction project of the Observatory under the supervision of the NRAO Director and the management oversight of Associated Universities, Inc. The relationships are shown on the organization chart, Appendix B.

An unfortunate effect of separating the MMA project into an initial three-year Design and Development Phase to be followed, pending approval, by a six-year construction phase, is to limit the opportunity to gather the entire MMA team at one place early in the project. The uncertainty associated with the long-term prospect for the project beyond the first three years implies that staff may need to relocate for a period of less than three years only to be faced with the prospect of again moving should the construction phase of the MMA be delayed or canceled. The only practical alternative, adopted for the MMA D&D phase, is to make use of the people involved in the development and prototyping activities at the locations where they are currently employed. Development of the SIS mixer devices, the transistor (HFET) amplifiers and design of the correlator will be done at the NRAO Central Development Laboratory in Charlottesville, Virginia; the prototype receiver system (cryogenic dewar, refrigerator and control instrumentation) and the antenna design will be done at the NRAO facilities in Tucson, Arizona; the array software development, IF transmission system, operational planning, and system integration on the test interferometer will be done at the NRAO in Socorro, New Mexico. The organizational challenge to the management of the D&D program is coordination of the efforts of these geographically separate groups. Management of the NRAO as a whole involves these same challenges, the issue for the MMA is not unique.

The MMA D&D tasks will be conducted by a full-time staff assigned to the project. These people will be NRAO employees. The major D&D tasks will be managed by *Project Division Heads* whose responsibility it is to organize the efforts of the staff assigned to the task. Each major task will have a *Working Group*, a committee of experts made up of individuals at the NRAO, assigned to the MMA project, and individuals among the university groups who can advise and guide MMA work being done at the NRAO. There are four such joint NRAO-university working groups that meet at regular intervals:

- Antenna;
- Receiver;
- System;
- and Computing.

In addition, there are two others: a site testing group made up wholly of NRAO/MMA staff, and a science working group, comprised wholly of university-based astronomers whose purpose it is to advise the MMA Project Scientist. Written reports are kept for all six Working Group meetings and these reports, together with the relevant ancillary information, are posted to the WWW so as to be available to all those interested in progress of the MMA project.

The organization chart for the MMA project, illustrating the activities to which the working groups contribute, is given in Appendix C. An important part of that organization is the Millimeter Array Development Consortium (MDC). The MDC is a collaboration between the NRAO and the university groups that operate millimeter arrays in the U.S., namely, the Caltech Owens Valley Radio Observatory (OVRO) and

the Berkeley-Illinois-Maryland Association (BIMA). By means of participation in the MDC Executive Steering Committee, OVRO and BIMA are fully involved in the decision making process for the MMA development.

From its very inception, the Millimeter Array has been a collaboration between the NRAO and the U.S. astronomical community. The ideas that form the backbone of the instrument definition are contributed by interested individuals in the form of MMA Memos. The memo series provides a forum for considered analysis of the issues facing a project of the magnitude and importance of the MMA; it provides a permanent record of the views and analysis that have gone into the definition of the MMA. More than 100 people have participated as authors of the series of MMA memos that now spans the past sixteen years of MMA development. The MMA memo series is accessible via the WWW (<http://www.nrao.tuc.edu/memolist>). Appendix D is a summary of the titles and authors of the MMA Memos. It is an important and effective means of maintaining communication about MMA planning with the community of interested U.S. astronomers.

#### IV. INSTRUMENTATION DEVELOPMENT FOR THE MMA

The instrumentation sought by astronomers for the MMA extends significantly the capabilities available at present from instrumentation on existing millimeter-wave synthesis arrays. To achieve the MMA specifications in some instances will require an escalation of design techniques presently in use; in others it will require a wholly new design approach. In either case, the opportunity provided by the MMA D&D phase will permit the design approach adopted to be verified for each of the major MMA instrumentation tasks.

A condensed overview of the MMA instrumentation design goals as presently planned compared to the current state-of-the-art on operational arrays (OVRO, BIMA, the Nobeyama Radio Observatory (NRO) array, and the Institut Radio Astronomie Millimetrique (IRAM) array) is given in Table 4.1 below.

**TABLE 4.1 OVERVIEW AND COMPARISON OF MMA INSTRUMENTATION GOALS**

	MMA Spec	Capabilities of Currently Operating Arrays
<b>ANTENNAS</b>		
RSS Surface Accuracy	< 25 microns	30-80 microns
Pointing Precision	0"8	> 3"
Fast Switching	Cycle < 10s	No Capability
Total Power Observing	Yes	No Capability
<b>RECEIVERS</b>		
28-45 GHz HFET	Yes	Special Purpose only
67-95 GHz HFET	Yes	No Capability
91-119 GHz SIS or HFET	Yes	Yes
125-163 GHz SIS	Yes	NRO only
163-211 GHz SIS	Yes	No capability
211-275 GHz SIS	Yes	Yes
275-370 GHz SIS	Yes	No capability
385-500 GHz SIS	Yes	No capability
602-720 GHz SIS	Yes	No capability
787-950 GHz SIS	Planned	No capability
SIS Balanced Mixers	Yes	No
SIS Image Separating	Yes	No
SIS Integrated with IF	Yes	No
Dual Polarization	Yes	No
IF Bandwidth	2 x 8 GHz	2 x 1 GHz

A brief description of the principal challenges for development of the MMA instrumentation in the areas of antennas, system, receivers, correlator, and computing is given below; these comments are amplified by material referenced in the Appendices to this volume.

#### 4.1 Antenna

The antennas are the single most costly part of the MMA, the most visible, and the most likely to have the longest life in service. The scientific requirement that the MMA have good mosaicking capability has a strong effect on the antenna design: it means that the antennas have to point exceptionally well and that the sidelobe response cannot vary appreciably with time or antenna orientation. Because the array needs to be reconfigurable, the antennas must be transportable and this in turn means that they cannot be secured in an enclosure; they must be in the open air and meet their performance specifications fully exposed to the environment (e.g. sun and wind). Moreover, the MMA will be built at a high altitude, remote site. This implies that the antennas should be designed for low maintenance and long component life.

The MMA antenna specifications are described in detail in MMA Memo 145, included here as Appendix E. Table 4.2 shows a concise summary of the specifications.

**TABLE 4.2 ANTENNA SPECIFICATIONS**

<b>Frequency Range</b>	30 to 950 GHz
<b>Surface Accuracy</b>	< 25 micrometers RMS
<b>Pointing Accuracy</b>	< 0".8 RMS 50% of the time < 2".5 RMS 75% of the time
<b>Phase Stability</b>	< 10 micrometers RMS 25% of the time < 22 micrometers RMS 50% of the time < 56 micrometers RMS 75% of the time
<b>Dynamical Performance</b>	Switch 1.5 degrees within 1 second of time
<b>Subreflector Nutation</b>	3 beamwidths at 86 GHz
<b>Close Packing</b>	< 1.3 times the antenna diameter
<b>Physical Design</b>	Simple and durable.

The antennas proposed for the MMA in 1990 were conceived of as being 8 m in diameter. The fiducial design was for a passive antenna, one with no active elements working to adjust the antenna shape or pointing. The possibility of securing partnership in the MMA with the Europeans or the Japanese, as described in Section VII, has served to focus MMA antenna design studies on a larger, 10 m diameter, design that would achieve the scientific goals of the MMA and the complementary goals of the Europeans and/or Japanese. Such a change provides a foundation for a partnership and yet allows a stand-alone MMA to be built of 36 such antennas, should these particular partnership initiatives fail.

The MMA antennas will be built under contract. In the MMA Design and Development plan, a contract will be let for an initial prototype antenna, with an option for a second antenna. This will be a design/build to performance contract. Although the ability of the design to meet the specifications will be the responsibility of the contractor, the MMA antenna group will engineer a concept design that they believe meets the MMA specs; that design will be given to all contractors interested in bidding on the antenna contract. At their discretion, they may use and modify that design or not. In either case, having the in-house design will give the MMA antenna engineers a tool with which to compare and assess the contractor's design. After the design is accepted, the MMA engineering team will monitor the progress of the contractor's fabrication efforts and they will be in a position to evaluate the desirability of making specific engineering refinements prior to contracting for the production suite of MMA antennas. The antenna design and all the drawings done by the contractor will become the property of AUI.

The production quantity of MMA antennas will be bid separately from the prototyping work on the initial one or two antennas. Quantity antenna procurement will be done in the construction phase of the MMA. The production procurement will be a build-to-print contract, not a build-to-spec contract. The purpose of the antenna prototyping in the D&D phase is precisely to allow us to assess the as-built design in sufficient detail that we can be confident that there is little risk associated with a build-to-print quantity antenna procurement. Such an approach will enlarge the pool of contractors interested in bidding on the MMA antenna contract and capable of performing the work satisfactorily. We anticipate a substantial cost saving will be realized by this approach and the competition it will foster.

#### 4.2 System

The electronics system for a large synthesis array such as the MMA is complex, with the signals received by the antennas undergoing numerous frequency conversions using local oscillators with precisely controlled phases. The current concept for the MMA system design is given in MMA Memo 190, included here as Appendix F. The principal parts of the electronics system are receivers, local oscillator, wide bandwidth transmission system, and correlator. Some of these sub-systems are discussed in more detail below. The detailed design of this system is an important task for the design and development phase of the project.

Some of the major technical challenges for the overall system design are the maintenance of phase stability adequate for the highest observing frequency in the various signal paths and provision of an accurate total power measurement capability. The remote location of the MMA requires that the system be designed for easy operation and maintenance, implying a monitoring system adequate for off-site fault diagnosis and the packaging of all electronics in easily replaceable modules.

#### 4.3 Receivers

The receiver plan for the MMA envisions use of transistor amplifiers, HFETs (heterostructure field effect transistor) for the frequency bands near 30 and 90 GHz, and use of SIS mixers at higher frequencies. For the

2.6 mm band that includes the CO(J=1-0) transition at 115 GHz a choice between HFET and SIS will be made based on the performance figures demonstrated by the prototype HFET amplifier in this band.

HFET amplifiers at 30 and 90 GHz with performance specifications similar to those of the MMA are being fabricated now at the NRAO Central Development Laboratory (CDL) for use on the Very Large Array (VLA), the Very Long Baseline Array (VLBA), and for the NASA Microwave Anisotropy Probe (MAP) spacecraft. Little work is necessary to refine these designs for the specific needs of the MMA.

SIS Mixers for use on the NRAO 12 Meter Telescope at frequencies from 70 to 300 GHz are also produced as needed at the CDL. However, because the sites under consideration for the MMA are so dry with such little emission from atmospheric water vapor, there are significant gains in sensitivity to be realized if it is possible to provide the MMA with truly quantum-limited SIS mixer receivers. Presently the best SIS receivers have noise temperatures in the range two to four times the photon temperature,  $hf/k$ . This receiver noise contribution can be exceeded by emission from atmospheric water vapor in the unwanted (image) sideband and it can be degraded by noise from the local oscillator. The MMA goal is to minimize both these effects through the use of balanced, image-separating SIS mixers.

While most SIS mixer receivers respond to both upper and lower sidebands, few astronomical observations require this capability; most observations seek to employ one sideband or the other. Nevertheless, for a double sideband system the unwanted response of the image sideband adds atmospheric emission to the system temperature increasing the observing time required to reach a given sensitivity. The approach to be taken in design of the MMA SIS mixers is to use microfabricated LO or IF quadrature hybrids to combine the signal from a pair of mixers and in and out of phase so as to separate the sidebands. The approach to be taken is outlined in Appendix G.

Local oscillator power is usually coupled into a SIS mixer using a directional coupler or beam splitter. If the signal path loss through the LO coupler is to be kept small, the LO loss will be large, typically 15-20 dB. In addition to wasting LO power, noise from the LO source in the signal and image bands is coupled into the mixer. A balanced mixer minimizes both these effects. It has a separate LO port for efficient coupling to a pair of mixers so that the LO power is reduced relative to the single-ended mixer. Sideband noise is also reduced by phase and amplitude balance through the mixer. See Appendix G.

In the MMA Design and Development program a balanced, image-separating SIS mixer will be developed at 230 GHz. The device will be integrated with an HFET IF amplifier for broadband performance. The goal of the work is to demonstrate both that the design approach is sound and to produce an SIS design that can be scaled to all the MMA frequencies at which SIS mixer receivers will be used. The 230 GHz SIS mixer will be incorporated in the prototype receiver that will go on Antenna #1 in June 2001.

#### 4.4 Local Oscillator

The MMA Design and Development plan provides support to parallel efforts for development of the local oscillator system: a conventional microwave source multiplied by varactor diodes will be designed and built for the 230 GHz band of the prototype receiver and, simultaneously, a photonic system will be built. The

photonic approach offers, potentially, greater simplicity and reliability at lower cost but it will require substantial development effort if it is to be adopted for the MMA.

The conventional LO development planned in the MMA D&D phase will be done in three phases. First, several 100 GHz phase-locked LO chains will be built and evaluated on the basis of available power, as well as on phase and amplitude noise. Second, the optimum design will be adapted for the specific MMA needs (capable of appropriate fringe rotation, tuning range). The third phase will involve extending the 100 GHz system to 230 GHz through the use of a fixed-tuned, planar varactor frequency multiplier. Fiducial designs for higher frequency bands will follow.

The photonic LO will involve phase-locking the difference frequency of two solid-state lasers operating near 1550 nanometers. As applied to the MMA, the pair of laser signals would be sent along a single fiber (for each antenna) from a central building to the antennas. There the signals would be put into a photomixer with the difference frequency becoming the receiver local oscillator. A contract is in place with UCLA for development of a velocity-matched traveling-wave photodetector for the WR-10 waveguide band (75-110 GHz). When this is delivered the complete photonic local oscillator will be assembled and compared with the conventional LO for noise and stability. One of the two approaches will be adopted for the MMA and developed further.

#### 4.5 Correlator

The plans for the MMA correlator development begin with the design and fabrication of an early-generation correlator that can be used with the test interferometer to evaluate the first antenna prototypes and to assess the performance of the initial prototype instrumentation. This is a single baseline cross-correlator, with spectroscopic capability, built around the chip developed for the spectrometer on the Green Bank Telescope.

Design of the MMA correlator itself will begin immediately but it is a much longer term effort. The plan calls for it to be built in a modular form such that it can be delivered one-quarter at a time. This staged delivery not only permits early analysis and debugging of the correlator in an operational setting but it also provides for a realistic appraisal of the controlling software and for an opportunity to use early subsets of the correlator to support interim operations of the array as it is assembled. The basic specifications for the correlator are that it will support:

- 40 antennas;
- eight IFs per antenna (maximum bandwidth per antenna of 16 GHz);
- 4 GHz maximum sampling per IF;
- 2 bit, 4 level sampling;
- 1024 lags per baseline with a 2 GHz bandwidth, minimum;
- four product pairs (RR, RL, LR, LL) possible for polarization;
- 30 kilometer maximum baseline delay range.

The correlator planning is outlined in MMA Memo 166, included here as Appendix H.

## 4.6 Computing

Specification of the appropriate computing environment for the MMA needs to combine the needs of controlling the instrumentation in real time with the needs of people and hardware to monitor the performance of those instruments and with the needs of the astronomer to interpret quickly the scientific product of the observations. Fortunately, there is an enormous amount of experience at the NRAO and in the community that may be brought to bear on the MMA computing task. The MMA D&D planning emphasizes the need to recruit that expertise.

Appendix I, MMA Memo 164, is a report of the MMA Computing Working Group. It lays out the high level requirements for the computing task. Especially important among the conclusions in this report are these:

- A fundamental product of the MMA will be images, as well as visibility data.
- The astronomer will interact with the MMA by specifying scientific goals, not instrumental parameters.

Both of these requirements demand that the software supporting the MMA have more information available to it than is presently the case with operating radio synthesis arrays. This imposes a burden on the MMA hardware designs in many areas; it also means that the computing system must be capable of evolving as techniques that are useful to the astronomer/users are developed.

In the D&D program the opportunity will be taken to experiment with software tools, techniques, and interfaces on existing arrays through the Millimeter Array Development Consortium (MDC) collaboration, while at the same time sticking to the delivery schedule needed for software for support of early testing at the test interferometer.

## V. IMPLICATIONS OF A REMOTE SITE FOR THE MMA: ROLE OF THE TEST INTERFEROMETER

Regardless of whether the MMA is located on Mauna Kea or on the Chilean Altiplano, construction of the array will involve trans-oceanic shipment of materials. As long as such materials can be packaged in standard ocean shipping containers the shipping cost is determined by the number of containers shipped: the cost is all in the loading and unloading. Given this, one may consider either to accumulate and ship construction materials for assembly of the instrument on-site, or alternatively, to fabricate and test large sub-assemblies in the continental U.S. and ship them as modular units. The latter approach is preferable because it permits high-level MMA staff to assemble and test MMA instrumentation in existing NRAO laboratories where the staff are currently located; there is no expense associated with relocating staff with sophisticated technical skills to a remote location for instrument assembly. Ideally, the work on-site can be reduced to that of connecting major sub-systems and testing.

Taking one step back from construction and considering this same issue for the development phase of the project one reaches the identical conclusion. Namely, the process of verifying the performance of prototype instrumentation for the MMA is best done by the designers of that instrumentation in a controlled, but realistic, environment whenever possible. The MMA D&D plan envisions the construction of a test interferometer comprised of two prototype MMA antennas, located at the VLA site and used to mount and test all the prototype instrumentation and software built during the D&D phase. This provides both a comprehensive system test for the MMA prototype assembly and it provides a test facility for the evaluation of successive iterations of hardware and software developments. Once performance and system compatibility is established on the test interferometer for each representative piece of MMA instrumentation one can build production quantities of that device and ship it directly to the array site confident that it will integrate smoothly into the overall array assembly on-site. The test interferometer will also be used for the initial training of the MMA operational staff.

At the conclusion of the three-year MMA D&D phase the prototype antenna and representative prototypes of all the MMA radiometric instrumentation will be complete and delivered to the VLA site. Specifically, the following deliverables, that are the product of the D&D effort, will be present on 1 June 2001 at the test interferometer:

<b>Antennas</b>	The first prototype, designed and built under contract by an antenna fabricator. An option for the second prototype antenna will have been exercised and funded from the MMA construction phase of the project.
<b>Receivers</b>	Prototype MMA cryogenic dewar and compressor. Three frequency inserts, at 30, 90, and 230 GHz. The initial 230 GHz SIS receiver is the prototype, balanced, image-separating mixer integrated with the broadband HFET IF amplifier. The design is scalable to the other MMA frequencies.
<b>LO</b>	Low frequency Gunn; multiplied by prototype broadband planar varactor diodes for 230 GHz.

<b>IF</b>	Lowest 1 GHz of the MMA 4-12 GHz system. Baseband converters are MMA design. Fiber optic transmitters/receivers are MMA design.
<b>Correlator</b>	Single baseline with 1 GHz bandwidth in each of two polarizations. Spectroscopic capability. Built around existing GBT chip, not final MMA. Holography back-end.
<b>M/C Software</b>	Monitor and Control bus is MMA prototype. Single antenna and interferometer control. Rudimentary operator interface. Rudimentary astronomer interface. Mapping program for testing purposes. Fast-switch positioning capability.

The next phases of the project, construction and operations, will begin with the detailed evaluation of the prototype hardware using the test interferometer (the first two prototype antennas) to be followed by design refinements and ultimately production fabrication of assemblies to be shipped directly to the array site.

The specific tests to be done with the prototype interferometer in the first 6-12 months of its operation in the construction phase of the MMA project include:

- Test and development of control software.
- Adjust the antenna surfaces using holography from a spacecraft or from a local beacon.
- Check the mechanical performance of the antennas.
- Check pointing and tracking using the strongest celestial sources.
- Verify the performance of any active elements used to point the antennas.
- Check the fast switching capability of the antenna servo and its control software.
- Check the coherence of the interferometer.
- Make an accurate measurement of the antenna phase stability and gain as a function of elevation.
- Verify the interferometer phase stability with solar heating, and with wind speed.
- Measure the polarization purity of the antenna and optics.

## VI. WORK BREAKDOWN STRUCTURE

The tasks to be accomplished in the MMA Design and Development phase are enumerated on the D&D Gantt Chart, Table 6.1. This outlines the general steps to be taken in each of the MMA development areas, a time estimate for each and the personnel resources needed to address the tasks. The MMA D&D program is done to prepare for MMA construction and as such the *deliverables* are designs, decisions, and prototypes, not production quantities of any of the array hardware. In the final year of the program, approximately June 2000 to June 2001, many of the D&D tasks will have been completed and their outputs delivered to the appropriate site for testing or incorporation in larger parts of the prototype hardware. The staff involved with such completed tasks will, at that time, be transferred either to the construction phase of the MMA which is anticipated to begin in FY2001 (October of 2000) or to the operations phase of the project which should begin in 2001.

Tables 6.2 and 6.3 present a summary of the Milestones and Deliverables of the project as abstracted from the Gantt Chart so that they may be easily reviewed either by task (Table 6.2) or by date (Table 6.3). Tables 6.4 and 6.5 summarize the personnel assignments by skill and task respectively.

Table 6.6 is an illustration of the breakdown of expenditures planned in support of the Design and Development work. The total cost for the three-year Design and Development program given here, \$26.0M in current dollars, is only incrementally larger than the \$22.3M cost estimated for the 1992 D&D plan, also in current dollars (see Volume I). An annual inflation of 2.6 percent will wholly account for this increase over the intervening six years.



MMA Design and Development 980127.1

Task Name	Resources	Start Date	Effort	End Date	1998	1999	2000	2001
<b>ADMINISTRATION</b>		<b>6/1/98</b>	<b>5,905.50d</b>	<b>6/1/01</b>				
<b>Project Management</b>		<b>6/1/98</b>	<b>5,905.50d</b>	<b>5/31/01</b>				
Coordination	Project Director, Schedul	6/1/98	228.60w	5/31/01				
Engineering	Project Manager	6/1/98	152.40w	5/31/01				
Software & Computing	Scientist	6/1/98	152.40w	5/31/01				
Science	Project Scientist, Progra	6/1/98	228.60w	5/31/01				
Site Affairs	Scientist	6/1/98	266.70w	5/31/01				
Business & Contracts	Business Manager, Buy	6/1/98	152.40w	5/31/01				
Deliver Initial MMA Cost Est		6/1/98	0mon	6/1/98				
Deliver Midterm MMA Cost Est		6/1/99	0mon	6/1/99				
Deliver Final MMA Cost Est		6/1/01	0mon	6/1/01				
<b>ARRAY SITE</b>		<b>6/1/98</b>	<b>3,576.00d</b>	<b>6/1/01</b>				
Site Recommendation		6/1/98	0d	6/1/98				
<b>Site Evaluation</b>		<b>6/1/98</b>	<b>2,415.00d</b>	<b>6/1/01</b>				
Testing Program	Scientist	6/1/98	152.40w	5/31/01				
Test Equip Maintenance	Technician	6/1/98	152.40w	5/31/01				
Data Analysis	Scientist	6/1/98	76.20w	5/31/01				
Design/Build Phase Cal Demo	Technician, Scientist	6/1/99	102.00w	6/1/01				
<b>Site Development</b>		<b>6/1/98</b>	<b>561.00d</b>	<b>5/31/01</b>				
Site Use Civil Engineering	Engineer	6/1/98	76.20w	5/31/01				
Site Use Ops Planning	Manager	6/1/99	24.00w	4/19/01				
Soil Sampling	Engineer	1/4/99	4.00w	10/14/99				
Safety Analysis & Procedure	Engineer	1/4/99	8.00w	7/28/00				
Configuration Design	Scientist	6/1/98	102.00w	6/2/00				
Configuration Review		3/1/00	0d	3/1/00				
A & E Contract Work	Engineer	1/3/00	18.00w	5/31/01				
<b>Site Permissions</b>		<b>12/31/99</b>	<b>0d</b>	<b>12/31/99</b>				
Signed Array Site Use		12/31/99	0d	12/31/99				
Signed Support Facil Use		12/31/99	0d	12/31/99				
<b>ANTENNA DEVELOPMENT</b>		<b>6/1/98</b>	<b>2,990.00d</b>	<b>6/1/01</b>				
Evaluate Design Concepts	Engineer	6/1/98	24.00d	7/2/98				
Preliminary Design Review		7/1/98	0mon	7/1/98				
<b>Design Antenna</b>		<b>7/1/98</b>	<b>28.97mon</b>	<b>3/2/99</b>				
Mount/Reflector Analysis	Engineer, Technician	7/1/98	42.00w	3/2/99				
Pointing/Metrology Studies	Engineer, Technician	7/1/98	42.00w	3/2/99				
Drive & Servo Studies	Engineer, Technician	7/1/98	42.00w	3/2/99				
Critical Design Review		1/1/99	0d	1/1/99				
<b>Prepare Antenna RFP</b>		<b>3/1/99</b>	<b>210.00d</b>	<b>5/3/99</b>				
Mount & Reflector Analysis	Engineer, Technician	3/1/99	16.00w	5/3/99				
Pointing/Metrology Studies	Engineer, Technician	3/1/99	16.00w	5/3/99				
Drive & Servo Studies	Engineer, Technician	3/1/99	10.00w	4/23/99				
Bid Prototype (#1+option #2)		6/1/99	0mon	6/1/99				
<b>Prelim Design Related Syst</b>		<b>4/1/99</b>	<b>16.00mon</b>	<b>9/2/99</b>				
Nutator	Engineer	6/1/99	3.00mon	9/1/99				
Transporter	Engineer	4/1/99	5.00mon	9/2/99				
Metrology Subsystem	Engineer	6/1/99	3.00mon	9/1/99				
Foundation	Engineer	4/1/99	5.00mon	9/2/99				
Receive Bid Response		9/1/99	0d	9/1/99				
Evaluate Bids	Engineer, Technician	9/1/99	32.00w	12/27/99				
Sign Contract (#1+option #2)		1/1/00	0d	1/1/00				
Parallel Analysis with Contractor	Engineer, Technician	1/3/00	66.39mon	6/1/01				



MMA Design and Development 980127.1

Task Name	Resources	Start Date	Effort	End Date	1998	1999	2000	2001
<b>Design of Related Systems</b>		<b>5/1/00</b>	<b>8.00mon</b>	<b>9/1/00</b>				
Transporter	Engineer	5/1/00	2.00mon	6/30/00				
Issue Transporter RFP		9/1/00	0mon	9/1/00				
Receive Transporter Bids		11/1/00	0mon	11/1/00				
Sign Transporter Contract		1/1/01	0mon	1/1/01				
Deliver Transporter		6/1/01	0mon	6/1/01				
Nutator	Engineer	7/3/00	2.00mon	9/1/00				
Foundation	Engineer	5/1/00	2.00mon	6/30/00				
Metrology Subsystem	Engineer	7/3/00	2.00mon	9/1/00				
Exercise Option Antenna #2		10/1/00	0d	10/1/00				
Delivery/Accept #1 at VLA Site		6/1/01	0d	6/1/01				
<b>SIS MIXER</b>		<b>6/1/98</b>	<b>6,366.75d</b>	<b>6/15/01</b>				
<b>Instrumentation Developme</b>		<b>6/1/98</b>	<b>171.95mon</b>	<b>6/15/01</b>				
Design On-wafer Monitor	Engineer	6/1/98	8.00w	1/18/99				
Wideband 1-12 GHz IF	Engineer	6/1/98	8.00w	1/18/99				
Window & IR Filter	Engineer	6/1/98	20.00w	12/29/99				
Sideband Meas Facility	Technician	6/1/98	7.00w	12/17/98				
IF Switches and Hybrids	Engineer	6/1/98	64.00w	12/6/00				
Enhance Network Analyzer	Engineer, Technician	10/1/98	36.00w	9/13/99				
Sources 180-320 GHz	Engineer	6/1/98	32.00w	12/6/00				
Sources 110-950GHz, begin	Engineer	6/1/99	52.00w	6/15/01				
4K Test Stations	Technician	6/1/98	64.00w	12/6/00				
SIS Support	Technician, Machinist	6/1/98	457.00w	5/31/01				
<b>SIS Mixer Development</b>		<b>6/1/98</b>	<b>120.77mon</b>	<b>6/1/01</b>				
200-300 GHz Elements	Engineer	6/1/98	3.00mon	9/1/98				
200-300 GHz Image-Sep (IS)	Engineer	6/1/98	45.00w	1/4/99				
200-300 GHz Balanced (Bal)	Engineer	6/1/98	54.00w	6/23/99				
200-300 GHz Bal, IS	Engineer	1/4/99	50.80w	1/3/00				
4-12 GHz Integrated IF	Engineer	6/1/98	80.00w	12/29/99				
SIS Preliminary Design Rev		1/1/00	0mon	1/1/00				
Deliver Proto 230 GHz to Tuc		4/1/00	0mon	4/1/00				
Build MMA 230 GHz Band	Engineer	1/3/00	60.00w	3/7/01				
Design MMA Bands	Engineer	1/3/00	41.49mon	6/1/01				
Proto & Dev MMA Bands	Engineer, Technician	1/2/01	42.00w	5/30/01				
SIS Critical Design Review		1/1/01	0mon	1/1/01				
Deliver MMA 230 GHz		4/1/01	0mon	4/1/01				
<b>HFET AMPLIFIER</b>		<b>6/1/98</b>	<b>980.00d</b>	<b>5/29/01</b>				
MMA Designs RF & IF	Engineer, Technician	6/1/98	152.00w	5/29/01				
Prototype 33-50 GHz	Engineer, Technician	6/1/98	20.00w	10/20/98				
Prototype 86-115 GHz	Engineer, Technician	11/2/98	24.00w	6/7/99				
Procure HFET Wafer		1/1/99	0w	12/31/99				
Deliver 30 GHz to Tucson		1/1/99	0d	1/1/99				
Deliver 90 GHz to Tucson		9/1/99	0mon	9/1/99				
<b>LOCAL OSCILLATOR</b>		<b>6/1/98</b>	<b>3,594.00d</b>	<b>6/8/01</b>				
<b>Conventional LO</b>		<b>6/1/98</b>	<b>1,520.00d</b>	<b>6/8/01</b>				
Design/Test 230GHz Doubl	Engineer, Technician	6/1/98	24.00w	11/18/98				
Demo 230 GHz Doubler		12/1/98	0mon	12/1/98				
Inst for 230 GHz PLL Dev	Technician	6/1/98	20.00w	10/20/98				
Design/build PLLs	Engineer, Technician	9/1/98	24.00w	2/23/99				
Preliminary Design Review		9/1/98	0mon	9/1/98				
Measure PLL Performance	Engineer, Technician	1/4/99	32.00w	8/18/99				
Design/test Filter	Engineer, Technician	3/1/99	24.00w	8/17/99				
Critical Design Review		6/1/99	0mon	6/1/99				
Breadboard PLL Demo		9/1/99	0mon	9/1/99				
230 GHz LO Demo		12/1/99	0mon	12/1/99				
Deliver LO to Tucson		3/1/00	0mon	6/1/00				



MMA Design and Development 980127.1

Task Name	Resources	Start Date	Effort	End Date	1998	1999	2000	2001
MMA Freqs Design & Proto	Engineer, Technician	9/1/99	180.00w	6/8/01				
<b>Photonic Local Oscill</b>		<b>6/1/98</b>	<b>2,074.00d</b>	<b>5/31/01</b>				
Design 75-110 GHz	Engineer	6/1/98	28.00w	12/17/98				
Gen/Test Phas-lock beat	Engineer, Technician	6/1/98	84.00w	7/8/99				
Receive 3mm Photodetector		9/1/99	0mon	12/6/99				
Build/Test 75-110 GHz	Engineer, Technician	1/4/99	76.00w	1/3/00				
Compare Photo/Conv 75-110	Engineer, Technician	3/1/00	24.00w	8/17/00				
Contract 230 GHz Photodet		6/1/99	0mon	12/13/00				
Design/Build/Test 230 GHz	Engineer, Technician	6/1/00	50.80w	5/31/01				
Design MMA Freq Bands	Engineer, Technician	6/1/99	152.00w	5/29/01				
Preliminary Design Review		1/1/99	0mon	1/1/99				
Critical Design Review		6/1/00	0mon	6/1/00				
<b>RECEIVER SYSTEMS</b>		<b>6/1/98</b>	<b>4,400.00d</b>	<b>6/8/01</b>				
Dewar Mechanical Design	Engineer, Technician	6/1/98	26.00w	6/9/99				
Cryogenics Options Evaluate	Engineer, Technician	6/1/98	24.00w	5/11/99				
Cryo & Refrigerator Design	Engineer, Technician	1/4/99	10.00w	5/24/99				
Receiver Optical Design	Engineer, Technician	6/1/98	36.00w	10/29/99				
Receiver RF Design	Engineer, Technician	6/1/98	36.00w	10/29/99				
Receiver Inst/Control Design	Engineer	6/1/98	52.00w	6/9/99				
Quasi-Optical Comp Develop	Engineer	6/1/98	78.00w	12/14/99				
Electromagnetic Test Instrum	Technician	6/1/98	52.00w	6/9/99				
Rx Package Critical Review		1/1/01	0d	1/1/01				
Construction Rx Packages	Engineer, Technician, M	6/1/99	360.00w	6/8/01				
Ass'y & Test 30 GHz Insert	Engineer, Technician, M	3/1/99	26.00w	6/30/99				
Ass'y & Test 90 GHz Insert	Engineer, Technician, M	8/2/99	26.00w	12/3/99				
Ass'y & Test 230 GHz Insert	Engineer, Technician, M	3/1/00	26.00w	6/30/00				
Ass'y Proto Rx (30/90/230 GHz)	Engineer, Technician	6/1/00	52.00w	12/4/00				
Integrate Proto Rx, Proto LO & IF	Engineer, Technician	1/2/01	26.00w	3/5/01				
Deliver Proto Rx to VLA Site		6/1/01	0d	6/1/01				
Prime Focus Holography Rx	Engineer	6/1/00	24.00w	5/10/01				
Holography Backend	Engineer, Technician	6/1/00	26.00w	12/4/00				
Deliver Holography Sys to VLA		6/1/01	0d	6/1/01				
<b>CORRELATOR</b>		<b>6/1/98</b>	<b>3,290.75d</b>	<b>5/31/01</b>				
<b>Test Correlator</b>		<b>7/1/98</b>	<b>154.00w</b>	<b>1/5/00</b>				
Build	Engineer, Technician	7/1/98	102.00w	7/2/99				
Test	Engineer, Technician	7/1/99	52.00w	1/5/00				
Deliver Test Correlator		1/3/00	0mon	1/3/00				
<b>Preliminary Design</b>		<b>6/1/98</b>	<b>14.79mon</b>	<b>1/4/99</b>				
Preliminary Studies	Engineer	6/1/98	1.00mon	6/30/98				
Design Architecture	Engineer	6/1/98	60.00w	1/4/99				
Preliminary Design Review		1/1/99	0mon	1/1/99				
<b>Detailed Design</b>		<b>1/4/99</b>	<b>49.66mon</b>	<b>6/1/00</b>				
Design Boards	Engineer	1/4/99	72.00w	6/1/00				
Design Rack	Engineer	1/4/99	72.00w	6/1/00				
Design Chip	Engineer	1/4/99	72.00w	6/1/00				
Critical Design Review		6/1/00	0mon	6/1/00				
<b>Prototype Correlator</b>		<b>6/1/00</b>	<b>51.45mon</b>	<b>5/31/01</b>				
Build Boards	Engineer, Technician	6/1/00	76.00w	5/31/01				
Build Racks	Engineer, Technician	6/1/00	76.00w	5/31/01				
Fabricate Chips	Engineer	6/1/00	50.80w	5/31/01				
Hardware Tests	Engineer, Technician	1/2/01	21.00w	5/30/01				
<b>SIGNAL TRANSMISSION</b>		<b>6/1/98</b>	<b>3,175.25d</b>	<b>9/4/01</b>				
<b>Design and Documentation</b>		<b>6/1/98</b>	<b>46.71mon</b>	<b>6/1/99</b>				
Local Oscillator	Engineer	6/1/98	50.80w	6/1/99				



MMA Design and Development 980127.1

Task Name	Resources	Start Date	Effort	End Date	1998	1999	2000	2001
IF	Engineer	6/1/98	50.80w	6/1/99				
Fiber Optics	Engineer	6/1/98	50.80w	6/1/99				
M&C Hard/Software	Engineer	6/1/98	50.80w	6/1/99				
Preliminary Design Review		10/1/98	0mon	10/1/98				
Critical Design Review		6/1/99	0mon	6/1/99				
<b>Build Prototype Modules</b>		<b>6/1/99</b>	<b>58.39mon</b>	<b>5/30/00</b>				
Local Oscillator	Engineer	6/1/99	50.80w	5/30/00				
IF	Engineer	6/1/99	50.80w	5/30/00				
Fiber Optics	Engineer	6/1/99	50.80w	5/30/00				
M&C Hard/Software	Engineer	6/1/99	50.80w	5/30/00				
Laboratory Test & Rework	Technician	6/1/99	50.80w	5/30/00				
Build Ant#1 Infrastr at VLA	Technician	9/1/00	38.00w	6/1/01				
<b>Build Testbed &amp; Ant#1 sub</b>		<b>6/1/00</b>	<b>32.15mon</b>	<b>9/4/01</b>				
Fabrication	Engineer	6/1/00	76.00w	5/31/01				
Lab Test & Rework	Engineer	6/1/00	50.80w	5/31/01				
Begin: Install and Test	Engineer	6/1/01	3.00mon	9/4/01				
<b>COMPUTING</b>		<b>6/1/98</b>	<b>4,900.00d</b>	<b>6/6/01</b>				
M/C Bus Evaluate & Prototype	Engineer, Programmer	6/1/98	36.00w	2/16/99				
<b>Correlator Realtime/Interfa</b>		<b>6/1/98</b>	<b>35.03mon</b>	<b>5/31/01</b>				
Design/Program Corr Interf	Programmer	6/1/98	101.60w	5/31/00				
PDR: Test Corr Interface		3/1/99	0mon	3/1/99				
CDR: Test Corr Interface		6/1/99	0mon	6/1/99				
Deliver Test Corr Interface		1/3/00	0mon	1/3/00				
Begin Proto Corr Interface	Programmer	6/1/00	50.80w	5/31/01				
<b>Project Support</b>		<b>6/1/98</b>	<b>316.80w</b>	<b>5/31/01</b>				
Build test/dev facilities	Programmer	6/1/98	152.40w	5/31/01				
Holography System	Programmer	6/1/00	12.00w	11/17/00				
<b>System Design</b>		<b>6/1/98</b>	<b>304.80w</b>	<b>5/31/01</b>				
PDR: Single Dish System		3/1/99	0d	3/1/99				
CDR: Single Dish System		1/1/01	0mon	1/1/01				
Deliver Sngl Dsh Sys to VLA		6/1/01	0d	6/1/01				
PDR: System Design		6/1/00	0w	6/1/00				
CDR: System Design		1/1/01	0w	1/1/01				
Begin Proto Array Control/Interf	Programmer	1/2/01	21.00w	5/30/01				
Automated Image Production	Programmer	1/2/01	11.00w	6/6/01				
Data Access and Archive	Programmer	1/2/01	11.00w	6/6/01				
Operator/Astronomer GUI	Programmer	6/1/98	76.00w	5/29/01				
<b>SYSTEM INTEGRATION AND</b>		<b>6/1/98</b>	<b>1,822.00d</b>	<b>7/10/01</b>				
<b>System Engineering</b>		<b>6/1/98</b>	<b>35.03mon</b>	<b>6/1/01</b>				
System Interface Control	System Engineer	6/1/98	50.80w	6/1/01				
Equipment Config Control	System Engineer	6/1/98	50.80w	6/1/01				
Documentation Control	System Engineer	6/1/98	50.80w	6/1/01				
Project Book version 1		6/1/98	0d	6/1/98				
Project Preliminary Review		7/1/98	0mon	7/1/98				
Project Book version 2		6/1/00	0mon	6/1/00				
Project Critical Review		1/1/01	0d	1/1/01				
<b>Scientific Issue Analysis</b>		<b>6/1/98</b>	<b>24.83mon</b>	<b>7/10/01</b>				
Contingency Scheduling	Programmer	1/4/99	32.00w	7/10/01				
Project Support	Scientist	6/1/98	76.00w	5/29/01				
<b>Test Interferometer</b>		<b>6/1/99</b>	<b>520.00d</b>	<b>9/8/00</b>				
Prepare Site at VLA	Engineer, Technician	6/1/99	26.00w	8/31/99				
Antenna Pads and Utilities	Engineer, Technician	9/1/99	52.00w	9/8/00				
Building Preparation	Engineer, Technician	3/1/00	26.00w	8/31/00				
Test Interf. Site Complete		6/1/01	0d	6/1/01				



**TABLE 6.2 MILESTONES AND DELIVERABLES BY TASK**

<b>ADMINISTRATION</b>	
Deliver Initial MMA Cost Estimate	Jun 1998
Deliver Midterm MMA Cost Estimate	Jun 1999
Deliver Final MMA Cost Estimate	Jun 2001
<b>SITE</b>	
Site Recommendation	Jun 1998
Signed Array Site Use Permission	Dec 1999
Configuration Review	Mar 2000
Signed Support Facility Use Permission	Dec 1999
<b>ANTENNA</b>	
Preliminary Design Review	Jul 1998
Critical Design Review	Jan 1999
Bid Prototype Antenna (#1+option #2)	Jun 1999
Receive Bid Response	Sep 1999
Sign Antenna Contract	Jan 2000
Issue Transporter RFF	Sep 2000
Exercise Option Ant #2	Oct 2000
Receive Transporter Bids	Nov 2000
Sign Transporter Contract	Jan 2001
Deliver/Accept Ant #1	Jun 2001
Receive/Accept Transporter	Jun 2001
<b>SIS MIXER</b>	
Preliminary Design Review	Jan 2000
Deliver Proto 230 GHz	Apr 2000
Critical Design Review	Jan 2001
Deliver MMA 230 GHz	Apr 2001
<b>HFET AMPLIFIER</b>	
Procure HFET Wafer	Jan 1999
Deliver 30 GHz	Jan 1999
Deliver 90 GHz	Sep 1999
<b>LOCAL OSCILLATOR</b>	
Preliminary Design Review: Conventional	Sep 1998
Demo 230 GHz Doubler	Dec 1998
Preliminary Design Review: Photonic	Jan 1999
Critical Design Review: Conventional	Jun 1999
Breadboard PLL Demonstration	Sep 1999
Receive 3 mm Photodetector	Sep 1999
230 GHz LO Demonstration	Dec 1999
Deliver LO to Tucson	Mar 2000
Critical Design Review Photonic: Decision	Jun 2000

<b>RECEIVER SYSTEM</b>	
Receiver Package Preliminary Review	Apr 1999
Receiver Package Critical Review	Jan 2001
Deliver Prototype Receiver	Jun 2001
Deliver Holography System	Jun 2001
<b>CORRELATOR</b>	
PDR Correlator Design	Jan 1999
Deliver Test Correlator	Jan 2000
CDR Correlator Design	Jul 2000
<b>SIGNAL TRANSMISSION</b>	
Preliminary Design Review	Oct 1998
Critical Design Review	Jun 1999
<b>COMPUTING</b>	
PDR: Test Correlator Interface	Mar 1999
PDR: Single Dish System	Mar 1999
CDR: Test Correlator Interface	Jun 1999
Deliver Test Correlator Interface	Jan 2000
PDR: Computing System	Jun 2000
CDR: Single Dish System	Jun 2000
CDR: Computing System	Jan 2001
Deliver Single Dish System	Jan 2001
<b>SYSTEM INTEGRATION AND TEST</b>	
Project Book Version 1	Jun 1998
Project Preliminary Review	Jul 1998
Project Book Version 2	Jun 2000
Project Critical Review	Jan 2001
Test Interferometer Site Complete	Jun 2001

**TABLE 6.3 MILESTONES AND DELIVERABLES: CHRONOLOGICAL**

<b>CALENDAR YEAR 1998</b>	
June	Deliver Initial MMA Cost Estimate
	Site Recommendation
	Project Book Version 1
July	PDR: Antenna Design
	Project Preliminary Review
September	PDR: Conventional LO
October	PDR: Signal Transmission System
December	230 GHz LO Doubler Demonstration
<b>CALENDAR YEAR 1999</b>	
January	CDR: Antenna Design
	Procure HFET Wafer
	Deliver 30 GHz Amplifier
	PDR: Photonic LO Design
	PDR: Correlator Design
April	Receiver Package Preliminary Review
March	PDR: Test Correlator Interface
	PDR: Single Dish Software System
June	Deliver Midterm MMA Cost Estimate
	Bid Prototype Antenna (#1+option #2)
	CDR: Conventional LO Design
	CDR: Signal Transmission System Design
	CDR: Test Correlator Interface
September	Receive Antenna Bid Response
	Deliver 90 GHz HFET Amplifier
	Demonstrate Breadboard PLL
	Receive 3mm Photodetector
December	Signed Array Site Use Permission
	Signed Ops Facility Site Use Permission
	230 GHz Conventional LO Demonstration
<b>CALENDAR YEAR 2000</b>	
January	Sign Antenna Contract Ant #1
	PDR: SIS Mixer Design
	Deliver Test Correlator
	Deliver Test Correlator Interface
March	Deliver Completed LO to Tucson
	Configuration Review
April	Deliver Proto 230 GHz
June	CDR: Photonic LO, Decision to Continue
	PDR: Computing System Design
	CDR: Single Dish Computing System
	Project Book Version 2
July	CDR: Correlator Design

September	Issue Transporter RFP
October	Exercise Option on Antenna #2
November	Receive Transporter Bids
<b>CALENDAR YEAR 2001</b>	
January	CDR: SIS Mixer Design
	CDR: Receiver Package
	CDR: Computing System
	Deliver Single Dish Computing System
	Project Critical Review
	Sign Transporter Contract
April	Deliver MMA 230 GHz SIS Mixer
June	Deliver Final MMA Cost Estimate
	Receive/Accept Antenna #1
	Deliver Prototype Receiver to VLA Site
	Deliver Holography System to VLA Site
	Test Interferometer Site Complete
	Receive/Accept Transporter

#### 6.4 Personnel Projections

The personnel required to carry out the tasks of the MMA Design and Development program and those needed to prepare for the construction phase of the project are summarized in the tables below. Table 6.4 presents the distribution of staff by calendar year. These are numbers of full-time employees, to be distinguished from years-worked for 1998 where the project begins in June, and for 2001 where the D&D phase is completed in June. Table 6.5 shows the distribution of staff by task for 1999 where the project is fully staffed and the project extends for the entire calendar year. The personnel allocation for other years is essentially identical to that in 1999; in the final year personnel will begin to be transferred to construction or operations.

The MDC university-based people working on the project are among those included in this table.

The MMA D&D personnel projection given here, approximately fifty full-time employees, is identical to the number of employees projected as being needed in the MMA D&D plan, Volume I, as presented to the NSF in 1992. The distribution of skills required, and the task assignments, is also little changed from the 1992 plan. The goals of the plan as presented here are, however, much refined over the plan as given in Volume I.

#### 6.5 Budget

The budget plan for the MMA Design and Development project is shown in Table 6.6. Entries are in dollars of the year of expenditure (current dollars). Personnel cost estimates are consistent with the personnel plan presented in Section 6.4 above. Cost estimates for all of the electronic sub-systems have been made by NRAO engineers experienced in building equipment similar to that needed for the MMA. These tasks together account for approximately 75 percent of the expense of the D&D program. The current allocation for contingency, \$1266 K, is low but is considered acceptable because of the small fraction (approximately 25

percent of the total budget) of the development work being done as contracts to commercial companies. The cost of the major contract, the antenna design and first element construction, has been estimated from budgetary figures provided at our request by three companies experienced in millimeter wavelength design and construction.

**TABLE 6.4 PERSONNEL PROJECTIONS BY CALENDAR YEAR**

	1998	1999	2000	2001
Scientist (S)	5.75	6.00	6.75	5.75
Engineer (E)	23.50	24.75	23.25	23.25
Programmer (P)	5.50	5.75	5.75	7.25
Technician (T)	11.00	12.00	12.5	12.00
Machinist (M)	1.00	2.00	2.00	2.00
Administrative/Other (A)	3.50	3.75	3.75	3.75

**TABLE 6.5 PERSONNEL PROJECTIONS BY TASK: CALENDAR YEAR 1999**

	S	E	P	T	M	A	Total
Administration	3.75		.50			3.50	7.75
Array Site	1.75	0.75		1.25		0.25	4.00
Antenna Development		3.00		1.00			4.00
SIS Mixer		5.00		3.00	1.00		9.00
HFET Amplifier		1.00		1.00			2.00
LO: Conventional		1.00		1.00			2.00
LO: Photonic		1.50		1.00			2.50
Receiver Systems		3.0		2.00	1.00		6.00
Correlator		4.0		1.00			5.00
Signal Transmission		4.0		0.50			4.50
Computing			5.00				5.00
System Integration	0.50	1.50	0.25	0.25			2.50
<b>TOTAL</b>	<b>6.00</b>	<b>24.75</b>	<b>5.75</b>	<b>12.00</b>	<b>2.00</b>	<b>3.75</b>	<b>54.25</b>

**TABLE 6.6 MMA DESIGN AND DEVELOPMENT: TOTAL COST**  
(in Thousands of Dollars)

	<b>CY1998</b>	<b>1999</b>	<b>2000</b>	<b>2001</b>	<b>SUBTOTAL</b>	<b>TOTAL</b>
<b>ADMINISTRATION</b>						
Labor	\$345	\$585	\$537	\$195	\$1,662	\$3,112
Facilities/Rent	50	200	200	100	550	
Communications	50	75	75	50	250	
Travel	150	200	200	100	650	
<b>ARRAY SITE</b>						
Labor	187	391	397	146	1,121	\$1,481
Mining Rights/EIS	60	100			160	
Materials	50	50	50	50	200	
<b>ANTENNA</b>						
Labor	192	340	352	60	944	\$6,464
Materials	25	50	50	25	150	
Study Contracts	50	200			250	
Prototype Antenna		2,500	2,620		5,120	
<b>SIS MIXER</b>						
Labor	247	264	325	101	937	\$2,837
Materials	100	100	100	50	350	
Test/Lab Equipment	250	250	100	50	650	
Contract Fabrication	300	300	300		900	
<b>HFET AMPLIFIER</b>						
Labor	91	110	83	34	318	\$568
Materials	50	50	50		150	
Wafer Fabrication		100			100	
<b>LOCAL OSCILLATOR</b>						
Labor	214	431	339	113	1,097	\$2,247
Lasers	100	50	50	25	225	
Photodetectors		150	50	50	250	
Multipliers	100	50	50	25	225	
Lab/Test Equipment	100	100	150	100	450	
<b>RECEIVER SYSTEMS</b>						
Labor	257	531	474	187	1,449	\$2,224
Contract Services	25	50	50	50	175	
Materials	75	100	100	75	350	
Lab/Test Equipment	50	100	100		250	
<b>CORRELATOR</b>						
Labor	217	487	333	117	1,154	\$1,304
Materials	25	50	50	25	150	
<b>SIGNAL TRANSMISSION</b>						
Labor	251	462	351	113	1,177	\$2,002
Lab/Test Equipment	150	150	50	25	375	
Materials	50	100	200	100	450	
<b>COMPUTING</b>						
Labor	280	437	416	243	1,376	\$1,526
Materials	25	50	50	25	150	
<b>SYSTEM INTEGRATION</b>						
Labor	87	239	270	73	669	\$969
Materials & Contracts	50	100	100	50	300	
<b>SUBTOTAL LABOR</b>	<b>\$2,368</b>	<b>\$4,277</b>	<b>\$3,877</b>	<b>\$1,382</b>	<b>\$11,904</b>	
<b>CONTINGENCY</b>						<b>\$1,266</b>
<b>GRAND TOTAL</b>	<b>\$4,253</b>	<b>\$9,502</b>	<b>\$8,622</b>	<b>\$2,357</b>	<b>\$24,734</b>	<b>\$26,000</b>

## VII. DESIGN AND DEVELOPMENT IN THE MMA PROJECT CONTEXT

### 7.1 Operations

At the conclusion of the Design and Development phase the prototype antenna will be delivered and accepted at the VLA where MMA system testing will be done. That antenna will be outfitted with the prototype receiver and controlled by prototype software written for the purpose. There will be a correlator to use as an autocorrelator for spectroscopic tests and as a cross correlator when the second prototype antenna arrives at the test site. As described above, the test instrument will be used to evaluate the antenna performance and to verify the performance and compatibility of successive iterations of all the MMA instrumentation. The test interferometer also plays a pivotal role in software development. All this can be done in a facility convenient for the MMA development staff.

The operating staff for the test interferometer will be the initial members of the MMA operations staff. These people will be among the first assigned to the MMA site itself and they will be used both to establish and document operational procedures, and to train additional hires to operations. Once the MMA site construction is in progress and some of these individuals are assigned to that location to initiate on-site operations, the MMA operations will be expanded to include operation of both the test interferometer on the VLA site and to interim MMA operations at the MMA site.

A timely start to the gradual build-up of MMA operations beginning in June of 2001 with the access to a prototype antenna provided by the MMA D&D program is important to the orderly development of MMA operations.

### 7.2 Construction: Role of MMA Partnerships

Among the *deliverables* of the MMA Design and Development initiative is an agreed partnership in the array by foreign countries or by U.S. agencies other than the NSF. Partners in the project will have their own ideas as to the structure of the construction project—they will need to be included in the intellectual and financial description of MMA construction—and, owing to this, it is not possible to lay out the entire construction project in detail. Moreover, some crucial aspects of the instrument construction await the design decisions to be made in the next three years of the D&D effort. All this means that one can present an overview of how the construction project could go, understanding that this will need modification as the partnerships and the D&D progresses. Such an overview is given in the Gantt Chart, Table 7.1. Its value is in the illustration it provides for the interrelation between Design and Development, Construction and Operations. Note that the construction work begins promptly at the start of FY2001 (October 2000) and smooths the transition between the D&D activities and the construction efforts task by task.

Two partnership possibilities may have a significant effect on the construction phase planning. These are the possibility of joining the MMA with the Japanese project, the Large Millimeter and Submillimeter Array (LMSA), or with the European Large Southern Array (LSA). Both of these initiatives have considerable support among their respective scientific communities and the leaders of both have expressed interest in

discussing how their projects could be joined with the MMA to the benefit of all. Either combination with the MMA, or better, a combination of all three, would provide such a truly powerful imaging instrument. The U.S. community has been supportive of efforts by the MMA staff to secure such a partnership. One barrier to a joint project is the dissimilar antenna diameters considered by the three; the MMA has planned 8 m antennas, the LMSA 10 m antennas, and the LSA 15 m antennas. Recent discussions among the three groups have led to successive compromises on the diameter to the range 10–12 m. The MMA Design and Development antenna design efforts will therefore focus on antennas of 10 m diameter to facilitate a partnership with one or both of these groups. Should the partnership initiatives fail, the MMA construction budget estimates would allow an array of approximately 36 antennas to be built. Such an array could accomplish all the scientific goals projected for an array of forty 8-m antennas, but would do so with nearly fifty percent more collecting area. This subtle change in the baseline MMA planning is therefore an asset to be used to court partnership with the LMSA or LSA and an asset to the sensitivity of the MMA as a stand alone instrument. Progress in securing partnerships for the MMA, as indeed progress in realizing the technology to achieve the capabilities desired of the MMA itself, begins with the efforts outlined in the MMA Design and Development Plan.

MMA Project Overview 980127.1

Task Name	Start Date	End Date	1998	1999	2000	2001	2002	2003	2004	2005	2006	2007	
<b>ADMINISTRATION</b>	<b>6/1/98</b>	<b>10/1/07</b>	[Gantt bar spanning 1998-2007]										
Design and Development	6/1/98	5/31/01	[Gantt bar from 6/1/98 to 5/31/01]										
Organize Project Management	6/1/98	5/31/01	[Gantt bar from 6/1/98 to 5/31/01]										
<b>Construction</b>	<b>10/2/00</b>	<b>10/1/07</b>	[Gantt bar spanning 10/2/00-10/1/07]										
Manage Production and Procurement	10/2/00	10/1/07	[Gantt bar from 10/2/00 to 10/1/07]										
<b>Operations</b>	<b>1/2/01</b>	<b>10/1/07</b>	[Gantt bar spanning 1/2/01-10/1/07]										
Plan and Develop Site Operations	1/2/01	10/1/07	[Gantt bar from 1/2/01 to 10/1/07]										
<b>ARRAY SITE</b>	<b>6/1/98</b>	<b>10/1/07</b>	[Gantt bar spanning 6/1/98-10/1/07]										
Design and Development	6/1/98	5/31/01	[Gantt bar from 6/1/98 to 5/31/01]										
Site Civil Engineering	6/1/98	5/31/01	[Gantt bar from 6/1/98 to 5/31/01]										
Site Use Permission	1/1/00	1/1/00	[Gantt bar at 1/1/00 with triangle marker]										
Preliminary A&E Contract	6/1/98	10/29/98	[Gantt bar from 6/1/98 to 10/29/98]										
<b>Construction</b>	<b>1/2/01</b>	<b>12/31/04</b>	[Gantt bar spanning 1/2/01-12/31/04]										
A&E Contract Engineering	1/2/01	12/31/04	[Gantt bar from 1/2/01 to 12/31/04]										
Ops Facility Construction	6/1/01	5/30/03	[Gantt bar from 6/1/01 to 5/30/03]										
Site Construction	6/1/01	6/1/04	[Gantt bar from 6/1/01 to 6/1/04]										
<b>Operations</b>	<b>6/1/01</b>	<b>10/1/07</b>	[Gantt bar spanning 6/1/01-10/1/07]										
Hire/Train Site Ops Staff	6/1/01	10/1/07	[Gantt bar from 6/1/01 to 10/1/07]										
<b>ANTENNA DEVELOPMENT</b>	<b>6/1/98</b>	<b>10/1/07</b>	[Gantt bar spanning 6/1/98-10/1/07]										
Design and Development	6/1/98	6/1/01	[Gantt bar from 6/1/98 to 6/1/01]										
Antenna Design	6/1/98	6/1/01	[Gantt bar from 6/1/98 to 6/1/01]										
Sign Contract (Ant#1+option Ant#2)	1/1/00	1/1/00	[Gantt bar at 1/1/00 with triangle marker]										
Receive/Accept Ant#1	6/1/01	6/1/01	[Gantt bar at 6/1/01 with triangle marker]										
<b>Construction</b>	<b>1/1/02</b>	<b>10/1/07</b>	[Gantt bar spanning 1/1/02-10/1/07]										
Receive/Accept Ant#2	1/1/02	1/1/02	[Gantt bar at 1/1/02 with triangle marker]										
Accept/Approve Antenna Design	1/1/03	1/1/03	[Gantt bar at 1/1/03 with triangle marker]										
Contract for Antenna Production	6/2/03	10/1/07	[Gantt bar from 6/2/03 to 10/1/07]										
Receive Antennas #3-11	3/1/04	3/1/05	[Gantt bar from 3/1/04 to 3/1/05]										
Receive Antennas #12-20	3/1/05	3/1/06	[Gantt bar from 3/1/05 to 3/1/06]										
Receive Antennas #21-29	3/1/06	3/1/07	[Gantt bar from 3/1/06 to 3/1/07]										
Receive Antennas #30-36	3/1/07	10/1/07	[Gantt bar from 3/1/07 to 10/1/07]										
<b>Operations</b>	<b>6/1/01</b>	<b>10/1/07</b>	[Gantt bar spanning 6/1/01-10/1/07]										
Evaluate Ant#1,2 on Test Interf	6/1/01	12/31/02	[Gantt bar from 6/1/01 to 12/31/02]										
Train Site Antenna Ops/Maint Staff	6/1/01	10/1/07	[Gantt bar from 6/1/01 to 10/1/07]										
<b>SIS MIXER</b>	<b>1/3/00</b>	<b>10/1/07</b>	[Gantt bar spanning 1/3/00-10/1/07]										
Design and Development	1/3/00	6/1/00	[Gantt bar from 1/3/00 to 6/1/00]										
Design MMA Bands	1/3/00	6/1/00	[Gantt bar from 1/3/00 to 6/1/00]										
Deliver MMA 230 GHz	4/1/00	4/1/00	[Gantt bar at 4/1/00 with triangle marker]										
<b>Construction</b>	<b>10/2/00</b>	<b>6/1/07</b>	[Gantt bar spanning 10/2/00-6/1/07]										
Design mm SIS	10/2/00	12/31/03	[Gantt bar from 10/2/00 to 12/31/03]										
Design mm bal, Im-Sep, SIS	10/2/00	5/30/03	[Gantt bar from 10/2/00 to 5/30/03]										
Design submm trav Wave SIS	10/2/00	5/30/03	[Gantt bar from 10/2/00 to 5/30/03]										
Design submm bal, Im-Sep, trav Wave SI	1/2/02	6/1/04	[Gantt bar from 1/2/02 to 6/1/04]										
Produce mm bal, Im-Sep, SIS	6/1/01	6/1/06	[Gantt bar from 6/1/01 to 6/1/06]										
Produce submm bal, Im-Sep, trav Wave	6/2/03	6/1/07	[Gantt bar from 6/2/03 to 6/1/07]										
<b>Operations</b>	<b>1/2/02</b>	<b>10/1/07</b>	[Gantt bar spanning 1/2/02-10/1/07]										
SIS Evaluation on Test Interferometer	1/2/02	12/31/04	[Gantt bar from 1/2/02 to 12/31/04]										
SIS Evaluation on Interim MMA	1/2/04	10/1/07	[Gantt bar from 1/2/04 to 10/1/07]										
<b>HFET AMPLIFIER</b>	<b>6/1/98</b>	<b>10/1/07</b>	[Gantt bar spanning 6/1/98-10/1/07]										
Design and Development	6/1/98	6/1/01	[Gantt bar from 6/1/98 to 6/1/01]										
MMA Designs	6/1/98	6/1/01	[Gantt bar from 6/1/98 to 6/1/01]										
MMA 30 and 90 GHz Prototypes	6/1/98	6/1/99	[Gantt bar from 6/1/98 to 6/1/99]										
<b>Construction</b>	<b>10/2/00</b>	<b>12/31/02</b>	[Gantt bar spanning 10/2/00-12/31/02]										
Production: 33-50 GHz	10/2/00	5/31/02	[Gantt bar from 10/2/00 to 5/31/02]										
Production: 67-90 GHz	3/1/01	8/30/02	[Gantt bar from 3/1/01 to 8/30/02]										
Production: 85-120 GHz	6/1/01	12/31/02	[Gantt bar from 6/1/01 to 12/31/02]										



## MMA Project Overview 980127.1

Task Name	Start Date	End Date	1998	1999	2000	2001	2002	2003	2004	2005	2006	2007
<b>Operations</b>	<b>6/1/01</b>	<b>10/1/07</b>										
Evaluation on Test Interferometer	1/2/02	12/31/04										
Evaluation on Interim MMA	1/2/04	9/28/07										
Train Site HFET Maintenance Staff	6/1/01	10/1/07										
<b>LOCAL OSCILLATOR</b>	<b>6/1/98</b>	<b>10/1/07</b>										
Design and Development	6/1/98	6/1/01										
Design & Prototype 230 GHz Convention	6/1/98	6/1/01										
Design & Prototype 230 GHz Photonic	6/1/98	6/30/98										
<b>Construction</b>	<b>1/1/02</b>	<b>6/1/06</b>										
Decision: Conventional or Photonic	1/1/02	1/1/02										
Design MMA LO System	1/2/02	5/30/03										
Produce Millimeter Bands LO	1/2/03	12/30/05										
Produce Submillimeter Bands LO	6/2/03	6/1/06										
<b>Operations</b>	<b>6/1/01</b>	<b>10/1/07</b>										
Evaluate mm LO on Test Interferometer	6/1/01	6/2/03										
Evaluate submm LO on Interim MMA	1/2/04	10/1/07										
Train MMA LO Maintenance Staff	6/3/02	10/1/07										
<b>RECEIVER SYSTEMS</b>	<b>6/1/98</b>	<b>10/1/07</b>										
Design and Development	6/1/98	6/1/00										
Design Cryo Refrigerator and Dewar	6/1/98	12/31/99										
Design and Prototype Receiver Package	6/1/98	6/1/00										
<b>Construction</b>	<b>1/2/01</b>	<b>10/1/07</b>										
Contract Machining	1/2/01	6/1/07										
Contract Subsystem Assembly	1/2/01	10/1/07										
Insert Assembly and Test	1/2/01	10/1/07										
Mechanical Assembly and Test	1/2/01	10/1/07										
Delivery of Receiver Packages	1/2/02	10/1/07										
<b>Operations</b>	<b>6/1/01</b>	<b>10/1/07</b>										
Engineering Evaluation on Test Interferom	1/2/02	12/31/03										
Progressive Insert Installation on MMA Sit	1/2/03	10/1/07										
Training of Site Ops/Maint Receiver Staff	6/1/01	10/1/07										
<b>CORRELATOR</b>	<b>6/1/98</b>	<b>10/1/07</b>										
Design and Development	6/1/98	6/1/01										
Build and Deliver Test Correlator	6/1/98	12/31/99										
MMA Design	1/4/99	6/1/00										
Design/Assemble Proto Correlator (1/4)	6/1/00	6/1/01										
<b>Construction</b>	<b>6/1/01</b>	<b>12/29/06</b>										
Build and Deliver Proto Corr (1/4) to Test I	6/1/01	5/31/02										
Build and Deliver first 1/4 to MMA Site	1/2/02	12/31/03										
Build and Deliver second 1/4 to MMA Site	1/2/03	12/31/04										
Build and Deliver third 1/4 to MMA Site	1/2/04	12/30/05										
Build and Deliver fourth 1/4 to MMA Site	1/3/05	12/29/06										
<b>Operations</b>	<b>6/1/01</b>	<b>10/1/07</b>										
Operate/debug Test Corr at Test Interf	6/1/01	5/31/02										
Operate/debug Proto Corr at Test Interf	6/3/02	6/1/04										
Operate Test Corr at MMA Site	1/2/03	12/31/03										
Operate/debug MMA Corr at MMA Site	1/2/04	10/1/07										
Train Correlator Ops and Maint Staff	6/1/01	10/1/07										
<b>SIGNAL TRANSMISSION</b>	<b>6/1/98</b>	<b>10/1/07</b>										
Design and Development	6/1/98	6/1/01										
System Design and Prototype	6/1/98	6/1/01										
Assemble/debug Proto Sys at Test Interf	6/1/00	6/1/01										
<b>Construction</b>	<b>1/2/02</b>	<b>6/1/04</b>										
Contract Subsystem Assembly	1/2/02	12/31/03										
Assembly and Test	1/2/02	12/31/03										
Installation at MMA Site	6/3/02	6/1/04										



MMA Project Overview 980127.1

Task Name	Start Date	End Date	1998	1999	2000	2001	2002	2003	2004	2005	2006	2007
<b>Operations</b>	<b>1/2/02</b>	<b>10/1/07</b>										
Training of Operations and Maint Staff	1/2/02	10/1/07										
<b>COMPUTING</b>	<b>6/1/98</b>	<b>9/28/07</b>										
Design and Development	6/1/98	6/1/01										
Design and Programming Correlator Inter	6/1/98	6/1/01										
Real-time Array System Design	6/1/98	6/1/01										
Operator & Astronomer Interface Spec	1/2/01	6/1/01										
<b>Construction</b>	<b>1/2/01</b>	<b>9/28/07</b>										
Program Correlator Reat-time	1/2/01	9/28/07										
Program Array System	1/2/01	9/28/07										
Program Interfaces	1/2/01	9/28/07										
Evaluate Proto Systems on Existing Array	1/2/02	12/31/04										
<b>Operations</b>	<b>1/2/01</b>	<b>9/28/07</b>										
Train & Involve Site Ops Prog Staff	1/2/01	9/28/07										
Support Test Interferometer Operations	6/1/01	6/1/07										
Support Interim Operations at MMA Site	6/2/03	9/28/07										
<b>SYSTEM INTEGRATION AND TEST</b>	<b>6/1/98</b>	<b>9/28/07</b>										
Design and Development	6/1/98	6/1/01										
Define System Standards	6/1/98	6/1/01										
Prepare Test Interferometer Site	6/1/99	6/1/01										
<b>Construction</b>	<b>1/2/01</b>	<b>9/28/07</b>										
Establish MMA Site Operations Procedur	1/2/01	12/31/04										
Establish MMA Site Engineering Standard	1/2/01	12/31/04										
Establish Site Assembly/Integration Proce	1/2/01	9/28/07										
<b>Operations</b>	<b>6/1/01</b>	<b>9/28/07</b>										
Operations and Analysis of Test Interfero	6/1/01	6/1/07										
Interface to Science & Engineering Staff	6/1/01	6/1/07										
Operate Interim MMA	6/1/04	9/28/07										



# Radio-interferometric imaging of very large objects: implications for array design

T.J. Cornwell, M.A. Holdaway, and J.M. Uson

National Radio Astronomy Observatory,\* Socorro, New Mexico, 87801, USA

Received September 30, accepted January 4, 1993

**Abstract.** High-quality images of fields larger than the field-of-view of the elements of an array of radio telescopes can be obtained from a mosaic of overlapping pointings. The addition of “single-dish” observations made with a telescope of the same size as the array elements suffices to produce images in which all Fourier components from the zero spatial frequency up to the maximum allowed by the array are properly represented. Image quality is then limited by systematic errors. Images with dynamic range exceeding 1000:1 and a fidelity index of about 20 require antennas with rms surface accuracy of  $\sim\lambda/40$  and pointing accuracy of  $\sim 6\%$  of the half-power beamwidth.

**Key words:** image processing – interferometry – observational methods

## 1. Introduction

Astronomically interesting objects are often larger than the field of view of the telescopes that are used to study them. A previous paper (Cornwell 1988, hereafter paper I) outlined the principles of radio-interferometric imaging of such objects and described observational and data reduction techniques for constructing “mosaic” images of large fields of view. In order to mosaic, data are collected by pointing an interferometric array to a number of positions spanning the region of interest and an image is generated by combining the data. Appropriate algorithms and a sampling theorem were derived in paper I. Mosaic observations can be and are being made using existing interferometric arrays (see for example Mundy et al. 1988). However, existing arrays are not optimally designed for measuring large structures and so the full promise of mosaicing techniques is likely to be fulfilled only by new arrays designed for mosaicing. The design of such mosaicing arrays is the subject of this paper.

*Send offprint requests to:* T.J. Cornwell

\* Associated Universities Inc. operates the National Radio Astronomy Observatory under National Science Foundation Cooperative Agreement No. AST-8814515

It is often the case that structures of interest correspond to baselines that are much smaller than the diameter of the telescopes — this is the so-called “short-spacing” problem. It is desirable to measure the corresponding visibilities with an interferometer because of its well-known rejection of systematic errors. However, this would seem to require an additional interferometric array consisting of a large number of small elements. A more practical approach is to synthesize the necessary small elements and spacings by combining the spacings measured by the interferometer with those measured by a single-dish. Such “element synthesis” can be achieved with a “homogeneous array” in which the single-dish(es) and the array elements are of the same size and can indeed be the same telescopes.

Since the field of view of an antenna is proportional to the observing wavelength, these techniques will be most important in the millimeter and sub-millimeter wavelength bands. Indeed, they should determine the design of imaging arrays operating in these bands. In this paper, we concentrate upon the issues involved in designing an array suitable for use in mosaicing. We show that:

1. Mosaicing requires some tightening of the performance specifications of array elements, particularly antenna rms surface accuracy and pointing accuracy, and
2. High-quality imaging can be performed by an array of equal-size elements which is capable of providing all the required measurements. A larger size single-dish is thus not necessary.

We support these conclusions by theoretical arguments, by computer simulations of one such array, and by an experimental demonstration using a currently-existing centimeter-wavelength array, the Very Large Array.

Before describing the **homogeneous array** concept, we first review the theory of mosaicing (Sect. 2), extend the discussion of mosaicing algorithms presented in Paper I (Sect. 3), and discuss how to evaluate imaging performance (Sect. 4). We then go on to investigate the issues involved in array design for mosaicing (Sect. 5), and to describe our numerical simulations (Sect. 6) and observational demonstration (Sect. 7). We conclude with some recommendations for the design of imaging arrays (Sect. 8) and some final comments (Sect. 9).

The homogeneous array concept has been adopted by the National Radio Astronomy Observatory for its proposed Millimeter Array (MMA). We illustrate some of our arguments with the specific example of an imaging array consisting of 39 elements of diameter 7.5m, operating at a wavelength of  $\lambda = 1.3$  mm. Although this configuration is close to that of the proposed MMA, our conclusions are fairly general. We shall note in the sections below those that are specific to the MMA.

## 2. Mosaicing theory

The fundamental observable for an imaging radio telescope can be written as the Fourier transform of the sky brightness  $I(\mathbf{x})$  weighted by a primary beam pattern  $A_p(\mathbf{x})$ :

$$V_p(\mathbf{u}) = \int A_p(\mathbf{x}) I(\mathbf{x}) e^{j2\pi\mathbf{u}\cdot\mathbf{x}} d\mathbf{x} \quad (1)$$

We will use the notation of Paper I: let  $\mathbf{u}$  be the vector separation of the telescopes measured in wavelengths, as seen from some direction which gives the phase reference. We describe the "primary beam" or sensitivity to emission of an element by the power pattern  $A_p(\mathbf{x})$ , which tapers off to zero for large offsets from the pointing center  $\mathbf{x}_p$ . This can be extended to the case of different elements by using instead the corresponding voltage patterns. The unknown object brightness at position  $\mathbf{x}$  is  $I(\mathbf{x})$ .

For a single-dish radio telescope  $\mathbf{u}$  is zero and the Fourier transform is just the measured total power:

$$V_p(0) = \int A_p(\mathbf{x}) I(\mathbf{x}) d\mathbf{x} \quad (2)$$

From here on, we will call  $V_p(\mathbf{u})$  the visibility function, even though it includes the total power measurement,  $V_p(0)$ , which is not normally considered a visibility sample. For notational simplicity we have denoted the pointing by a discrete variable  $p$ , but it could easily be written as a continuous variable, such as would be relevant for a continuously scanned telescope.

If the visibility function  $V_p(\mathbf{u})$  is known for all points  $\mathbf{u}$  in the Fourier plane, then Eq. 1 can be inverted to yield the true sky brightness:

$$I(\mathbf{x}) = \frac{\int V_p(\mathbf{u}) e^{-j2\pi\mathbf{u}\cdot\mathbf{x}} d\mathbf{u}}{A_p(\mathbf{x})} \quad (3)$$

For objects that exceed the field of view of the elements of the array, some combination of different pointings must be made. A least squares algorithm can be invoked to form an optimum estimate of the sky brightness distribution from data obtained using several pointing centers. We call this the "linear mosaic" image:

$$I^{LM}(\mathbf{x}) = \frac{\sum_p A_p(\mathbf{x}) \int V_p(\mathbf{u}) e^{-j2\pi\mathbf{u}\cdot\mathbf{x}} d\mathbf{u}}{\sum_p A_p^2(\mathbf{x})} \quad (4)$$

Generalization to different weights is straightforward.

This linear mosaic image has two principal uses. First, it provides a computationally inexpensive estimate of the true sky

brightness that is sufficiently accurate for moderate signal-to-noise ratio ( $\text{SNR} \leq 100$ , depending on the accuracy to which the primary beam is known as well as on the uv coverage of the observations), and, second, it is very useful for performing an approximate error analysis of the general case. We elaborate on these two points below.

Mosaicing observations require good sampling in both the image and Fourier planes. Fourier-plane sampling for any one pointing must allow good quality imaging of that pointing by itself. The image-plane sampling requirements are determined by the size of the primary beam pattern  $A_p(\mathbf{x})$ . This is obtained by squaring the Fourier transform of the illumination pattern of the array elements and it is therefore band-limited with support in the Fourier plane given by  $\pm D/\lambda$  where  $D$  is the element diameter and  $\lambda$  is the observing wavelength. An image plane sampling theorem shows that the pointings must be spaced every  $\lambda/(2D)$  in the image plane (paper I). This limit is often violated in single-dish observing because of the mistaken idea that if the actual sampling interval is  $\Delta x$  then only spatial frequencies higher than  $2/\Delta x$  are corrupted. This is not so: aliasing produces intermodulations of spatial frequencies down to  $2/\Delta x - D/\lambda$  resulting in a loss of information on the corresponding scale sizes. Hence for an image which is undersampled by the common factor of two, all spatial frequencies are corrupted. Although this is mitigated by the high degree of tapering of the illumination pattern often used in single-dishes (10-13 dB in power at the edge of the aperture), some information is inevitably lost.

For non-coplanar arrays such as the VLA, it is sometimes necessary to replace the 2-D Fourier inversion by a constrained 3-D inversion. This is especially important for long wavelengths, where it is often required even for single-pointing images, as well as for very large fields of view in which case 2-D algorithms might suffice for the individual pointings while the actual mosaic will require 3-D processing (Cornwell & Perley 1992).

## 3. Mosaicing algorithms

In practice, it is not possible to invert the Fourier relationship because only limited sampling of the Fourier plane  $\mathbf{u}$  is available. Let the sampling for a given pointing center be described by a function  $s_p(\mathbf{u})$ , which is usually representable by a collection of Dirac  $\delta$ -distributions, and let its Fourier transform with respect to  $\mathbf{u}$  be  $S_p(\mathbf{x})$ . Then it is simple to show that Fourier inversion of the sampled visibility function yields the so-called "dirty image":

$$I_p^D(\mathbf{x}) = S_p(\mathbf{x}) * [A_p(\mathbf{x})I(\mathbf{x})] \quad (5)$$

Inserting this relationship into the least squares estimate of the sky brightness, we find that we obtain a "dirty" linear mosaic image given by:

$$I^{LM}(\mathbf{x}) = \frac{\sum_p A_p(\mathbf{x}) (S_p(\mathbf{x}) * [A_p(\mathbf{x})I(\mathbf{x})]) w_p}{\sum_p A_p^2(\mathbf{x}) w_p} \quad (6)$$

where the weight is usually taken to be:

$$w_p = \frac{1}{\sigma_{I_p}^2} \quad (7)$$

This represents an imaging system in which the point spread function (PSF) is manifestly position dependent: as a point source moves around the whole field of view, different dirty PSFs  $S_p(\mathbf{x})$  are emphasized. To give us some understanding of this relation, let us make the approximation that all dirty PSFs are identical. The response to a point source at the origin of the coordinate system is then:

$$S^{LM}(\mathbf{x}) = S(\mathbf{x}) \left[ \frac{\sum_p A_p(\mathbf{x}) A_p(0) w_p}{\sum_p A_p^2(\mathbf{x}) w_p} \right] \quad (8)$$

In the second term in this equation, the denominator is approximately constant while the numerator can be thought of as a convolution of the primary beam with itself. In the Fourier plane, this convolution is equivalent to a squaring of the sensitivity patterns. Hence this dirty least squares PSF is roughly equivalent to convolving the Fourier plane sampling pattern with the *square* of the transform of the primary beam  $A(\mathbf{x})$ .

With this approximation, the “dirty” linear mosaic image can be written as:

$$I^{LM}(\mathbf{x}) \approx S^{LM}(\mathbf{x}) * I(\mathbf{x}) \quad (9)$$

It is worth noting that:

- This combination optimizes SNR in the Fourier plane since it weights the various spatial frequencies by the inverse variance of the errors.
- Conceptually, the Fourier plane coverage for a mosaicing experiment is obtained by convolving a typical Fourier plane coverage for an individual pointing with the square of the sensitivity pattern corresponding to the element primary beam. One goal of the design of mosaicing arrays might be then to ensure that this effective Fourier plane coverage is as complete as possible.
- An approximate correction of the Fourier plane sampling may be made by deconvolving  $S^{LM}(\mathbf{x})$  from the dirty least squares image.
- If the Fourier transform of  $S^{LM}(\mathbf{x})$  has no zeroes (out to some maximum spatial frequency) then imaging can be performed using simple inverse filtering or Wiener filtering. If zeroes are present then non-linear deconvolution using some form of the CLEAN (Högbom 1974) or MEM (e.g. Narayan & Nityananda 1986) algorithms may be worthwhile.

There are some limitations to this “linear mosaicing”. First, Eq. 6 is actually not a simple convolution and so deconvolution is not strictly feasible. The approximation is fairly good as long as the array size is much bigger than the element size. Second, the PSFs for each field may actually differ and so the deconvolution will be in error. Third, for a field which is incompletely sampled in the image plane (such as is obtained when the emission continues outside the sampled region), some correction of

edge effects must be made. We have found that simply removing the normalization by  $\sum_p A_p^2(\mathbf{x})$  weights down the outer edges satisfactorily (see Sect. 6).

A fully correct approach to mosaicing which overcomes these problems was described in Paper I. We perform a joint deconvolution of all the relevant data using, for example, a Maximum Entropy (MEM) method (e.g. Narayan & Nityananda 1986). We call this “non-linear mosaicing” since it incorporates a non-linear deconvolution at the heart of the mosaicing process.

To describe non-linear mosaicing, it is convenient to consider the measured Fourier plane data. For each pointing we obtain visibility samples  $V_p(\mathbf{u}_i)$  at the  $N_p$  sample points  $\mathbf{u}_i$ . We wish to estimate the sky brightness from the complete set of samples. We choose that image,  $I^{MEM}$ , which fits all the data within some tolerance and has maximum entropy:

$$\mathcal{H}(I) = - \int I(\mathbf{x}) \ln \left( \frac{I(\mathbf{x})}{eM(\mathbf{x})} \right) dx \quad (10)$$

where  $e$  is the base of natural logarithms and  $M(\mathbf{x})$  is a default image to which  $I^{MEM}$  is forced to in the absence of data (usually chosen to be flat). The entropy is maximized subject to the constraint that the fit, as measured by  $\chi^2$  be adequate:

$$\chi^2 = \sum_p \sum_i^{N_p} |V_p(\mathbf{u}_i) - \hat{V}_p(\mathbf{u}_i)|^2 w_{p,i} \quad (11)$$

where  $\hat{V}_p(\mathbf{u}_i)$  denotes the value of the visibility at a sample point as predicted from the MEM image.

There is no closed form solution but  $I^{MEM}$  may be found numerically using one of a number of algorithms (see Paper I) based upon variants of gradient search. The MEM image can usually be found in about 50-100 2D FFTs per pointing (the actual number depends on the complexity of the image and the data obtained).

The MEM image thus obtained has a number of defects, including variable resolution across the field and a bias term at low signal-to-noise levels. We minimize these defects by working mainly with the “restored” MEM image  $\tilde{I}^{MEM}$  which is obtained from the original MEM image by first smoothing with a two dimensional Gaussian of size comparable to array resolution, and second adding back the residuals of the fitting process. This is analogous to the restoration process used in CLEAN (Schwarz 1978).

The advantages of the non-linear approach are that, first, each pointing may have substantially different Fourier plane coverage, second, noise is accounted for properly (in the definition of  $\chi^2$ ), and, third, that since we are not attempting to solve a pure deconvolution relation, edge effects are treated correctly. The disadvantages lie mainly in the large computing resources required. Separate deconvolution of the individual pointings followed by least squares combination is possible but produces inferior results and saves only a factor of about 3 in computing time (see Paper I).

To summarize, we have described two methods for generating images from mosaic data: one linear, least squares based

approach and one non-linear, Maximum Entropy joint deconvolution. The former is expected to be most useful for imaging with low signal-to-noise ratio ( $\text{SNR} \leq 100$ ) and is also useful for analyzing the errors of mosaicing, while the latter is a fully correct approach which should result in the highest quality images.

#### 4. Imaging performance

In assessing the imaging performance of an array, it is important to consider the scientific questions that may be pursued using an image. Interferometric arrays are indirect imaging instruments, and do not provide an accurate image of the sky brightness directly. An image is available only after lengthy and complicated data processing often involving poorly understood, non-linear algorithms. For this reason, if a scientific question can be answered without making an image, it is best to do so. For example, the most accurate strength, size and shape determinations of simple isolated objects are derived by fitting analytical models to the observed visibility samples rather than to an image. Most often, however, visibility-based analysis is not possible, either because the objects of interest are not isolated and so the visibility information is confused, or because the scientific question is not sufficiently narrow. In these circumstances an image must be made, using whatever algorithms are available, and the scientific question must be answered using the image.

How we quantify the quality of an image depends upon the scientific question being addressed. For example, in high-resolution observations of extragalactic radio jets, a typical goal is to place limits on the strength of any low level emission close to the nucleus. Here the noise level away from the brightest regions is important, and indeed, the VLBI literature often quote this in the form of a dynamic range as a measure of image quality. However, this measure neglects imaging performance on the bright regions of the source which may be more important if, for example, one is studying filamentary structure in the lobes of radio sources. Then the on-source accuracy of reconstruction is the relevant parameter. While these two measures of image quality are often correlated, there is no reason to expect any simple, universal relationship. Inadequate calibration will limit the accuracy of an image but will be most noticeable off-source with little impact upon the on-source accuracy (in the absence of a global calibration error), while poor Fourier plane coverage will lead to serious errors in the reconstruction of the brightness distribution with only a secondary effect off-source. A drawback of both measures is that they are specific to a particular scale size: the natural resolution of the image, and are therefore relatively insensitive to errors on larger scale sizes. One could calculate both for a variety of smoothed images, but a simpler approach is to look at the accuracy of the reconstruction of various spatial frequencies.

Other measures of image quality arise in different scientific applications (see for example Cohen 1991 for a summary relevant to the Hubble Space Telescope).

In thinking about imaging performance and in evaluating the results of our analytical and numerical work, we have found three particular measures of image quality to be useful:

- The “**fidelity**” defined as the ratio of the value of a pixel to the error between the true sky distribution  $T(\mathbf{x})$  and the reconstructed image  $I(\mathbf{x})$ . The fidelity is therefore an image that expresses an estimate of the signal-to-noise ratio (SNR) for each pixel.
- The “**dynamic range**” is defined as the ratio of the peak brightness in an image to the off-source error level. The dynamic range is a single number representing the degree of contrast visible in an image.
- The **visibility SNR curve**. The **VSNR** curve is constructed by differencing the reconstructed image and the convolved model, Fourier transforming, averaging in radial bins, and dividing it into the radially-binned Fourier transform of the model. This is a measure of the fidelity averaged over areas of the Fourier plane.

For actual observations, only the dynamic range can be calculated. Both the fidelity and **VSNR** curves can only be evaluated if the true brightness distribution is known either, for example, from measurements made by some other instrument or given a priori as in analytical or numerical calculations.

All three measures can be calculated analytically but the fidelity is most easily derived. We apply below straightforward error propagation to the linear mosaic image. We will use simple models of the errors, assuming either complete correlation or complete independence of errors between pointings, and we will largely ignore the fact that an array is composed of many elements, each of which will have its own errors. This first attempt at error analysis will help us develop an intuitive picture of the importance of various types of errors. A more complete picture will emerge from the numerical simulations discussed below.

Propagation of errors through Eq. 4 is quite straightforward. For simplicity, we quote the results when the weights for all pointings are the same. We have the following results:

**Additive errors** originating in system noise produce a background of noise in the images. If the noise in all pointings is  $\sigma_{ID}$ , then the noise in the least squares image is:

$$\sigma_{ILM} = \frac{\sigma_{ID}}{\sqrt{\sum_p A_p^2(\mathbf{x})}} \quad (12)$$

The term  $\sqrt{\sum_p A_p^2(\mathbf{x})}$  represents an improvement in sensitivity due to the overlapping of primary beams. For a typical beam, this lies in the range 2-3 and so for cases where each pointing has the same level of noise, the linear mosaic image has a noise level which is about 2-3 times lower than that in the images made from the individual pointings. Note that noise can vary substantially across the field. In particular, it inevitably rises at the edge of the sampled region.

**Primary beam errors** (or more strictly errors in the assumed model of the primary beam  $A_p(\mathbf{x})$ ) limit our ability to esti-

mate the sky brightness. For uncorrelated errors of variance  $\sigma_{A_p}^2$ , the image fidelity is:

$$\Lambda^{PBE} \cong \frac{\sum_p A_p^2(\mathbf{x})}{\sqrt{\sum_p \sigma_{A_p}^2 A_p^2(\mathbf{x})}} \quad (13)$$

In the limit in which the errors are totally correlated between pointings the fidelity is limited to:

$$\Lambda^{PBE} \cong \frac{1}{\sigma_A} \quad (14)$$

Pointing errors are expected to be important in limiting the quality of mosaiced images. In single pointing images of objects smaller than the primary beam, errors in the visibility are of second order in the pointing errors of the elements of the array. For mosaiced images where the emission fills the antenna primary beam, the dependence is of first order. The effect of pointing errors can be analysed using Eq. 14. If the FWHM of the primary beam is  $\theta_A$ , then we find that, using a Gaussian approximation to the primary beam, the image plane fidelity is limited to:

$$\Lambda^{PE} = \left[ \frac{\sqrt{\sum_p A_p^2(\mathbf{x})}}{2\sqrt{2 \ln(2)}} \right] \frac{\theta_A}{\sigma_x} \quad (15)$$

where the pointing errors are uncorrelated and have variance  $\sigma_x^2$  per pointing. Typically, the numerical factor on the right hand side of this equation is close to unity and so the fidelity limitation due to pointing errors is approximately  $\theta_A/\sigma_x$ .

Surface errors can be thought of as leading to an error in the assumed primary beam model and can therefore also be analysed using Eq. 14. The power in the error beam due to surface errors having a variance  $\sigma_S$  is  $1 - e^{-\sigma_S^2/2}$ . If the surface errors are small then  $\sigma_A \approx \sigma_S^2/2$ , and the fidelity is limited to:

$$\Lambda^{SE} = \frac{1}{2\sigma_S^2} \quad (16)$$

This analysis assumes that all array elements have the same errors. Overcoming this limitation is difficult but one might expect that, in the most favorable cases of uncorrelated errors, the fidelity would improve by  $\sim \sqrt{N_A}$  (where  $N_A$  is the number of array elements) so that, for example, the fidelity would be limited to about  $\sqrt{N_A}/\sigma_A$  due to primary beam errors and would be limited to about  $\sqrt{N_A}\theta_A/\sigma_x$  due to pointing errors. Partial correlation of such errors would lessen this improvement.

Another limitation of our analysis is that we have neglected the effects of the limited Fourier-plane coverage for each pointing. Our results predict the fidelity and say nothing about the dynamic range. Intuitively, one would expect that on-source errors are scattered into the surrounding emission, and generate errors at a level which is lower by the ratio of the typical sidelobe level in the synthesized beam to its peak response. If so, then deconvolution should, in principle, restore these errors back to their origins, and so the dynamic range must be related to the difference in sidelobes between adjacent pointings. In addition, calibration errors of various origins will also limit the dynamic range.

These limitations of our analysis are best addressed using simulated observations incorporating some of the sources of errors which we have discussed (Sect. 6). Since the simulations require an initial design for a mosaicing array, we must first examine the implications of mosaicing for array design (next section).

## 5. Array design for mosaicing

Interferometric array design has been well covered by many authors (see for example Thompson et al. 1986; Hjellming 1989). So we will address only those issues raised by mosaicing. The principal questions are:

- How should the visibilities on spacings comparable to and less than the diameter of an array element be obtained?
- How would the array configuration be affected? One useful criterion for array design is the completeness of the instantaneous Fourier plane coverage implicit in the PSF of the dirty linear mosaic  $S^{LM}(\mathbf{x})$ .
- What antenna specifications would be needed to mosaic? For example, how accurate must the element pointing be? Our results of the previous section can be used to provide general guidelines but we expect that more accurate answers must come from numerical simulations and actual observational tests.
- What special measurement strategies would be required? In particular should the total power and the visibility measurements be made simultaneously?
- How would the calibration of the array be affected by mosaicing?

We address these points in turn.

### 5.1. Array concepts

Let us begin by assuming a conventional interferometric array. Mosaicing of the interferometric observations provides information on spacings longwards of some minimum spacing which can be written as  $B_{min} - \alpha_I D$  where  $B_{min}$  is the shortest (projected) spacing between antenna pointing centers and  $\alpha_I < 1$ . Similarly, single-dish observations using an antenna of diameter  $D_S$  provide information on spacings shortwards of some maximum spacing which we will write as  $\alpha_S D_S$  where  $0 < \alpha_S < 1$ . In the absence of systematic errors,  $\alpha_I$  and  $\alpha_S$  can be arbitrarily close to unity and, provided  $B_{min}$  is less than  $2D$ , all spacings can be recovered by mosaicing using the standard interferometric measurements taken with an array together with total power measurements made with the same array elements. We will call this idea of imaging with only one size element the “homogeneous array” concept. In principle, it would seem possible to make the total-power and interferometric observations synchronously. However, beam-switching will always be required in total-power mode in order to remove the effects of the atmospheric emission. Simultaneous observations would require a synchronization of the switching devices on all of the antennas. In addition, the interferometric observations would have to be gated accordingly (the off-positions would be useful as well if

contained within the source of interest). While this might indeed be a practical scheme, it is likely that the total-power measurements might be dominated by systematic effects such as ground spillover pickup which would be minimized by tapering the illumination pattern of the antennas for total power observations. Notice that this is possible while still measuring all spacings (provided that  $B_{min}$  is sufficiently small).

A common objection to the **homogeneous array** concept is that, in practice, both  $\alpha_I$  and  $\alpha_S$  are much less than unity and so a method of bridging the gap in spacings is required. We will call the idea of using another telescope, either a big single-dish or another array of different size elements, the “**heterogeneous array**” concept. There are a number of possible **heterogeneous array** schemes:

**Larger single-dish:** a large single-dish could be used to provide spacings close to the array element diameter. With  $D_S \sim (2 - 3)D$ , one can afford to have  $\alpha_S \sim 0.3 - 0.5$ . Total power observations from the single-dish can easily be included in the mosaic to form an image with all the necessary spatial frequencies. Since a single feed single-dish of the same collecting area as an array would be much slower in imaging than the interferometric array, a focal plane feed array must be used to speed up the observations. A different feed array would be needed for each observing band. Even with the conservative assumption that pointing errors are independent of telescope size these would affect measurements made with the larger single-dish worse than those made with the **homogeneous array**. Indeed, the need to deal with pointing errors drives the optimum element size smaller rather than larger.

**Element sub-illumination:** Woody et al. (1991) have described a scheme for obtaining short spacings by illuminating two patches on one array element to form an interferometer of spacing  $\sim D/2$ . While this bridges the gap, it does so at the cost of sensitivity and a small mosaic is then more efficient. Furthermore the Woody *et al.* scheme does nothing to measure even shorter spacings and so total power observations must still be performed. To obtain sensitivity approaching that of the **homogeneous array**, it is necessary to install such systems on all array elements, and even then not all the collecting area can be used in the observations.

**Smaller array:** an array of a moderate number (e.g. 10-20) of smaller (e.g.  $D_t = D/3$ ) telescopes could be combined into a separate interferometric array. While this solves the problem of obtaining spacings of  $\sim D$ , the same problem still holds for spacings of  $D_t$ . One obvious method is to then use the large array elements in total power mode to measure spacings down to much less than  $D_t$ . Finally, one could use the smaller array elements to get spacings from much less than  $D_t$  down to zero. This scheme involves therefore the use of two **homogeneous arrays**. As we show below, one such array is sufficient.

**Hierarchy of smaller arrays:** The need for any total power measurement can be obviated if we follow the same approach of downscaling iteratively to obtain a hierarchy of arrays, each scaled by a factor  $\sim \sqrt{N_A}$  in size ( $N_A$  is the

number of elements of each array). The smallest dish diameter is related to the largest field of view desired: for example, if we set this to half a degree at a wavelength  $\lambda = 1.3$  mm, then we find that the smallest array must be composed of horns with a diameter of about 0.06 m. To reach a reasonable sensitivity with a moderate number of array elements (say 25), the largest array element must be about (6 – 10) m in diameter, so we would need 4 different arrays with elements of diameters about 0.06, 0.3, 1.5, 7.5 m.

**Array of very small elements:** for completeness, we mention another possible scheme in which an array is formed entirely of feeds of diameter 0.06 m. To get the same collecting area as an array of  $N_A$ , each of diameter 7.5 m, the array of very small elements would require about  $4 \times 10^5 N_A$  individual telescopes.

## 5.2. Assessment of array concepts

Of these **heterogeneous array** schemes, simplicity makes the first option the most attractive one. In judging the relative merits of the **homogeneous array** and a conventional array supplemented by a large single-dish telescope we have to consider three principal areas of concern: random errors, systematic errors and design constraints (including cost-effectiveness).

Let us consider first the effect of random errors on the **homogeneous array**. This translates into a question of the relative amount of time required to make the total power and interferometric measurements. There are two different ways of estimating the required observing time, one based upon matching sensitivity and one based upon matching signal-to-noise ratio. Before delving into these, we must consider for what type of astronomical objects mosaicing will most useful. This affects the required observing time since in a typical mosaicing observation, the signal in the shorter spacings will most often be substantially greater than that in the larger ones. To demonstrate this, let us consider five illustrative, but not exhaustive, classes of objects:

1. A uniform brightness distribution: the interferometric signal will be zero.
2. A point object: the signal will be the same for total power and interferometric observations.
3. An object which contains little fine-scale structure: the signal on the interferometric spacings is very low compared to the total power.
4. A random brightness distribution of  $P$  resolution “blobs” in every single pointing: If  $F$  is the total power then the rms visibility will be about  $F/\sqrt{P}$ , with peaks of several times higher. Suppose that each blob is the size of a resolution element, and that the emission fills the primary beam, then for a packed array of  $N_A$  elements,  $P$  is approximately  $N_A^2$  and so the signal-to-noise of the total power measurements will be about  $N_A$  times higher than that of the interferometric observations. Increasing the size of the blobs would decrease this ratio correspondingly.
5. A brightness distribution with no preferred scale size. The visibility function must go as  $\sim 1/\sqrt{u \cdot u}$  and is much

stronger for total power measurements than for interferometric measurements.

Mosaicing is not important for cases 1 and 2 since either total power measurements (case 1) or interferometric measurements (case 2) of a single pointing will suffice. Only cases 3, 4 and 5 provide good candidates for mosaicing. It is clear that in all three, the signal accessible to interferometric measurements must always be much less than that for total power measurements. Hence, equalizing the noise level across the Fourier plane will produce very high signal to noise on the very shortest spacings. The opposite tactic of equalizing typical signal to noise ratio must therefore require substantially less total power observing time. In practice, the SNR on the total power measurements is likely to be ultimately limited not by receiver noise but by calibration errors and systematic effects.

While the previous argument is basically correct, we need to deal with two subtleties. First, the center of the Fourier plane is not sampled with enough sensitivity. Taking into account the difficulties inherent in packing antennas closely, the best value for the packing density is about 0.4–0.5. Hence to equalize the noise level using all array elements to measure total power requires less time than for the interferometric observations by the square of this factor. Second, sensitive total-power measurements require beam-switching in order to subtract the contributions of the atmosphere, ground spillover and receiver noise. Large objects have to be scanned with the added complication that the “reference” beam might also observe the object under study. This results in a further factor of  $\sim 8$  in the observing time for the total-power measurements (Emerson et al., 1979). Putting these two factors together we find that to match noise levels typically about 1.6 more time must be spent observing in total-power than in interferometric mode. To match SNR, the time spent in total-power mode could be a few orders of magnitude less than that spent in interferometric observations.

This conclusion is in accord both with experience from existing millimeter wavelength interferometric arrays and with experience from centimeter wavelength multi-configuration observations of extended objects using the NRAO–VLA (Napier et al. 1983) where much less observing time is needed in the more compact configurations.

This discussion assumed that all antennas would be outfitted for total-power measurements. This might turn out not to be practical as the most sensitive total-power measurements will be limited by errors in the cancellation of atmospheric and ground pickup and other systematic errors and it could well be that only a few of the antennas could be optimized for total-power measurements at a reasonable cost. The ratio of time spent on interferometric and total-power measurements would have to be adjusted accordingly.

We now have to consider the effects of random errors on the large single-dish in the heterogeneous array. From the above argument about matching SNR, we have seen that for the homogeneous array there should be no problem obtaining sufficient observing time for the total power measurements. A large single-dish is slower than  $N_A$  smaller single-dishes for the total power measurements unless a focal plane array with

approximately  $N_A$  feeds is used on the large single-dish. Therefore, depending upon the exact shape of the visibility function, a large single-dish with a single feed might have to be dedicated solely to making short-spacing observations to complement the interferometric observations.

Random errors can be diminished in value by integration. However, systematic errors which do not integrate down will probably dominate in many observations and so it is important to consider what can be done to minimize their adverse effects. As the element size decreases, a given spatial frequency is measured with less sensitivity and so, in making an image, the measured value must be corrected by a larger numerical factor, thus boosting the deleterious effects of any systematic errors. In the case of a single-dish making total power observations, this is further exacerbated by the desire to limit spillover by tapering the illumination pattern. This is, in principle, a strong argument for a large single-dish if we recognize that total power observations are more prone to systematic errors than interferometer observations. In assessing the power of this line of argument we are considerably hindered by the lack of any hard evidence concerning the values of  $\alpha_S$  and  $\alpha_I$ , which we might call the degrees of trustworthiness of single-dish and interferometer observations. The conventional wisdom is that typically  $\alpha_S \sim 0.3 - 0.4$ . This, combined with the pessimistic assumption that  $\alpha_I \sim 0.0$ , leads to the conclusion that  $D_S \sim 2.5 - 3D$ . However, one of the few observational tests of  $\alpha_I$  produced the result that even for a poor model of the primary beam (known to about 10%)  $\alpha_I \sim 0.5$  (Paper I). Hence, if  $B_{min}$  is reduced by projection effects, then we require that  $\alpha_S D_S \sim 0.5D$  and thus if we can improve  $\alpha_S$  to about 0.5, then we can take  $D_S$  to be  $D$  and a special-purpose single-dish is not required. We should emphasize that the values of  $\alpha_I$  and  $\alpha_S$  are not well known. In view of the multitude of possible influences, we think that in the absence of firm experimental values, numerical simulation is the best way to evaluate them with more accuracy.

As for the value of  $B_{min}$ , the principal constraints come from antenna design considerations. For safety, each element should rotate inside a cylinder of diameter considerably less than  $B_{min}$  at the zenith. Typically, the diameter of this notional cylinder is about  $1.3 - 1.5D$ . Hence to reduce  $B_{min}$  further either a novel antenna design must be used or observations restricted in zenith angles (to reduce  $B_{min}$  to  $D$  would typically require zenith angles of less than about 40 degrees).

In summary, it is clear that both the homogeneous array and the heterogeneous arrays will allow good quality imaging. However, the necessary element specifications such as pointing and surface accuracy are easier to achieve with the smaller elements used by the homogeneous array. A more complete assessment of the performance of the homogeneous array depends upon simulation of typical sources of error.

### 5.3. Array configuration

For a single primary beam, the imaging speed of an array is proportional to the total collecting area  $N_A D^2$ . If mosaicing is important then the extra time required to form a mosaic must

be included and the imaging speed goes as  $N_A D$ . Thus mosaicing favors small array elements since a big penalty in speed is incurred for imaging with small fields of view. For a given imaging speed, however, the number of elements will eventually become prohibitive as  $D$  decreases since receiver, correlator and computing costs go as either the first or second power of  $N_A$ . The desire to limit the effects of pointing and surface errors also leads in the same direction of decreasing the element diameter.

Since mosaicing is designed for imaging objects larger than the element primary beam, good Fourier plane sampling must be obtained on all baselines bigger than an element diameter, ranging up to the maximum spacing for which mosaicing is expected to be important. Hence a very compact configuration is required. If we take as our design goal the quality of the linear mosaicing PSF,  $S^{LM}$ , then we might reasonably require that it has no zeroes in the Fourier transform for all spacings up to some limit. This can be achieved using any of a number of designs for the most compact configuration; virtually any array which is limited in packing by the antenna size will satisfy this criterion. We note that shadowing can potentially disrupt observations with a very compact array causing the loss of the shortest spacings. Although this is certainly an important issue at centimeter wavelengths, at millimeter wavelengths the desire to avoid high zenith angles (and concomitantly high opacities) minimizes shadowing. This leads on to a related point, that for mosaicing of many pointings (say  $10^2 - 10^4$ ), fast imaging is vital and so reliance upon Earth rotation synthesis to improve the Fourier plane coverage is unrealistic. Instead, a mosaicing array must possess complete instantaneous coverage. This, combined with the argument presented in the previous paragraph, drives the array to a large number of elements.

#### 5.4. Array element specifications

The array elements must point and track and have good surface accuracy. Good absolute pointing is not as important as the ability to track accurately over a relatively small range of hour angles. It is reasonable to expect that the pointing behaviour of each array element will be calibrated interferometrically during the most taxing observations. Global and slowly varying pointing errors could also be removed by some form of self-calibration (see e.g. Emerson, 1991). If we take as a specification that the fidelity be about 100, then the results of our analysis of linear mosaic imaging can be used to show that, for a 40-element array, the array elements must point to about a sixteenth of the full-width-half-maximum size of the primary beam (about 1.3 arcsec for an 8m diameter dish at 230GHz), the primary beam must be known to about 6% (rms), and the (rms) surface accuracy must be about  $\lambda/40$ . We note that the pointing and surface accuracy specifications are considerably tighter than those typically made for interferometer elements.

These arguments are further supported by the numerical simulations discussed in Sect. 6.

#### 5.5. Measurement and calibration strategies

High image quality can be aided by a number of measurement and calibration strategies. First, enforcing consistency in calibration will be vital. This can be achieved with relative ease by using the same antennas to do both the total power and the interferometric measurements (an overall calibration uncertainty is unlikely to be a serious problem). The cross-calibration between the single-dish and the interferometric measurements becomes a harder problem if different instruments are used as in the case of the heterogeneous array or, to some extent, if the total-power measurements made with the homogeneous array are done with somewhat underilluminated antennas (to avoid ground spillover). In the latter case, cross-calibration depends on the knowledge of the respective beam-patterns which is straightforward to obtain. Conventional interferometric measurements can achieve a dynamic range well in excess of 10000:1 through the use of antenna gain self-calibration algorithms (see for example Cornwell and Fomalont, 1989) and similar algorithms can be used to ensure accurate cross-calibration between the interferometric and the single-dish measurements. Along these lines, Emerson (1991) has demonstrated that even a simple consistency-enforcing algorithm can correct systematic antenna pointing errors.

The second important measurement strategy is to average over random errors. The most trivial example of this is the averaging down of receiver noise. A more important example is the averaging of random pointing errors by repeating scans across an object.

The third important point is to ensure complete sampling of both the image plane and the Fourier plane. For simple brightness distributions such the mainly empty sky seen at centimeter wavelengths, the prior information incorporated in deconvolution and self-calibration algorithms can be a powerful factor in overcoming poor sampling. However, for the complex brightness distributions which we expect to see at millimeter wavelengths, such prior information is likely to be less useful. An example of potentially misleading results of deconvolution comes from our observational test discussed in Sect. 7, where the image obtained from both total power and interferometric data has an apparently lower dynamic range than one obtained from interferometric data alone. It is clear that the image obtained from both total power and interferometric data more accurately represents the structure of the object.

Finally we should note that the experience with previous telescopes has been that the most effective measurement and calibration strategies have been developed after observations began. We expect this to be also true of a telescope developed for mosaicing. A particular area of concern must be the assessment and correction of subtle and difficult to model systematic errors such as spillover. It would be fruitful to explore such schemes using existing arrays or prototypes of future ones.

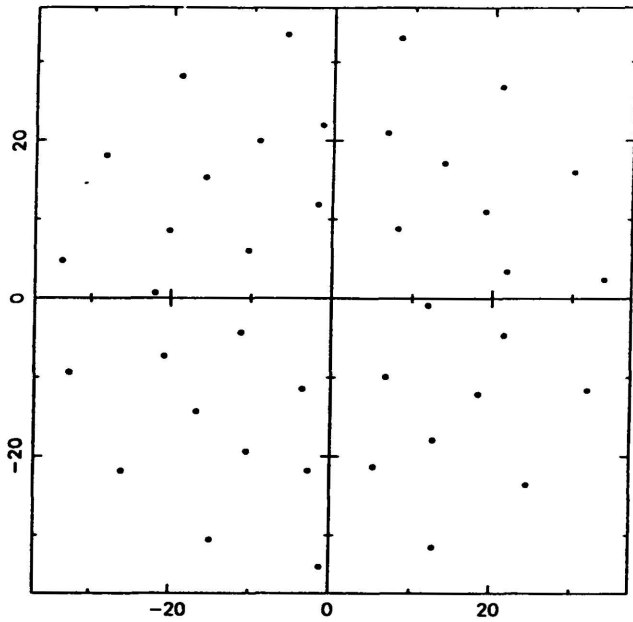


Fig. 1. Test Array Compact configuration antenna locations

## 6. Numerical simulations

Our analysis of the linear mosaic algorithm given above helps in the development of an intuitive understanding of the effects of various types of error. However, real observations will be considerably more complicated in various ways. First, complete and regular Fourier plane coverage will not be possible in practice. Second, totally correlated or uncorrelated errors are unlikely to occur in practice. Third, subtle observational errors such as slowly varying calibration errors are likely to be important.

For these reasons, we have undertaken an extensive set of numerical simulations. The topics addressed by our simulations include the following:

- Primary Beam Errors
- Noise
- Antenna Gain Instabilities
- Pointing Errors
- Linear Mosaic
- Simulations of a Planetary Observation

The model array was that of an early concept of the NRAO millimeter array which consisted of 39 antennas of diameter 7.5 meters positioned in three concentric circles of radii 12, 22, and 34 m (Braun, 1989). This array measures all spacings up to about  $9D$  (see Fig. 1) with 50% filling factor (i.e. the collecting area is about 50% of that of a filled aperture of similar diameter). The effective Fourier plane coverage obtained from mosaicing (shown in Fig. 2) has no regions of zero sensitivity for all spatial frequencies on baselines up to  $\sim 70m$ . The model brightness distribution for most of the simulations is based on an optical image of an HII region in M31, which was convolved with a 3.7arcsec beam (Fig. 3). Unless indicated otherwise, each simulated observation covered a grid of 7 by 7 pointings separated by  $\lambda/2D$  with one 60 second integration per

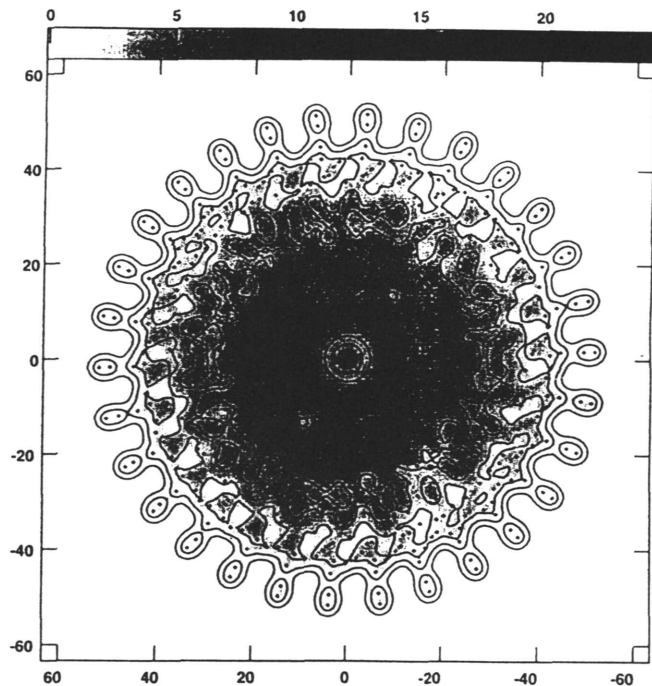


Fig. 2. Effective Fourier plane coverage of test array at 230 GHz. The dots denote sample points and the grey scale image denotes the Fourier plane coverage achieved by linear mosaicing of uniformly illuminated array element of 7.5m diameter. The contour levels are 2%, 5%, 10%, 20%, 40%, 60%, 80% and 100%. Notice the dip in sensitivity in the ring that corresponds to the scale of the diameter of the array elements

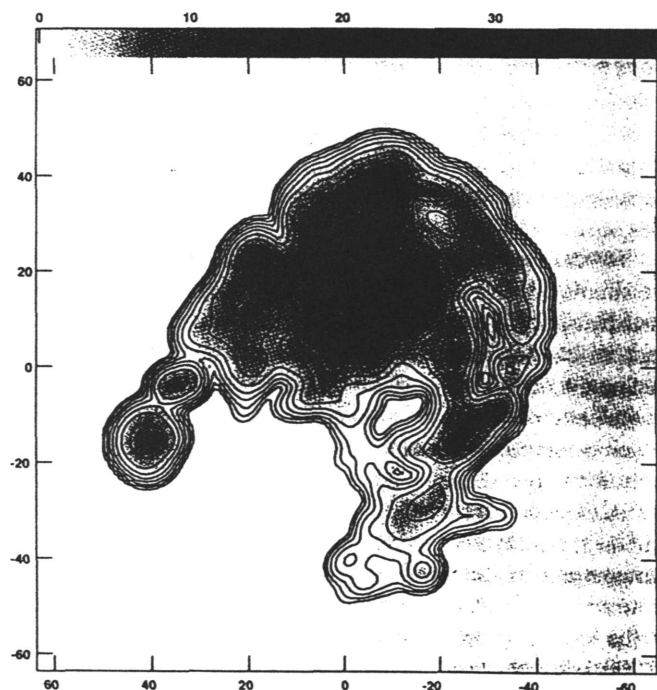


Fig. 3. The model brightness distribution used in the mosaicing simulations, convolved with a 3.7 arcsec beam. The greyscale runs from 0K to 40K and the contours are in a geometric progression in factors of two, starting at 0.05K

pointing, with  $\nu = 230$  GHz,  $\Delta\nu = 1$  MHz, and  $T_{sys} = 200$  K (all efficiency factors were assumed to be unity). Various model brightness temperatures were used. The model brightness distribution is sampled at each pointing by a primary beam given by the diffraction limited response of a uniformly illuminated 7.5m aperture with a 0.75m central circular blockage carried out to the second null. The source declination was equal to the array latitude ( $35^\circ$ ) and the observed hour angle ranged from  $-0.4$  to  $0.4$  to force the source to pass through the zenith, a worst case for measuring short spacing information as the baselines are not significantly foreshortened by projection, although a realistic one as it would seem desirable to avoid high opacities, especially at millimeter wavelengths.

### 6.1. Gauging image quality

Assessment of the results of a simulation requires both visual and numerical assessment of image quality. We will use the following ways to judge image quality:

- visual comparison of the resulting image with the model.
- estimation of the dynamic range **DR**, defined as the image peak divided by the off-source rms.
- estimation of the fidelity. Ideally, one would evaluate the on-source noise from a number of trials in a Monte Carlo method. However, since each of our simulations can be quite time-consuming we have instead used a single trial from which we estimate a fidelity index **FI** by taking the median value. Thus the fidelity index given here is only an approximation to the true fidelity described above.

$$FI \equiv \text{median} \left\{ \frac{I(\mathbf{x})}{\text{abs}[I(\mathbf{x}) - T(\mathbf{x})]} \right\} \quad (17)$$

- plotting of the visibility SNR curve.

To “calibrate” our understanding of these quality measures, we simulated VLA observations of the same model brightness distribution at a wavelength of  $\lambda = 20$  cm. While the compact millimeter array used in the mosaicing simulations has essentially complete Fourier plane coverage, the VLA has poor instantaneous Fourier plane coverage. To make a comparison which is representative of a very good image produced by each instrument, the VLA simulation required four hours in each of the B, C, and D arrays at 1.5 GHz yielding a 3.6 arcsec beam, and the test array required a mosaic of 49 pointings, one minute per pointing, at 230 GHz yielding a 3.7 arcsec beam. No errors were added to the simulated visibilities. A MEM deconvolution of the VLA data results in an image with  $FI = 120$  and  $DR = 27000$ , while the test array mosaic image has  $FI = 230$  and  $DR = 7000$ . The low fidelity indicates that on-source deconvolution errors are  $\sim 1 - 2$  orders of magnitude worse than off-source errors. If only snapshots from the B and D configurations of the VLA are used, then the fidelity index **FI** drops to 14 and the dynamic range **DR** drops to 1240.

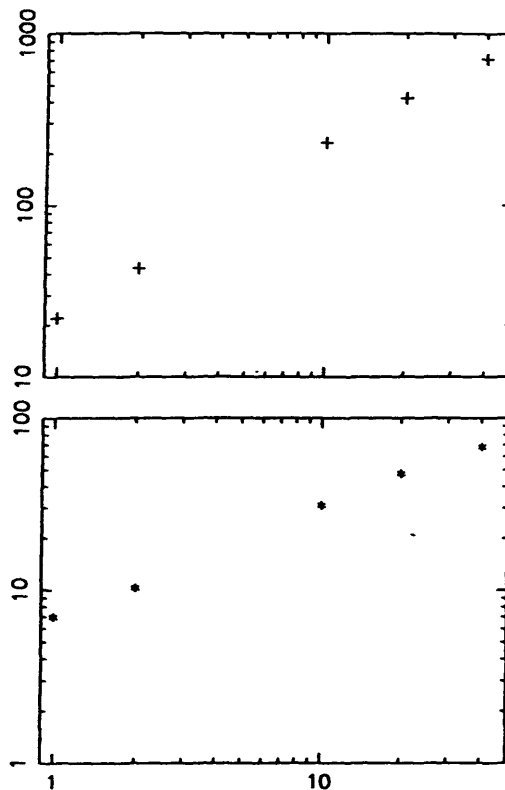


Fig. 4. Brightness temperature simulations: Dynamic range (+) and fidelity index (\*) as a function of peak  $T_B$  (K)

### 6.2. Primary beam errors

Errors in the reconstructed image result when the reconstruction is performed with an incorrect primary beam. To test this, the primary beam used in the reconstruction was the Airy disk, whereas the beam used in the simulation was an Airy disk spliced with a Gaussian before the 1st null. We found that  $DR \sim 3000$  and  $FI \sim 150$  can be obtained with a beam that is known with high accuracy down to about the 7% level, and is continued with a smooth gaussian below this level (equivalent to an overall knowledge of the primary beam to an rms error of  $\sim 1\%$ ). Departures from rotational symmetry of the primary beam due to, for example, feed leg blockage could be on the order of 1%, less than the errors in these simulations, and therefore are likely to be unimportant.

### 6.3. Noise

When observing with good Fourier plane coverage in the absence of noise, mosaicing should work extremely well at all places in the Fourier plane. However, it might be expected that when observing weak, noisy objects, the lowered sensitivity in the Fourier plane between the total power and the shortest interferometric observations would lead to problems in reconstructing those spacings. It is this sensitivity-related effect which we describe next.

The model image in Fig. 3 was scaled in brightness as Gaussian receiver and atmospheric noise was added. The simulations are labeled by the *peak* brightness temperature in the convolved

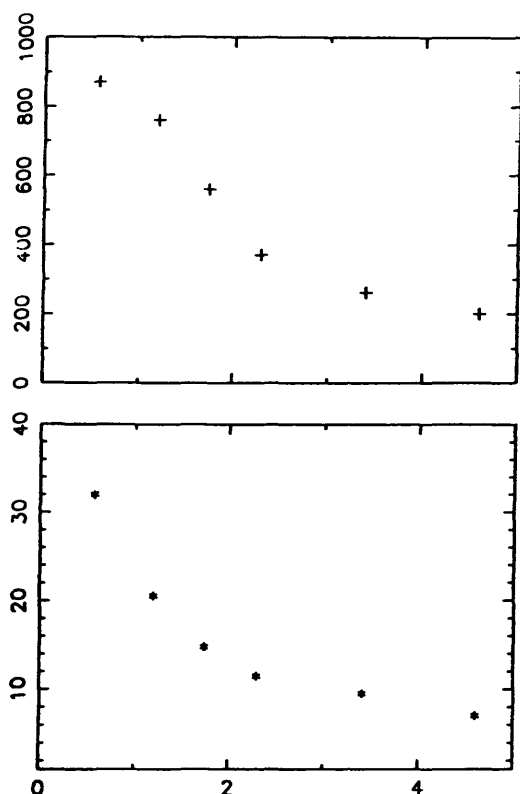


Fig. 5. Pointing error simulations: Dynamic range (+) and fidelity index (\*) as a function of rms pointing error (in arcsec)

model image. Peak source brightness temperatures range from 0.2K to 100K.

These simulations show that mosaic images are indeed linear: there is no threshold in brightness below which imaging falls apart. The dynamic range increases linearly with the source brightness as indicated by Fig. 4. The fidelity index, also shown in Fig. 4, increases linearly with source brightness for objects weaker than about 2K. Above 2K, the fidelity index continues to increase with the image peak brightness temperature, but there is a gradual roll off in fidelity index as on-source deconvolution errors become important. Another important result is that linear mosaicing can reconstruct spatial frequencies in the transition range between single-dish and interferometric measurements. Errors introduced on this range of spatial scales, 5-10m, are not disproportionate to the errors introduced by Gaussian noise on other spatial scales.

#### 6.4. Antenna gain instabilities

To simulate the effects of the atmosphere on mosaicing without simulating the atmosphere itself, we introduced antenna gain fluctuations to represent the residual effects of a changing atmosphere *after* calibration. Gaussian fluctuations in antenna gain of 7% are introduced for each antenna and for each pointing, and a linear drift is introduced of 5% to the total power gains only. At the very shortest spacings (0-5 meters) the drift dominates

and the total power measurements are off by about 6%. Above spacings of about 6 meters where the interferometer starts to dominate, the redundancy of the array averages errors down to a few percent. Finally at the longest spacings, where there is essentially no redundancy, the error is close to 5%. It was found that even with fluctuations of 14% and drifts of 10%, non-linear mosaicing produced reasonable results.

#### 6.5. Pointing errors

We allowed each antenna to have independent pointing errors which could change in time. The simulated visibility is then given by:

$$V_{1,2}(\mathbf{u}) = \int I(\mathbf{x}) E_1(\mathbf{x} - \mathbf{x}_{1p}) E_2^*(\mathbf{x} - \mathbf{x}_{2p}) e^{j2\pi \mathbf{u} \cdot \mathbf{x}} d\mathbf{x} \quad (18)$$

where  $V_{1,2}(\mathbf{u})$  is the visibility formed between antennas 1 and 2,  $I(\mathbf{x})$  is the model brightness distribution,  $E_1$  is the voltage pattern for antenna 1,  $\mathbf{x}_{1p}$  is the position to which antenna 1 is actually pointing, and  $\mathbf{u}$  and  $\mathbf{x}$  represent the vectors  $u, v$  and  $(x, y)$ . Our model for antenna pointing errors is based on observational experience. It has four terms:

1. a global pointing offset,  $G$ , for the entire array which is constant in time.
2. an initial pointing offset,  $I$ , which is random among all antennas but is constant in time.
3. a drift,  $D$ , in pointing throughout the observation which is uniform among antennas and changes uniformly with time.
4. a component,  $R$ , which is random among antennas and in time.

Each term has a component in azimuth and elevation. The simulations can be somewhat simplified by assuming that some kinds of errors (such as the random term) will not have a preferred direction setting the elevation and azimuth rms equal to each other, and others will have a particular preferred direction (such as the drift) fixing the ratio of the components of that error term. To control the number of degrees of freedom in this model, we have imposed a further observationally plausible restriction on the numerical values of the various terms:

$$G = (X, X) \quad D = (X/2, 0) \quad I = (X, X) \quad R = (X, X)$$

The first value of each pair is the azimuth error, the second is the elevation error. Images were generally produced for  $X = .25, .5, 1.0, 1.5,$  and  $2.0$  arcseconds, leading to rms pointing errors ranging from about .6 to 4.5 arcseconds.

Turning now to the results of the simulations, we first note that the visually obvious effect of the pointing errors was to introduce low spatial frequency ( $\sim 5$  m) positive and negative "ears" extending from the source. These ears are at the .2% level for 1.2 arcsec pointing errors. The quadrupole appearance of the ears in these simulations is actually due to the details of the pointing error model and the observing strategy and disappears when multiple scans are taken of the source.

The DR and FI are plotted against rms pointing error in Fig. 5. While DR is a useful image diagnostic for error processes which scatter power incoherently on fine scales (such as

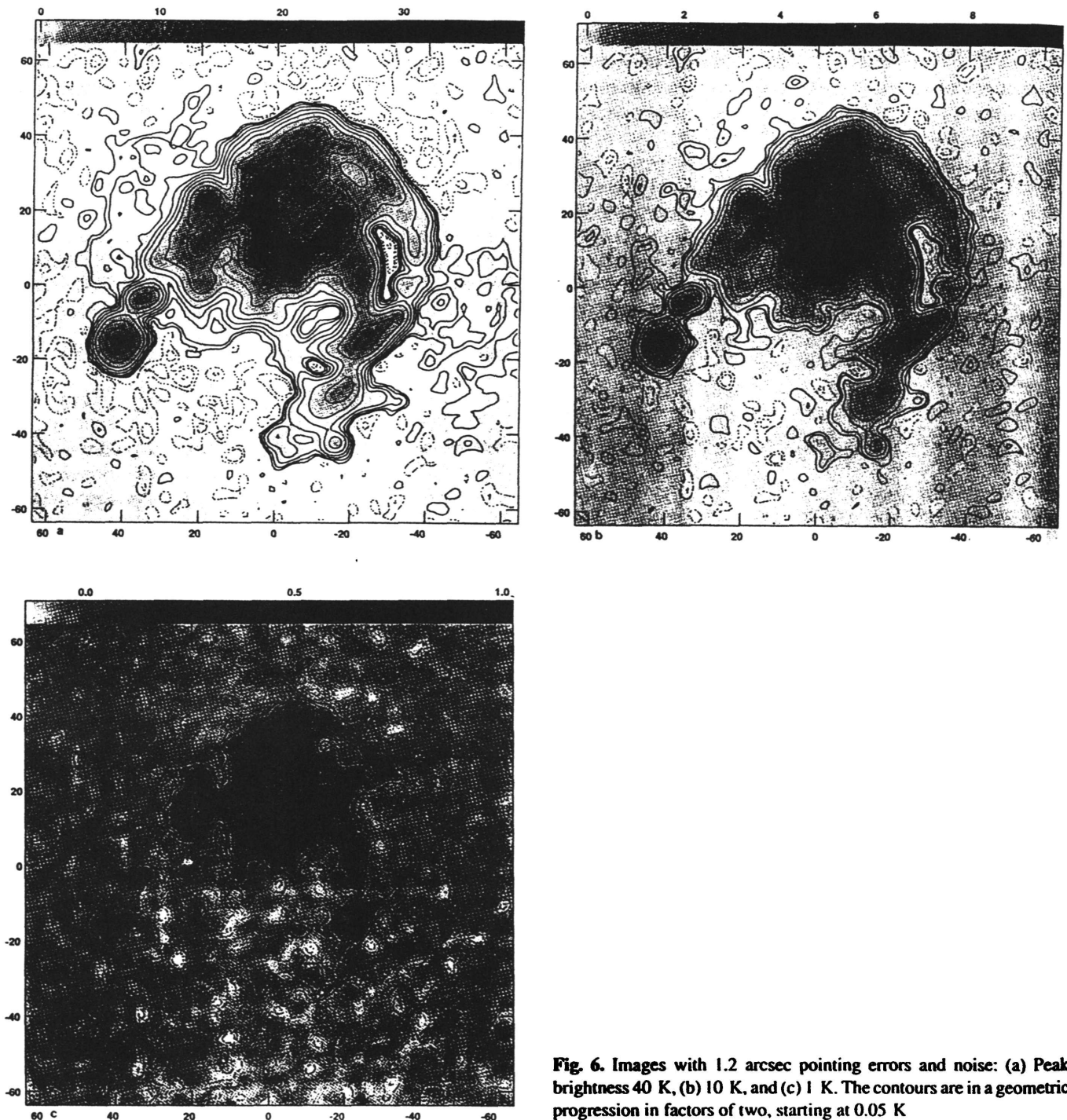


**Fig. 6.** Images with 1.2 arcsec pointing errors and noise: (a) Peak brightness 40 K, (b) 10 K, and (c) 1 K. The contours are in a geometric progression in factors of two, starting at 0.05 K

Gaussian noise), it is hard to evaluate for images with large scale coherent errors such as ears since the noise level varies considerably across the background. The fidelity index is a more reliable indicator. The simulations show that the FI is inversely proportional to the magnitude of the pointing error. Pointing errors of about 1 arcsec are required to reach a  $FI \sim 20$ .

Pointing error simulations in which the total power was measured with a 15m antenna resulted in much worse images for the same magnitude of pointing error as the pointing error is a

larger fraction of the primary beam. For an image in which total power measurements performed by a 15 meter single-dish with 1.2 arcsec rms pointing errors, the fidelity index was 11.8 and the dynamic range was 100.

To investigate possible coupling of the effects of pointing errors with those of additive noise, 1.2 arcsec rms pointing errors were simulated in concert with Gaussian noise as detailed above. The visually obvious effects of the pointing errors dominate the image errors above  $T_B = 40K$  but are masked by the noise for

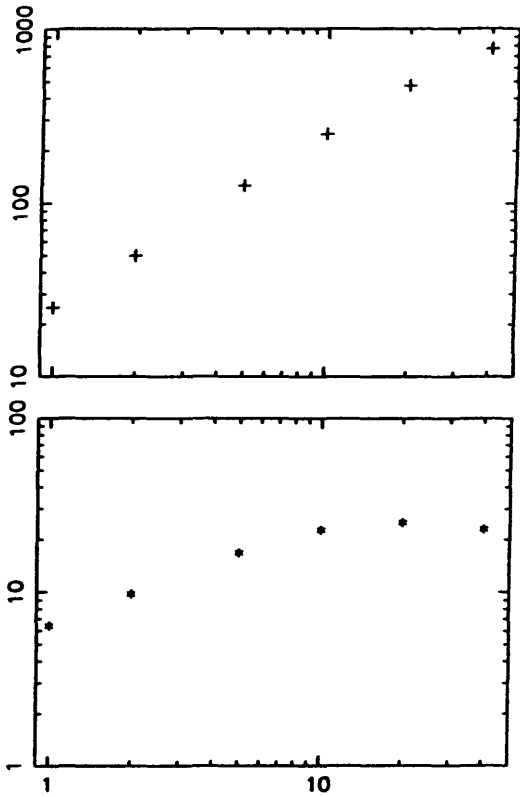


Fig. 7. Coupling of additive noise and pointing errors: Dynamic range and fidelity index as a function of peak  $T_B$  with 1.2 arcsec pointing errors

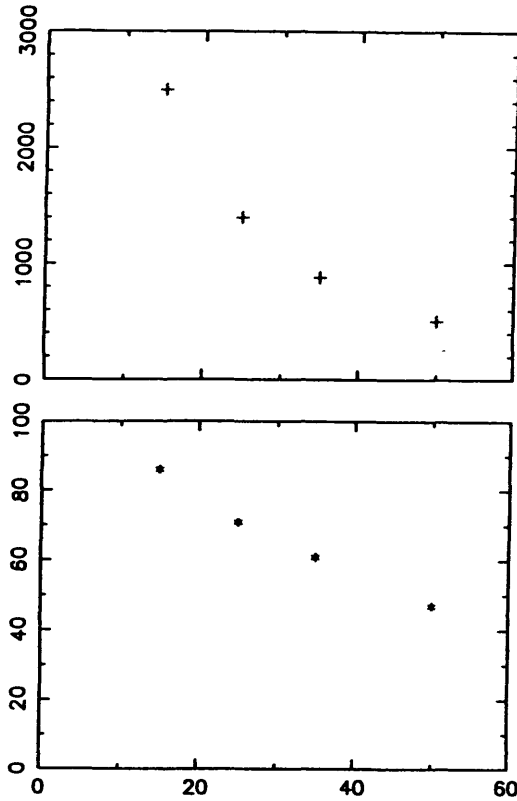


Fig. 8. Surface error simulations: Dynamic range (+) and fidelity index (\*) as a function of rms surface error (in microns)

lower brightness sources. Images with peak  $T_B = 40\text{K}$ ,  $10\text{K}$ , and  $1\text{K}$  are shown in Fig. 6. The dynamic range increases almost linearly with source brightness up to  $40\text{K}$  in Fig. 7, almost identical to the case with no pointing errors in Fig. 4. However, as we emphasized above, the image appearance and dynamic range are not good diagnostics of on-source errors. The fidelity index increases with brightness temperature up to  $T_B = 10\text{K}$ , above which the fidelity index saturates at about 20, indicating that pointing errors dominate the on-source reconstruction errors well before the effects of the pointing errors are recognizable in the images. For the  $1\text{K}$  image, VSNR curves with and without pointing errors indicate that the pointing errors have very little effect on the reconstruction. For the brighter  $10\text{K}$  image, the pointing errors show up on all spatial frequencies of the reconstruction but are most obvious on spacings between  $2\text{m}$  and  $8\text{m}$ .

Sensitivity considerations aside, pointing errors are the fundamental limitation to high quality image reconstruction using mosaicing at millimeter wavelengths. What can be done to improve the image quality? First, calibration of any global pointing error component will greatly improve the image quality as it has been shown that the global error is the most damaging component of the pointing error model. Second, scanning quickly over the source a number of times instead of just once will improve the image as the random and drift pointing error components will average down and any global component in *azimuth* and

*elevation* will change in right ascension and declination over the observations, causing it to average down as well (Holdaway 1990).

### 6.6. Surface errors

Surface errors lead to a decrease in antenna efficiency, which will affect the noise level in the mosaic images, and also to higher sidelobes or primary beam errors, which will limit the quality of the mosaic images. As demonstrated above, the SNR of a linear mosaic image subject to pointing errors alone is proportional to  $\lambda/D/\sigma_{PE}$ , while the SNR of a mosaic image subject to surface errors alone is proportional to  $(\lambda/\sigma_{SE})^2$ . Since the surface errors have a stronger frequency dependence, a millimeter array should have good enough surfaces so that surface errors and pointing errors will have roughly the same impact on the images at the highest observing frequency.

Surface errors introduce phase errors in the incoming wavefront as it reflects from the primary and secondary surfaces and  $E(\mathbf{x})$  is then given by

$$E(\mathbf{x}) = \int f(\mathbf{k}) e^{j4\pi\epsilon(\mathbf{k})/\lambda} e^{j2\pi\mathbf{k}\mathbf{x}} d\mathbf{k} \quad (19)$$

where  $f(\mathbf{k})$  is the aperture illumination,  $\epsilon(\mathbf{k})$  is the surface error distribution,  $\mathbf{k}$  is the antenna plane coordinate, and  $\mathbf{x}$  is the coor-

dinate of the voltage pattern. Given model surface error patterns for each antenna, the voltage pattern and thus the two dimensional primary beam for each antenna may be calculated. The effects of the surface errors on a single visibility sample can be simulated by computing the Fourier sum of the product of the model brightness distribution and the voltage patterns for the  $i^{\text{th}}$  and  $k^{\text{th}}$  antennas:

$$V_{i,k}(u) = \int I(x)E_i(x' - x_i)E_k^*(x' - x_k)e^{j2\pi x u} dx \quad (20)$$

where  $x'$  is related to  $x$  via a rotation through the parallactic angle of the antenna on the sky and  $x_i$  is the position on the sky to which the  $i^{\text{th}}$  antenna points. Pointing errors can be included at no extra computational cost.

If the antenna is made up of a number of panels, then surface errors will be correlated on scales of  $D/N$ , where  $N$  is the number of panels across the antenna. Surface errors due to gravitational and thermal effects will have correlation scale lengths on the order of  $D$  or  $D/2$  and will be time dependent with timescales of a few hours. If the mosaiced region is small and can be observed quickly ( $< 1$  hour) time dependent effects will not be important. On the other hand, if each field is observed a number of times at a range of hour angles, changes in the voltage pattern due to these time dependent effects will tend to average out and a better reconstruction may be possible. No time dependent surface errors have been modeled in these simulations. The simulated surface errors are assumed to have a power law spectrum of index  $-1.2$  between between 1 and 8 meters. Surface error models which have no correlation shorter than  $D/2$  (representing molded antennas with only large scale correlations) have also been explored (Holdaway, 1992).

The details of the simulated observations are similar to those described above except that the declination was chosen to be  $20^\circ$  to reduce the rate of change of the parallactic angle. Simulations were performed with rms surface errors of 15, 25, 35, and 50 microns. Although these simulations were performed at 230 GHz, results at other frequencies can be scaled as  $\lambda/\sigma_{SE}$ .

The resulting DR and FI for the surface error simulations are shown in Fig. 8.

The performance indicated is worsened in various ways if the details of the simulations are changed:

- We have assumed that all antennas in the array have different surface error distributions. If, however, the error patterns are identical for all antennas, then the DR is 2-3 times lower and the FI drops by about 2/3.
- In performing the reconstruction, we found that the best results were obtained using an empirically determined primary beam pattern. Since the computational costs can be reduced substantially by using an azimuthally symmetric beam, we have therefore obtained the PB model by averaging over antenna and over azimuth. However, if the theoretical PB is used in place of the empirical PB, the DR is 4-6 times lower and the FI is about 2 times lower.
- When 1.2 arcsec pointing errors are added, the FI is limited to 20-30 and the DR to about 1000.

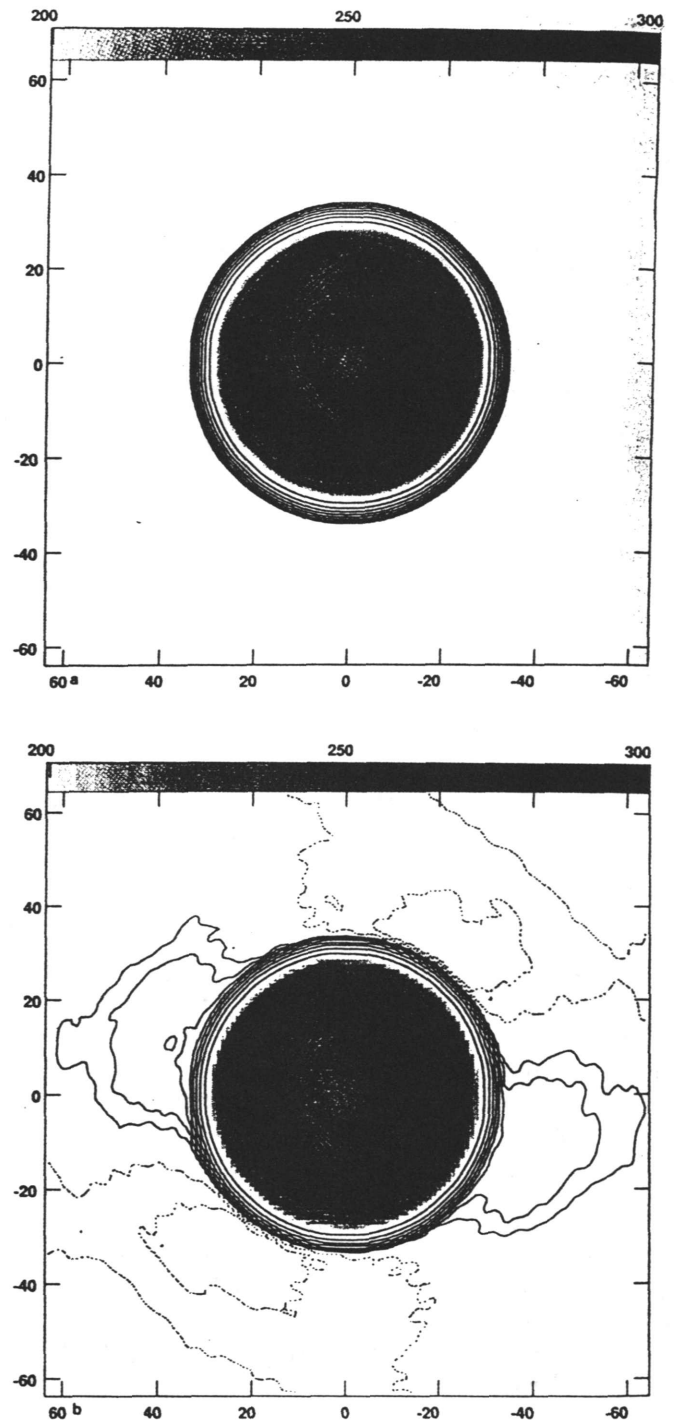


Fig. 9. Mosaic simulation of a planet with structure;  $T_B = 250K$ , 1.2 arcsec pointing errors. (a) Original model (b) reconstruction. The contour levels are chosen to emphasize slight gradients on the disk: -4, -2, -1, 1, 2, 4, 8, 16, 32, 64, 128, 246, 248, 250, 252, 254, 260, 270, 280, 290, 300 K. The peak brightness is 320 K

- Antennas with surface errors which are correlated down to  $D/2$  require  $\lambda/55$  accuracy to produce results which antennas with  $D/8$  minimum correlation scale can get with  $\lambda/40$ . Hence if antenna surfaces are produced as a single

piece from a mold, the correlation size is larger than for a paneled antenna, leading to larger and less symmetric near sidelobes and so the surface specifications must be somewhat tighter.

A more complete accounting of the effects of surface errors on mosaic images is given by Holdaway (1992).

### 6.7. Linear mosaic

With noise and pointing errors included in the simulations, linear mosaicing produces images which compare well with those from nonlinear mosaicing for dynamic range less than 500. The image obtained by linear reconstruction is essentially the same as that produced by the nonlinear reconstruction spacings ranging from 0 to 20 meters. It is slightly worse on spacings in the range from 20 to 50 meters, and significantly worse on spacings beyond 50 meters. This occurs because the approximation that the synthesized beams are identical for all pointings breaks down first for the long spacings which change the fastest.

### 6.8. Simulations of a planetary observation

In general, planets are difficult objects to image interferometrically (e.g. de Pater, 1990) and therefore present one of the most severe tests for an array. To investigate mosaic imaging of a planet, we used a sharp edged disk of 30 arcsecond radius for a model. To observe any emission on the disk (such as the planetary atmosphere) with good fidelity, several pointings beyond the disk must be observed. For our 30 arcsecond radius planet model, a rectangular grid of 5 by 5 pointings (spaced 17 arcsec apart) lead to .5% errors on disk but large holes –8% a few arcseconds away from the disk. A 5 by 5 pointing simulated observation of the larger model source did not show such defects. Emission off the disk can be imaged accurately only by extending the number of pointings to a 7 by 7 grid of pointings.

It is well-known that pre-tapering of visibility data can aid in the use of MEM algorithms (see e.g. Cornwell and Braun, 1989). In this case, a substantial reduction in the on-source error can be obtained when the visibilities are pre-tapered by a 2 arcsec beam. The error then drops from 0.08% to .02% rms. Similarly the off-disk error dropped from .1% of the disk to about .03% (corresponding to a dynamic range of about 3000).

Unlike most observations of molecular clouds, the quality of images of planets will be limited by pointing errors. We assume a 250K disk brightness temperature for a more complicated model and use the pointing error model described in Sect. 3. The model and the maximum entropy mosaic reconstruction are shown in Fig. 9. Features as weak as .2% of the brightness of the disk can be seen. The dynamic range is 430 and the fidelity index is 75. The fidelity index is relatively high because pointing errors have little effect on a source which changes little on the size scale of the pointing errors.

## 7. An observational test

To complement our extensive set of simulations of the homogeneous array concept, we have performed an observational test

using the VLA and a single VLBA element operating in total power mode (both the antennas at Pie Town and Los Alamos were used). For our purposes the principal attraction of using the VLBA element is that the pointing errors at 8.4GHz (~ 15 arcseconds) scale to those specified for our test array elements at 230GHz. Fortunately, although the VLBA elements were not specifically designed for total power observations, the stability of the VLBA electronics allow a measurement of total-power from the monitor data. While we cannot perform a comparison with a “true sky” image, we have obtained an image consistent with both sets of data and with good visual appearance.

The Crab Nebula subtends about 7 arcmin which is slightly larger than the primary beam of a 25m diameter telescope at 8.4GHz (5.4 arcmin FWHM). At the Nyquist sampling interval of about 2.7 arcmin, a minimum of ten pointings are required to span the object, allowing for a respectable guard band of pointings where the brightness is expected to be negligible. This, combined with its intrinsic brightness, makes the Crab Nebula an ideal target for a mosaicing test.

The VLA interferometric observations were kindly provided to us by Glen Langston. The Crab nebula was observed at 8.4GHz in the VLA D-configuration using 10 pointings at half-power spacings. These 10 pointings were observed in sequence 4 times, giving a total observing time of 18 minutes per pointing, and about 3 hours in total. The flux scale was established by referring the phase calibrator 0528+134 to 3C286. Before imaging, the visibility data sets were phase rotated to a common phase reference position and the  $u, v, w$  coordinates adjusted correspondingly.

Total power observations were obtained using the Los Alamos VLBA element. We fixed the electronic gain and monitored total power (TP) and switched power (SP) during the run. TP alone is strongly dependent upon elevation but TP/SP is not. TP/SP changes by a factor of 2 on observing the Crab, and is linear to about 2% over this range. We observed a 9 by 9 grid of pointings in azimuth-elevation coordinates, spaced by 2 arcmin, spending 25s on each sample. Every 3 samples we observed an off-source offset by 20 arcmin in azimuth which provided the adopted zero-level. The total observing time per 9 by 9 grid was therefore about 40 minutes. Calibration was performed on 3C84 (whose flux was in turn derived from those of several Baars calibrators by Craig Walker), and the primary beam was measured using an 18 by 18 1-arcmin grid, also on 3C84.

Since the Fourier plane coverage of the VLA observations was relatively poor, rather than use the linear mosaic image  $I^{LM}$ , we used the non-linear mosaic image  $I^{MEM}$ . The data constraints were the VLA visibility data for each pointing and the set of TP/SP measurements for the 9 by 9 grid observed using the VLBA element. The mosaicing algorithm relies upon a model for the primary beams of the elements used. For the VLA elements we used a polynomial model developed by Napier and Rots (1982). We have measured the beam of the VLBA antennas that we used and found that at our operating frequency the beams are well described by that of a uniformly illuminated, blocked aperture. We produced three images (shown in Fig. 10). First, an image from the VLA data alone, showing

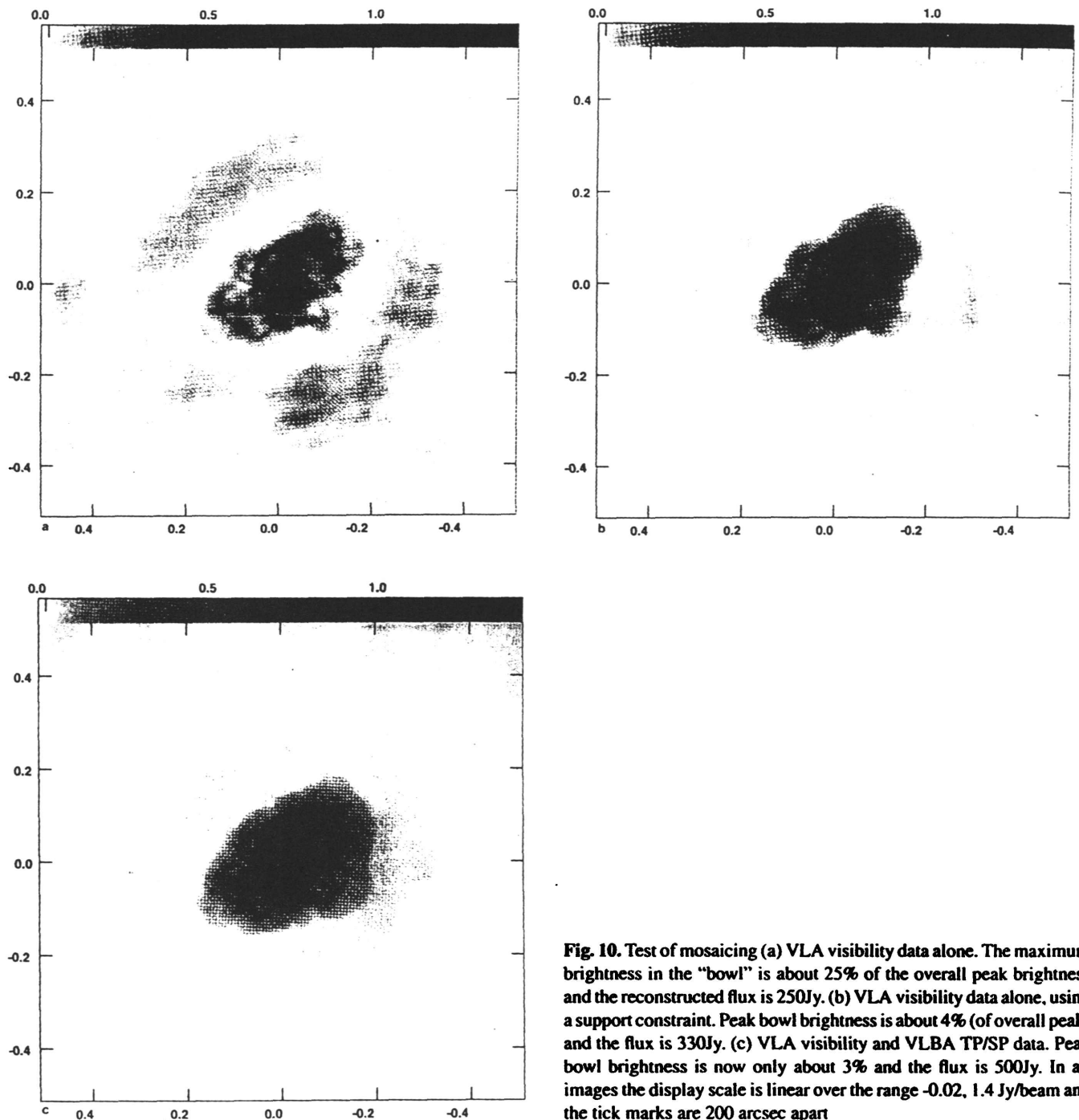


**Fig. 10.** Test of mosaicing (a) VLA visibility data alone. The maximum brightness in the “bowl” is about 25% of the overall peak brightness and the reconstructed flux is 250Jy. (b) VLA visibility data alone, using a support constraint. Peak bowl brightness is about 4% (of overall peak) and the flux is 330Jy. (c) VLA visibility and VLBA TP/SP data. Peak bowl brightness is now only about 3% and the flux is 500Jy. In all images the display scale is linear over the range  $-0.02, 1.4$  Jy/beam and the tick marks are 200 arcsec apart

a large bowl-like artifact due to the missing short spacing information. Second, we demonstrate that this can be improved substantially by using some prior knowledge about the support of the Crab Nebula: we masked the bowl-like region in the first image, and, after smoothing by a 10 arcsec Gaussian, used it as a default image  $M(x)$  in the non-linear mosaicing. The image has improved considerably in visual appearance and the restored flux has increased. Third, we added the VLBA TP/SP data. The image now has substantially more total flux than the other two images and has a higher peak brightness than the second image.

Although the noise is slightly higher than that in the previous image, we believe that the image is a more faithful representation of the true sky brightness distribution (the FI is certainly higher, although the DR is slightly lower).

The conclusions from this test are that:

- Despite the relative simplicity of our TP/SP observing scheme, we obtained a visually acceptable image which fits both data sets adequately.
- The level of residual noise off source (3% peak) is compatible with the level of non-linearity in the VLBA system

(about 2%) and the possible errors in cross calibration of the VLA and VLBA data (probably no better than 2-3%). Errors in the pointing and in the assumed primary beam models will probably be important at higher SNR levels than we reached in this experiment.

## 8. Recommendations for array design

We have found that the analytical expressions derived in this paper provide a good guide for the design of imaging arrays. Fine-tuning of a particular design can be then done with numerical simulations such as the ones described above. It is often difficult to simulate subtle systematic errors. Therefore, testing of a specific design with a prototype array is advisable.

The **homogeneous array** design is robust with respect to all errors we have simulated so far. Important design specifications that have been determined or reinforced by these simulations include:

- The primary beam must be well understood. For the test array, deviations from the beam model must be small down to or below the  $\sim 7\%$  level.
- Pointing accuracy must be better than for single field observations. For the test array that we have used, the requirement is  $\sim 1$  arcsec rms.
- The antennas must possess a better surface than is required for single field observations. For our, test array, the specification is  $25\mu\text{m}$  which corresponds to an rms surface accuracy of about  $\lambda/40$ . Errors which are coherent over large regions of the surface are most damaging.

Rules of thumb in mosaic imaging which have come out of these simulations include:

- For complicated fields of view as well as incompletely sampled, non-linear mosaicing must be employed. The resulting images are as accurate as images made from fields which are mostly empty.
- For low SNR observations, the computationally inexpensive linear mosaic can be employed if the object is sampled out to zero brightness.
- Linear mosaic images degrade gracefully as the SNR decreases.

## 9. Concluding remarks

We have seen that the **homogeneous array** concept allows high quality imaging. This conclusion arises from theoretical analysis, numerical simulations, and an observational test. The **homogeneous array** concept has been adopted for the Millimeter Array (MMA) recently proposed by the National Radio Astronomy Observatory.

The key distinguishing feature of the **homogeneous array** is that short spacings close to the dish diameter are measured using the array elements rather than via some other scheme. Given that the concept seems to work, we feel that its key advantage over rival concepts is its simplicity, which is particularly important in a large complex system such as the proposed Millimeter Array.

*Acknowledgements.* This work grew out of the NRAO Millimeter Array design work which has taken place over the past 9 years. The **homogeneous array** concept is the end-product of this work and has been influenced by many people: in particular we wish to thank Frazer Owen, Robert Braun, Bob Hjellming and Harvey Liszt. We are also indebted to many other people for useful discussions on mosaicing, but we especially wish to thank Darrel Emerson for many vigorous discussions on the virtues of the **homogeneous array** concept. We are very pleased that we were able to use a VLBA antenna at the opposite end of the spatial frequency domain to its designed use. For this and their help and patience, we thank the VLBA project staff, especially Durgadas Bagri for his advice and Craig Walker for a timely measurement of the flux of 3C84. We also thank Glen Langston for providing the VLA data.

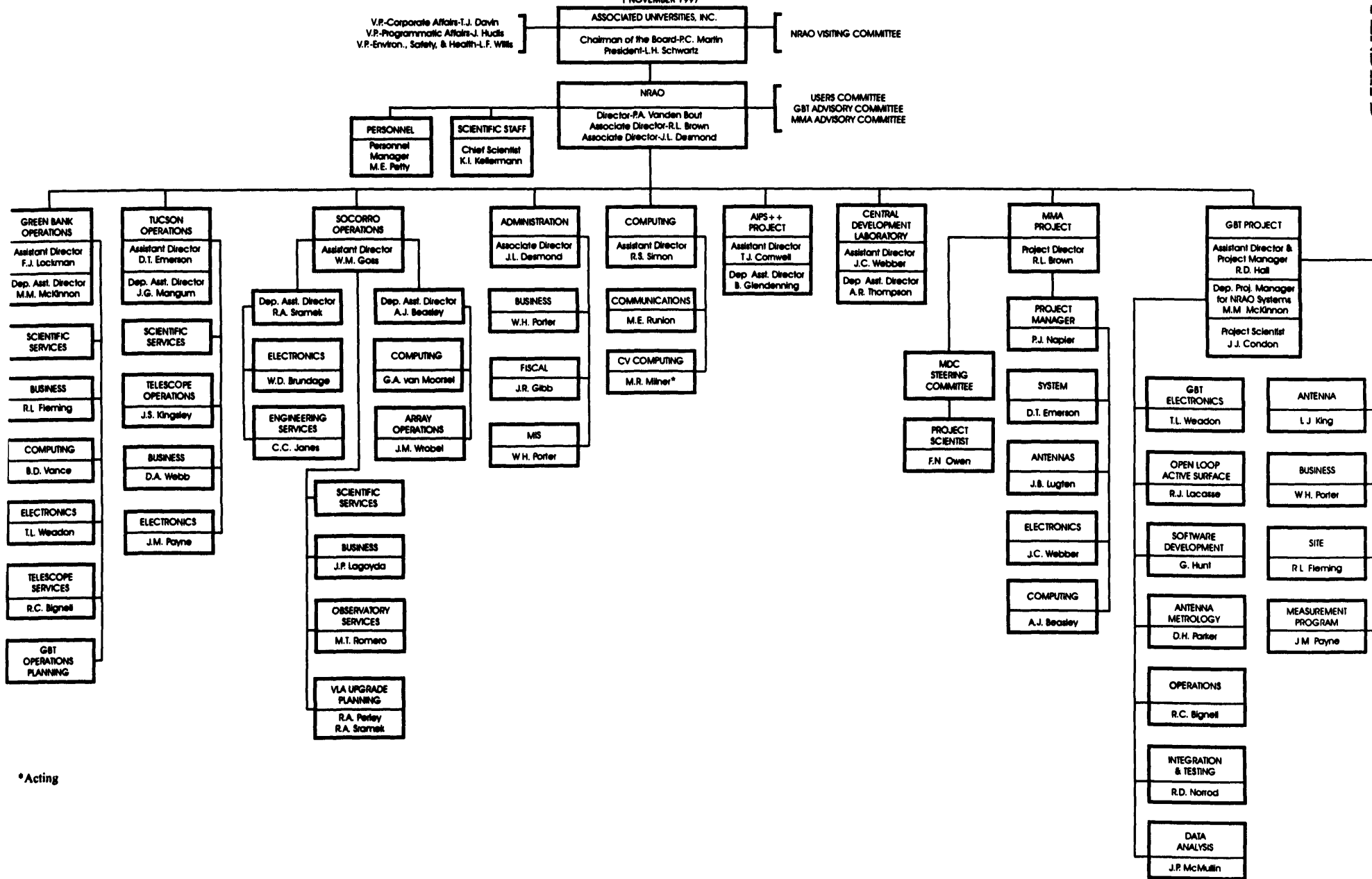
## References

- Braun, R., 1988, NRAO millimeter array memo 54, Socorro, NM  
 Cohen, J. G., 1991, AJ 101, 734  
 Cornwell, T. J., 1984, NRAO millimeter array memo 24, Socorro, NM  
 Cornwell, T. J., 1987, NRAO millimeter array memo 42, Socorro, NM  
 Cornwell, T. J., 1987, NRAO millimeter array memo 43, Socorro, NM  
 Cornwell, T. J., Evans K. F., 1985, A&A 143, 77  
 Cornwell, T. J., 1988, A&A 202, 316  
 Cornwell, T. J., Braun, R., 1989, In: Perley, R.A., Schwab, F.R., Bridle, A.H. (eds.), *Synthesis Imaging in Radio Astronomy*, A.S.P., Provo, Utah, p167  
 Cornwell, T. J., Fomalont E. B., 1989, In: Perley, R.A., Schwab, F.R., Bridle, A.H. (eds.), *Synthesis Imaging in Radio Astronomy*, A.S.P., Provo, Utah, p185.  
 Cornwell, T. J., Perley, R. A., 1992, A&A 261, 353  
 De Pater, I., 1990, ARA&A 28, 347  
 Ekers, R. D., Rots, A. H., 1979, In: C.van Schooneveld (ed.), *Proc. IAU Col. 49, Image Formation from Coherence Functions in Astronomy*. D.Reidel, p61.  
 Emerson, D. T., Klein, U., Haslam, C. G. T., 1979, A&A 76, 92  
 Emerson, D. T., 1991, In: Cornwell, T.J., and Perley, R.A. (eds.), *Proc. IAU Col. 131, Radio Interferometry: Theory, Techniques and Applications*, ASP, Provo, Utah, 441.  
 Hjellming, R. M., 1989, In: Perley, R.A., Schwab, F.R., Bridle, A.H. (eds.), *Synthesis Imaging in Radio Astronomy*, A.S.P., Provo, Utah, p167.  
 Högbom, J., 1974, ApJS 15, 417  
 Holdaway, M. A., 1990, NRAO millimeter array memo 61, Socorro, NM  
 Holdaway, M. A., 1992, NRAO millimeter array memo 74, Socorro, NM  
 Mundy, L. G., Cornwell, T. J., Masson C. R., Scoville, N. Z., Bååth, L. B., Johansson, L. E. B., 1988, ApJ 325, 382  
 Napier, P.J., Rots, A.H., 1982, NRAO test memo 134, Socorro, NM  
 Napier, P.J., Thompson, R.T., Ekers, R.D., 1983, *Proc. IEEE* 71, 1295  
 Narayan, R., Nityananda, R., 1986, ARA&A 24, 127  
 Pearson, T.J., Readhead, A.C.S., 1984, ARA&A 22, 97  
 Schwarz, U.J., 1978, A&A 65, 345  
 Thompson, A.R., Moran, J.M., Swenson, G.W., 1986, *Interferometry and Synthesis in Radio Astronomy*, Wiley-Interscience, New York  
 Woody, D. P., Scoville, N. Z., Mundy, L. G., 1991, In: Cornwell, T. J., Perley, R.A. (eds.), *Radio Interferometry: Theory, Techniques and Applications*, A.S.P., Provo, Utah, p81  
 This article was processed by the author using Springer-Verlag LaTeX A&A style file version 3.



NATIONAL RADIO ASTRONOMY OBSERVATORY  
ORGANIZATION CHART

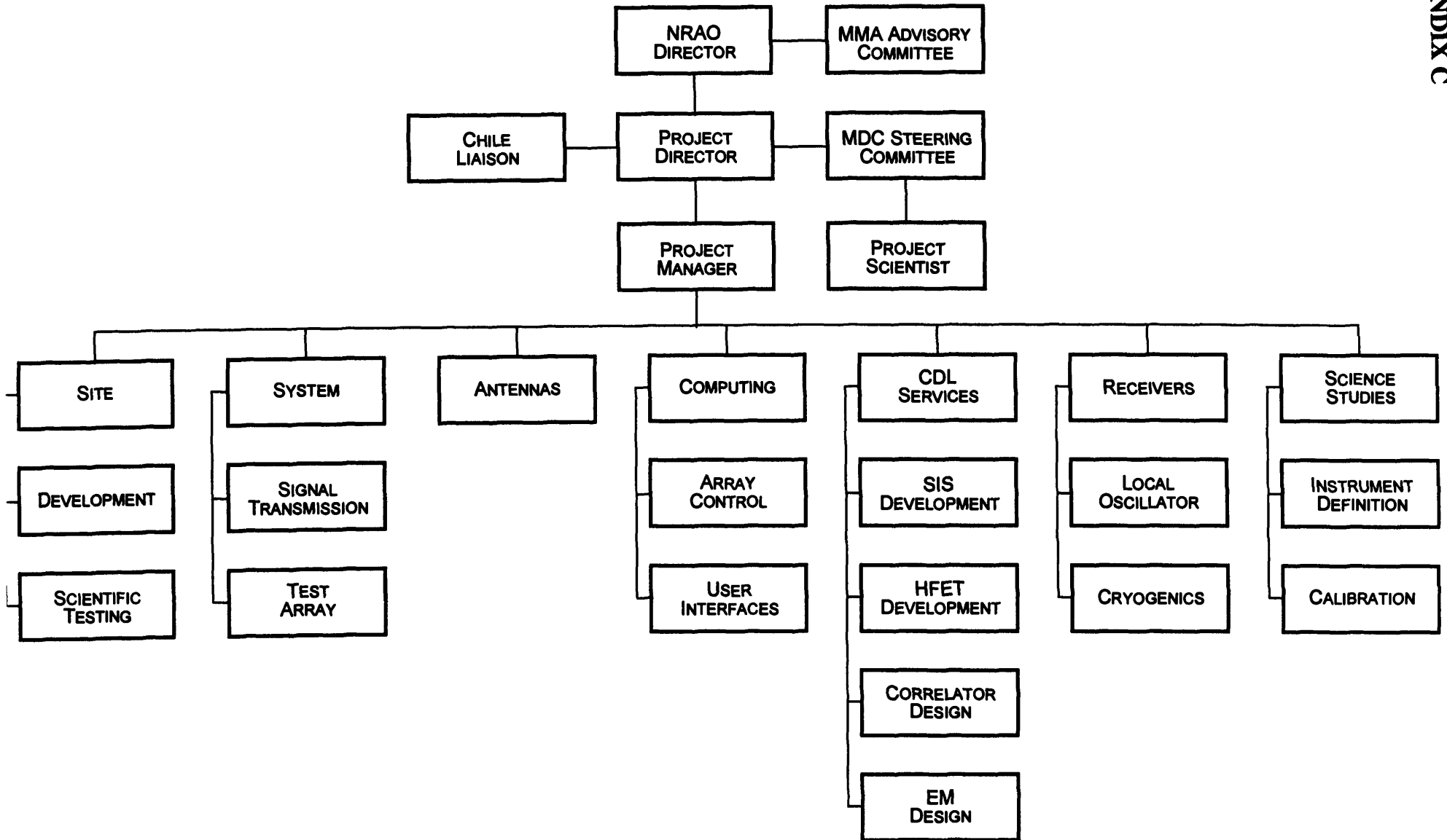
1 NOVEMBER 1997



\* Acting



# MMA DESIGN AND DEVELOPMENT PHASE ORGANIZATION AND TASKS





# Millimeter Array Memos

The Millimeter Array Memo series documents the development of the MMA project.

- Search the existing MMA Memo abstracts based on Title, Author, or Subject Keywords.
- Postscript files of selected MMA Memos are available in the FTP Directory.
- Subscribe to the mma-info electronic mailing list, the preferred mode of distributing new MMA Memos.
- Potential MMA Memo authors should read the MMA Memo Submission Guidelines
- For more information on the MMA memo series, contact Kate Weatherall at 505-835-7452 or by e-mail at [kweather@nrao.edu](mailto:kweather@nrao.edu).
- For back hardcopies of MMA memos, contact Lori Appel at 505-835-7310 or by e-mail at [lappel@nrao.edu](mailto:lappel@nrao.edu).

No.	Title	Author(s)	Date
193	<u>Report of the LSA/MMA Antenna Study Committee</u>	T. Andersen, J. Lugten, P. Napier, D. Plathner, D. Woody, M. Bremer, J. Cheng, J. Delannoy, R. Hills	12/97
192	<u>The Astronomical Case for Short Integration Times on the Millimeter Array</u>	Michael P. Rupen	11/97
191	<u>Feasibility Study of the Use of the White Mountain Research Station (WMRS) Laboratory to Measure the Effects of 27% Oxygen Enrichment at 5000 m Altitude on Human Cognitive Function</u>	J.B. West, F.L. Powell, A.M. Luks (Division of Physiology School of Medicine, UCSD)	11/97
190	<u>A System Design for the MMA</u>	A. R. Thompson	11/97
189	<u>Reference pointing of LSA/MMA antennas</u>	Robert Lucas	11/97
188	<u>Another look at anomalous refraction on Chajnantor</u>	Bryan Butler	10/97
187	<u>Modeling of the Submillimeter Opacity on Chajnantor</u>	M.A. Holdaway, Juan R. Pardo	10/97
186	<u>Calculation of Anomalous Refraction on Chajnantor</u>	M.A. Holdaway	9/97
185	<u>Review of Gifford-McMahon Refrigerators For 4K</u>	Larry R. D'Addario	9/97
184	<u>Cryogenics Options for the MMA</u>	Larry R. D'Addario	9/97
183	<u>A Suggested Receiver Layout for the MMA Antenna</u>	John Lugten, Jack Welch	9/97
182	<u>A 12-m Antenna Design for a Joint US-European Array</u>	Jingquan Cheng	9/97
181	<u>Notes on Possible Sensors for Improving the</u>	J. M. Payne	8/97

	<u>Pointing of MMA Antennas</u>		
180	<u>Imaging With Heterogeneous Arrays</u>	M.C.H. Wright	8/97
179	<u>Compatibility Issues for Joint Operation of the LMSA and MMA</u>	M. Ishiguro, P. Napier	7/97
178	<u>Effects of Pointing Errors on Mosaic Images with 8m, 12m, and 15m Dishes</u>	M.A. Holdaway	8/97
177	<u>Sensitivity Comparisons of the Various LSA/MMA Collaboration Options</u>	M.A. Holdaway	8/97
176	<u>Preliminary Phase Stability Comparison of the Chajnantor and Pampa la Bola sites</u>	M.A. Holdaway, Satoki Matsushita, M. Saito	7/97
175	<u>Gain Degradation in a Symmetrical Cassegrain Antenna Due to Laterally Offset Feeds</u>	Bill Shillue	6/97
174	<u>How Many Fast Switching Cycles Will the MMA Make in its Lifetime?</u>	M.A. Holdaway	6/97
173	<u>Application of Fast Switching Phase Calibration at mm Wavelengths on 33 km Baselines</u>	C.L. Carilli, M.A. Holdaway	5/97
172	<u>Comments on Minimum Sidelobe Configurations</u>	M.A. Holdaway	5/97
171	<u>Optimization of an array configuration minimizing side lobes.</u>	L.R. Kogan	5/97
170	<u>System Temperatures, Single Versus Double Sideband Operation, and Optimum Receiver Performance</u>	P. R. Jewell, J. G. Mangum	4/97
169	<u>Atmospheric Coherence Times at Chajnantor</u>	M.A. Holdaway	4/97
168	<u>Relative Sensitivities of Single and Double Sideband Receivers for the MMA</u>	A.R. Thompson, A.R. Kerr	4/97
167	<u>High Level Computing Information Flow for the MMA</u>	M.A. Holdaway	4/97
166	<u>The MMA Correlator</u>	Ray Escoffier	4/97
165	<u>System Design Considerations for the Atacama Array</u>	A. R. Thompson, D. Bagri, B. G. Clark, J. E. Carlstrom, L. R. D'Addario, D. Emerson, R. P. Escoffier, J. Romney, S. Padin, R. A. Sramek, D. Thornton, W. J. Welch	2/97
164	<u>MMA Computing Working Group Report</u>	Steve Scott, Darrel Emerson, Rick Fisher, Mark Holdaway, Jill Knapp, Lee Mundy, Remo Tilanus, Mel Wright	11/96
163	<u>A Strawman Optics Layout For The MMA Antenna</u>	P.Napier, J. Biegging, J. Cheng, D. Emerson, M. Gordon, M. Holdaway, J. Kingsley, J. Lugten, J. Payne, D. Woody	11/96

162	<u>Medical and Physiological Considerations for a High-Altitude MMA Site</u>	P.J.Napier, J.B.West (School of Medicine, UCSD, San Diego)	10/96
161	<u>Receiver Noise Temperature, the Quantum Noise Limit, and the Role of the Zero-Point Fluctuations</u>	A. R. Kerr, M. J. Feldman, S.-K. Pan	9/96
160	<u>Digital Elevation Models for the Chainantor Site</u>	M.A. Holdaway, M.A. Gordon, S.M. Foster, F.R. Schwab, Hernan Bustos	8/96
159	<u>Wind Velocities at the Chainantor and Mauna Kea Sites and the Effect on MMA Pointing</u>	M.A. Holdaway, S.M. Foster, Darrel Emerson, Jingquan Cheng, Fred Schwab	8/96
158	<u>Correlation Between Opacity and Surface Water Vapor Pressure Measurements at Rio Frio</u>	M.A. Holdaway, Masato Ishiguro, Naomasa Nakai, Satoki Matsushita	8/96
157	<u>Exploring the Clustered Array Concept for the Atacama Array</u>	M.A. Holdaway, P.J. Napier, F. Owen	8/96
156	<u>What Fourier Plane Coverage is Right for the MMA?</u>	M.A. Holdaway	7/96
155	<u>Evaluating the Minimum Baseline Constraints for the MMA D Array</u>	M.A. Holdaway, Scott M. Foster	7/96
154	<u>Visit by Thiokol and visit to EOS and SMT</u>	Jingquan Cheng, Jeffrey Kingsley	4/96
153	<u>Fitting a 12km Configuration on the Chainantor Site</u>	M.A. Holdaway, Scott M. Foster, K.-I. Morita	4/96
152	<u>Comparison of Rio Frio and Chainantor Site Testing Data</u>	M.A. Holdaway, M. Ishiguro, Scott M. Foster, R. Kawabe, K. Kohno, F.N. Owen, S.J.E. Radford, M. Saito	4/96
151	<u>Design of Planar Image Separating and Balanced SIS Mixers</u>	A.R. Kerr, S.-K. Pan	3/96
150	<u>SIS Mixer Analysis with Non-Zero Intermediate Frequencies</u>	S.-K. Pan, A.R. Kerr	3/96
149	<u>Flux Calibration of the MMA</u>	M.A. Holdaway	2/96
148	<u>Calibration of Submillimeter Observations with SiO Masers: Does the MMA Need Dual Band Capability?</u>	M.A. Holdaway	2/96
147	<u>How Quickly Can the MMA Reconfigure?</u>	M.A. Holdaway, F.N. Owen	2/96
146	<u>An MMA Lag Correlator Design</u>	R. Escofier	11/95
145	<u>Antennas for the Millimeter Wave Array</u>	P. J. Napier, J. Cheng, D. T. Emerson, M. A. Gordon, J. B. Lugten, J. M. Payne, W. J. Welch, D. P. Woody	10/95
144	<u>Report from the Phase Calibration Working Group</u>	David Woody, Mark Holdaway, Oliver Lay, Colin Masson, Frazer Owen, Dick Plambeck, Simon Radford, Ed Sutton	10/95

143	<u>Report of the Receiver Committee for the MMA</u>	Jack Welch, John Carlstrom, Darrel Emerson, Phil Jewell, Tony Kerr, Steve Padin, John Payne, Dick Plambeck, Marian Pospieszalski, Dave Woody	9/95
142	<u>MMA Systems Working Group Report</u>	A. R. Thompson, D. Bagri, B. G. Clark, J. E. Carlstrom, L. R. D'Addario, D. Emerson, R. P. Escoffier, J. Romney, S. Padin, R. A. Sramek, D. Thornton, W. J. Welch	9/95
141	<u>Thermal Behavior of BIMA Antenna Dish Structure</u>	J. Cheng	9/95
140	<u>Outrigger Stations for the MMA</u>	R. M. Hjellming	10/95
139	<u>Fast Switching Phase Calibration: Effectiveness at Mauna Kea and Chajnantor</u>	M.A. Holdaway, Simon J.E. Radford, F.N. Owen, Scott M. Foster	9/95
138	<u>Comparing MMA and VLA Capabilities in the 36-50 GHz Band</u>	M.A. Holdaway	9/95
137	<u>Removal of Atmospheric Emission from Total Power Continuum Observations</u>	M.A. Holdaway, F.N. Owen, Darrel T. Emerson	9/95
136	<u>Correcting for Decorrelation Due to Atmospheric Phase Errors</u>	M.A. Holdaway, F.N. Owen	9/95
135	<u>ELECTROMAGNETIC PERFORMANCE COMPARISON OF AN OFFSET AND A CONVENTIONAL MMA ANTENNA DESIGN</u>	P.J.Napier	9/95
134	<u>Some Comments on Sampling, Antenna Spacings, and Uniform Aperture Illumination</u>	Wm. J. Welch	8/95
133	<u>Visit to Thermoplastic Pultrusion, Inc.</u>	Jingquan Cheng	7/95
132	<u>Visit to SMA and Bosma</u>	Jingquan Cheng	5/95
131	<u>Gain and Phase Stabilities of Some Components Used in the BIMA Array</u>	Frye et al.	7/95
130	<u>Velocity of Winds Aloft from Site Test Interferometer Data</u>	M.A. Holdaway	7/95
129	<u>Data Processing for Site Test Interferometers</u>	M.A. Holdaway, Simon J.E. Radford, F.N. Owen, and Scott M. Foster	6/95
128	<u>Sensitivity of the MMA in Wide Field Imaging</u>	M.A. Holdaway, M.P. Rupen	6/95
127	<u>Experimental Determination of the Dependence of Tropospheric Pathlength Variation on Airmass</u>	M.A. Holdaway, M. Ishiguro	3/95
126	<u>A Test of Fast Switching Phase Calibration with the VLA at 22GHz</u>	M.A. Holdaway, F.N. Owen	4/95
125	<u>Damping and Vibration Control</u>	J. Cheng	10/94

124	<u>Distances to MMA Calibrators Based on 90 GHz Source Counts</u>	S.M. Foster	10/94
123	<u>Source Counts at 90 GHz</u>	M.A. Holdaway, F.N. Owen, M.P. Rupen	10/94
122	<u>On-The-Fly-Mosaicing</u>	M.A. Holdaway, S.M. Foster	10/94
121	<u>Rectangular Panels for Offset MMA Antennas</u>	J. Cheng	8/94
120	<u>Erratum for Memo</u>	James Lamb	7/94
119	<u>The Optimum Elongation of the MMA A Configuration</u>	S.M. Foster	7/94
118	<u>Atmospheric Opacity Observations from the VLBA and CSO Sites on Mauna Kea</u>	Fred Schwab	6/94
117	<u>The Minimum Separation Problem for an Offset Slant Axis Antenna</u>	J. Cheng	5/94
116	<u>The Effect of Beam Offsets on Polarization Measurements</u>	A.R. Thompson	5/94
115	<u>Polarization Properties of an Open Cassegrain Antenna</u>	Peter Napier	5/94
114	<u>An Integrated SIS Mixer and HEMT IF Amplifier</u>	S. Padin	4/94
113	<u>Weather Conditions at the Potential MMA Site on Mauna Kea</u>	P.J. Napier	4/94
112	<u>MMA Visibility from Hilo and Topographic Shadowing</u>	M.A. Holdaway	4/94
111	<u>Preliminary MMA Configurations for Mauna Kea</u>	M.A. Holdaway	3/94
110	<u>Homologous Offset Antenna Concept for the Millimeter Array Project</u>	Jingquan Cheng	3/94
109	<u>MMA Systems Update</u>	A.R. Thompson	3/94
108	<u>Single Dish Observing and Calibration Modes</u>	D.T. Emerson, P.R. Jewell	12/93
107	<u>Sharing Time and/or Antennas Between Total Power and Interferometric Observations</u>	A.R. Thompson	1/94
106	<u>A Slant-Axis Antenna for the MMA: Computer Simulation Results of Fast Switching</u>	Jingquan Cheng	1/94
105	<u>Rapid Position Switching in Radio Telescopes: Structural Damping using a Constrained Layer Treatment</u>	Jingquan Cheng	1/94
104	<u>Scientific Emphasis of the Millimeter Array</u>	R.L. Brown, D.E. Hogg, G.R. Knapp, H.S. Liszt, B.E. Turner, H.A. Wooten	10/93
103	<u>Some Fundamental and Practical Limits on Broadband Matching to Capacitive Devices, and</u>	A.R. Kerr	9/93

	<u>the Implications for SIS Mixer Design</u>		
102	<u>A Possible Receiver Optics Layout for the MMA</u>	J. Lamb	10/93
101	<u>Slanted-Axis Antenna Design II</u>	J.Cheng	10/93
100	<u>Temperature Measurements on BIMA 6-M Antennas - Part I: Backing Structure</u>	J. Lamb, Forster	10/93
99	<u>Search for Possible Millimeter Array Sites on the U.S. Mainland</u>	C.M. Wade	8/99
98	<u>Geometry of the Slant-Axis Antenna</u>	J. Lamb	7/93
97	<u>Slanted -Axis Antenna Design I</u>	J. Cheng	6/93
96	<u>Proposed Surface Error Budget for MMA Antennas</u>	J.Lamb	5/93
95	<u>Imaging with Known Pointing Errors</u>	M.A. Holdaway	4/93
94	<u>Discussion of Slant Axis Antenna Concept</u>	J. Cheng	11/92
93	<u>Springerville / Eager Trip</u>	D.A. Webb	11/92
92	<u>Timber Ridge A Configuration Out on a Limb</u>	M.A. Holdaway	11/92
91	<u>More Remarks on MMA System Design</u>	J. Granlund	9/92
90	<u>A Study of Materials for A Broadband Millimeter-Wave Quasi-Optical Vacuum Window</u>	A.R. Kerr, N.J. Bailey, D. E. Boyd, N. Horner	8/92
89	<u>MMA Downconversion to Baseband and Sampling</u>	A. Dowd	8/92
88	<u>Paired Antenna Phase Calibration: Residual Phase Errors and Configuration Study</u>	M.A. Holaway	8/92
87	<u>Progress on Tunerless SIS Mixer for the 200 - 300 GHz Band</u>	A.R. Kerr, S.K. Pan, A.W. Lichtenberger, D.M. Lea	7/92
86	<u>Possibilities for Wide - Angle Beam-Switching</u>	J. Lamb	6/92
85	<u>Some Remarks on MMA System Design</u>	B.G. Clark	6/92
84	<u>Possible Phase Calibration Schemes for the MMA</u>	M.A. Holdaway	6/92
83	<u>Thermal considerations for MMA Antennas</u>	J.Lamb	5/92
82	<u>List of MMA Memos</u>	Trujillo	3/92
81	<u>Evaluating the MMA Compact Configuration Designs</u>	M.A. Holdaway	3/92
80	<u>Further Simulations of (possible) MMA Configurations</u>	Jing -Ping - Ge	3/92
79	<u>A Summary of the Data Obtained During the MMA Site Survey</u>	D.E. Hogg	2/92
78	<u>Report on Visit to Hat Creek</u>	J. Lamb, J. Payne	1/92

77	<u>Road Feasibility Study for MMA Sites in the Magdalena Mountains</u>	P. J. Napier	1/92
76	<u>Radio-Frequency Interference and the MMA</u>	P.C. Crane	1/92
75	<u>Lower Tropospheric Wind Speed Statistics from Rawinsonde Observations at Albuquerque, New Mexico, Winslow, Arizona and Hilo, Hawaii</u>	F. Schwab	1/92
74	<u>Surface Accuracy Requirements for Mosaicing at Millimeter Wavelengths</u>	M.A. Holdaway	1/92
73	<u>Mosaicing with Even Higher Dynamic Range</u>	M.A. Holdaway	1/92
72	<u>Circular Polarization and Multi-Band Operation : Implications for MMA Receiver Design</u>	A.R. Kerr	1/92
71	<u>MMA Systems Engineering Questions and Comments</u>	A.R. Thompson	12/91
70	<u>Image Frequency Suppression on the MMA</u>	A.R. Kerr	12/91
69	<u>SIS Mixer and Lo Options for the Millimeter Array</u>	A.R. Kerr	12/91
68	<u>A Millimeter Phase Stability Analysis of the South Baldy and Springerville Sites</u>	M.A. Holdaway	11/91
67	<u>HFET's and Receivers for the Millimeter - Wave Array</u>	M.W. Pospieszalsi	8/91
66	<u>MMA Correlator Some Design Considerations</u>	A. Dowd	5/91
65	<u>Some Considerations on the IF and Transmission System of the Millimeter Array</u>	A.R. Thompson	4/91
64	<u>Minimum Spacing Constraints for MMA Antennas</u>	J.W. Lamb	3/91
63	<u>Pointing Errors and the Possibility of Pointing Calibration</u>	M.A. Holdaway	2/91
62	<u>An Independent Simulation of Imaging Characteristics of a Millimetre Array, With and Without a Single Large Element, and an LE Pointing Correction Algorithm</u>	D.T. Emerson	11/90
61	<u>Imaging Characteristics of a Homogeneous Millimeter Array</u>	M.A. Holdaway	6/90
60	<u>Furhter Study of the Magdalena Mountain Site and Two New Arizona Sites as Possible Locations for the Millimeter Array</u>	T.Calovini, F. Owen	5/90
59	<u>Update of MMA Sensitivity Estimates</u>	R. Hjellming	11/89
58	<u>Millimeter Wave Atmospheric Opacity and Transparency Curves</u>	F. Schwab, D. Hogg	10/89

57	<u>Related Observing Speed of Single Antennas and Packed Arrays</u>	R.M. Hjellming	1/89
56	<u>Millimeter Array Correlator: Further Design Details</u>	L.D'Addario	7/89
55	<u>Millimeter Array Correlator Cost Equation</u>	L.D'Addario	7/89
54	<u>Simulations of Primary Beam Truncation and Pointing Errors with the MMA</u>	R.Braun	7/89
53	<u>On the Feasibility of South Baldy as a Site for the MMA</u>	T. Calovini, F. Owen	5/89
52	<u>Preliminary Optics Design for the Millimeter Array Antennas</u>	J. Lamb, J. Payne	12/88
51	<u>Millimeter-Wave Seeing Inferred from Radiosonde Observation-Preliminary Results</u>	F.R. Schwab, D.E. Hogg	8/88
50	<u>Report of the Central Element Working Group</u>	T. Cornwell, R.Braun, D.Emerson, and J.Uson	2/88
49	<u>Measurement of Atmospheric Phase Stability with a 225 GHz Radiometer</u>	M.McKinnon	5/88
48	<u>List of Millimeter Array Memos</u>	P. Crane	3/88
47	<u>High Site Millimeter Array Configurations</u>	R. Hjellming	2/88
46	<u>Mosaicing with High Dynamic Range</u>	R. Braun	2/88
45	<u>First Results from the Site Testing Program of the Millimeter-Wave Array</u>	D. Hogg, F. Owen, M. McKinnon	2/88
44	<u>The Size of the Central Element: Pointing Considerations</u>	T.J. Cornwell	1/88
43	<u>A Comparison of a Mosaiced VLA Image and a Conventional Penticton Image</u>	T.J. Cornwell	0/87
42	<u>Analysis of the Ekers and Rots Method of Short-Spacing Estimation</u>	T.J. Cornwell	0/87
41	<u>225 GHz Atmospheric Receiver - User's Manual ( Electronic Division Internal Report</u>	Z-Y. Liu	8/87
40	<u>Measurement of Atmospheric Opacity Due to Water Vapor at 225 GHz</u>	M. McKinnon	6/87
39	<u>Comparison Study of Astronomical Site Quality of Mount Graham and Mauna Kea</u>	K.M. Merril, F.F. Forbes	3/87
38	<u>Crystalline Antenna Arrays</u>	T.J. Cornwell	0/86
37	<u>Atmospheric Opacity at the VLA (Scientific Memorandum No. 157)</u>	J.M. Uson	2/86
36	<u>An Interim mm Astronomy Instrument</u>	R.M. Hjellming	11/85

35	<u>Factors Affecting the Sensitivity of a Millimeter Array - Further Discussion</u>	P.R. Jewell	0/85
34	<u>The Summer 1985 Concept of the Proposed NRAO Millimeter Array</u>	R.M. Hjellming	0/85
33	<u>Factors Affecting Sensitivity for the Millimeter Arrays</u>	R.M. Hjellming	7/85
32	<u>Mosaicing with the mm Array</u>	T. J. Cornwell	0/85
31	<u>The Multi-Telescope Component of the Proposed mm Array</u>	R.M. Hjellming	2/85
30	<u>The 90 meter Configuration of the Proposed NRAO mm Array</u>	R.M. Hjellming	2/85
29	<u>Sensitivity Criteria for Aperture Synthesis Arrays</u>	R.M. Hjellming	2/85
28	<u>Longer Baselines</u>	R.C. Walker	11/84
27	<u>Evaluation of 1 KM Millimeter Array Configurations with Attention to RMS Sidelobe Level and Antenna Number</u>	G.S. Hennessy, R.M. Hjellming	12/84
26	<u>Response to MMA Memo No. 22</u>	A.A. Stark	10/84
25	<u>Are We Thinking Boldly Enough?</u>	M.A. Gordon	10/84
24	<u>Brightness Temperature Limits for Filled and Unfilled Apertures</u>	T.J. Cornwell	9/84
23	<u>Wide Bandwidth Correlator</u>	B.G. Clark	9/84
22	<u>Cost Diameter Curves</u>	D. Downes	8/84
21	<u>Evaluation of Some Initial Possibilities for the Large Configurations of the Proposed mm Array</u>	R.M. Hjellming	0/84
20	<u>Some Initial Parameters of the Proposed mm Array</u>	R.M. Hjellming	0/84
19	<u>VLA Atmospheric Opacity at 225 GHz mm Array</u>	S.A. Cota, R.A. Sramek	8/84
18	<u>Quality Indicators for the MM Array</u>	T.J. Cornwell	7/84
17	<u>A Possible Optics Plan for the Multi-element Antenna</u>	B. Martin	6/84
16	<u>Report of the Millimeter Array Technical Advisory Committee of March 1984</u>	-----	3/84
15	<u>SMT Technical Memorandum UA - 84-3 Appendices</u>	B.L. Ulich	3/84
14	<u>Notes on Millimeter Array Meeting</u>	J.M. Moran	3/84
13	<u>The Relation Between Optical Seeing and Radio Phase Stability</u>	T.J. Cornwell	3/84
12	<u>Imaging of Weak Sources with Compact Arrays</u>	T.J. Cornwell	3/84

11	<u>Multi-Element Array Configurations</u>	A. Moffet	3/84
10	<u>Concept of a Compound Millimeter Array</u>	F.N. Owen	12/83
9	<u>Report of Subcommittee on Millimeter and Submillimeter- Wavelength Astronomy</u>	NSF Astronomer Advisory Committee	4/83
8	<u>VLA Phase Stability at 22 GHz on Baselines of 100m to 3 km (VLA Test Memo 143)</u>	R.A. Sramek	10/83
7	<u>Performance Considerations for Correlating Acousto-Optic Spectrometers</u>	J.W. Archer	9/83
6	<u>Cost Equation of Millimeter Wave Array</u>	S. Weinreb	9/83
5	<u>Estimate Antenna Costs - Millimeter Array</u>	W. Horne	12/82
4	<u>A millimeter-Wave Array Development Plan</u>	S. Weinreb	9/83
3	<u>Fiber Optic Links in a Millimeter Wave Array</u>	S. Weinreb	6/83
2	<u>Science with a Millimeter Array</u>	Various	2/83
1	<u>The Concept of a Millimeter Array</u>	F.N. Owen	9/82

[MMA Home](#)[Development](#)[Partners](#)[Science](#)[Meetings](#)[News & Events](#)

For back hardcopies of MMA memos, contact Lori Appel at 505-835-7310 or by e-mail at [lappel@nrao.edu](mailto:lappel@nrao.edu).

For more information on the MMA memo series, Contact Kate Weatherall at 505-835-7452 or with e-mail at [kweather@aoe.nrao.edu](mailto:kweather@aoe.nrao.edu)



*Last update 14 January 98*

**Kate Weatherall**

[kweather@aoe.nrao.edu](mailto:kweather@aoe.nrao.edu)

**“Antennas for the Millimeter Wave Array”**

**MMA Antenna Working Group**

**October 20, 1995**



**NR10**

**NO. 145**



**Antennas**  
**for the**  
**Millimeter Wave Array**

20 October 1995

Prepared by the MMA Antenna Working Group

J. Cheng<sup>1</sup>  
D. T. Emerson<sup>1</sup>  
M. A. Gordon<sup>1</sup>  
J. B. Lugten<sup>2</sup>  
P. J. Napier<sup>1</sup> (chairman)  
J. M. Payne<sup>1</sup>  
W. J. Welch<sup>2</sup>  
D. P. Woody<sup>3</sup>

---

<sup>1</sup>National Radio Astronomy Observatory

<sup>2</sup>Berkeley-Illinois-Maryland Array

<sup>3</sup>Owens Valley Radio Observatory



## Summary

This report compares two existing 8m designs for the Millimeter Wave Array (MMA) antennas. One is a conventional elevation-over-azimuth design derived from the 6m antennas used in the Berkeley-Illinois-Maryland Array at Hat Creek, California. This design uses steel for both the mount and the back structure. The other is a slant-axis design using an offset paraboloid as the primary mirror, a combination seldom if ever used in radio astronomy. This design uses steel for the antenna mount and carbon fiber reinforced plastic (CFRP) for the back structure. Both designs use cast-aluminum surface plates, milled by a numerically controlled machine and stress-relieved by thermal cycling, to form the primary mirror.

This report lists the antenna specifications required by the MMA, describes the structural elements of both designs, evaluates the performance of the designs, and estimates their costs.

This report finds that although either design would be appropriate for the MMA, each has deficiencies. The conventional design has a strong dependence of phase errors with temperature and marginal pointing performance due principally to using a yoke to support the primary surface. The offset/slant-axis design has poor polarization and field-of-view performance unless equipped with supplemental mirrors to alter the optical path from the surface to the receiver location, a modification that reduces sensitivity. Both designs fall slightly short of the performance requirements needed to calibrate phase errors rapidly.

As evaluated, we estimate each antenna to cost to be \$1.3M and \$1.5M, respectively, for the conventional and offset/slant-axis designs.

At this writing, this report recommends the conventional design for the MMA antennas. Our evaluation presumes that the phase errors will be measured every few minutes and the pointing errors, every 30 minutes. In this case the conventional design *just* meets specifications. If this frequency of calibration cannot be met or if there is a desire for operation at higher frequencies, then a better design may result from combining the best features of the two designs considered here, that is, a conventional reflector on a CFRP backstructure on a slant-axis mount.

Whatever the choice, the committee strongly recommends that a prototype antenna be tested before committing to purchasing the 40 antennas needed for the MMA—especially if the choice is a offset/slant-axis design that would be new to radio astronomy.



## Table of Contents

Summary .....	i
1. Perspective .....	1
2. Specifications .....	1
3. Antenna Environment .....	3
4. Candidate Antenna Designs .....	4
A. Conventional Design .....	5
B. Offset/slant-axis Design .....	5
5. Electromagnetic Performance .....	6
A. Relative Sensitivity .....	7
B. Polarization Purity .....	7
C. Field-of-view .....	7
D. Sidelobe Asymmetry .....	7
6. Surface Error .....	8
A. Backstructure .....	8
B. Panels .....	8
C. Secondary Mirror .....	9
D. Holographic Setting .....	9
7. Pointing Performance .....	10
8. Phase Stability .....	12
9. Fast Switching .....	13
10. Close Packing .....	14
11. Cost .....	15
12. Conclusions .....	16
A. Conclusions regarding performance .....	16
B. Questions for astronomers .....	16
C. Recommendations .....	16
References .....	17

## List of Tables

<b>Table 1: Specifications</b> .....	<b>2</b>
<b>Table 2: Antenna Structural Elements</b> .....	<b>6</b>
<b>Table 3: Electromagnetic Performance</b> .....	<b>8</b>
<b>Table 4: RMS Surface Errors (<math>\mu\text{m}</math>)</b> .....	<b>10</b>
<b>Table 5: Estimated Pointing Errors</b> .....	<b>11</b>
<b>Table 6: Phase Errors</b> .....	<b>13</b>
<b>Table 7: Fast-Switching Performance</b> .....	<b>14</b>
<b>Table 8: Close-Packing Performance</b> .....	<b>15</b>
<b>Table 9: Estimated Cost of the Antenna Designs in 1994\$</b> .....	<b>15</b>

## List of Figures

Figure 1. Wind speeds at the VLBA site .....	3
Figure 2. Wind speeds at Llano de Chajnantor .....	3
Figure 3. Air temperatures at the VLBA site .....	4
Figure 4. Air temperatures at Llano de Chajnantor .....	4
Figure 5a. The conventional antenna design .....	5
Figure 5b. The Offset/slant-axis antenna design .....	5



## **1. Perspective**

The design and selection of antennas for the Millimeter Wave Array (MMA) are a paramount part of the project. Antennas are the most expensive part of the instrument, estimated to exceed 35% of the non-recurring costs. The construction, transportation, and installation of the antennas on a high-altitude site will be difficult. Unlike software or electronics, the antennas are unlikely to be changed over the lifetime of the instrument. They will be the most permanent part of the MMA. Accordingly, this portion of the MMA planning requires special attention.

## **2. Specifications**

Chapter VII of the proposal "The Millimeter Array", submitted to the National Science Foundation in July 1990 by Associated Universities, Inc., gives the basic antenna requirements. The specifications for the antennas result partly from the site environment like the range of ambient temperatures, the variation of insolation, the speed distribution of the winds, and snow accumulation; partly from radiometric requirements like surface accuracy, polarization characteristics, pointing accuracy, stability of its optical figure, and dynamic performance related to slewing speed; partly from the array's imaging requirements like the primary field of view and close packing possibilities; and partly from practical requirements like ease of installation, mobility, durability, servicing, and cost. Table 1 summarizes the antenna specifications as currently interpreted by the MMA Antenna Working Group (AG). The AG intends the design specifications to be a reasonable compromise between feasibility and cost on the one hand and performance on the other hand, based upon *its* understanding of astronomers' needs and upon the environmental conditions at the candidate sites. The AG will review and, if necessary, change these antenna specifications in response to comments from astronomers and new information regarding the site environment.

**Table 1: Specifications**

<i>Item</i>	<i>Specification</i>	<i>Notes</i>
Aperture size	8m	
Frequency Range	30 GHz to 350 GHz	The "low frequency" 30 GHz band will be supported, when required, by switching a flat plate reflector into the optics path to shunt the low frequency beam off to the side. This technique preserves the high frequency performance
Surface accuracy	$\leq 25\mu\text{m}$ RMS	Needed for "mosaicking", i.e., the merging of contiguous MMA images. Ensures low sidelobes to preserve image integrity. Provides an aperture efficiency at 300 GHz that is 90% of the "DC" maximum, i.e., $\text{RMS} = \lambda 1.0\text{mm}/40 = 25\mu\text{m}$ .
Pointing accuracy	$\leq 1''$ RMS, 50% of time  $\leq 3''$ RMS, 75% of time	Needed for "mosaicking". This accuracy equals approximately 1/20 of the beam width at half-power at 300GHz, i.e., $1/20 \times 20'' = 1''$ . Principally determined by wind, i.e., $\leq 1''$ RMS pointing for 50th percentile wind.
Phase stability	$\leq 10\mu\text{m}$ RMS 25% of time $\leq 22\mu\text{m}$ RMS 50% of time $\leq 56\mu\text{m}$ RMS 75% of time	Specifies change in path length from the radio source to the antenna focal point. Translates principally into antenna stiffness and resistance to thermal distortion.
Dynamic performance	Preferred: move to a calibration source $1.5^\circ$ from source within 1 timesec with $3''$ pointing accuracy  Acceptable: move to calibration source $1.5^\circ$ away within 2 timesec	Permits rapid calibration of the array. Very fast slew speed and rapid structural settling required.
Subreflector Nutation	3 beamwidths at 86 GHz	Needed for total power stabilization
Close Packing	$< 10.4$ m ( $1.3 \times$ diameter)	Minimum spacing between adjacent antennas. Needed for measuring shortest interferometer spacings.
Physical design	Simple but durable	Antennas must perform well after multiple moves associated with changing configurations of the MMA, must survive storm winds, lightning strikes and moderate snow loads, and must be easy to maintain.

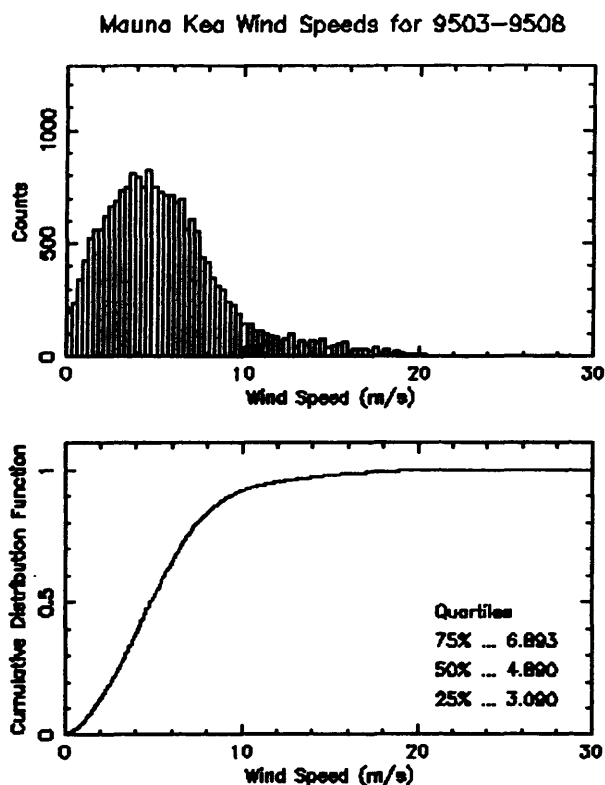


Figure 1. Distribution of wind speeds at the VLBA site on Mauna Kea, Hawaii, for March through August, 1995.

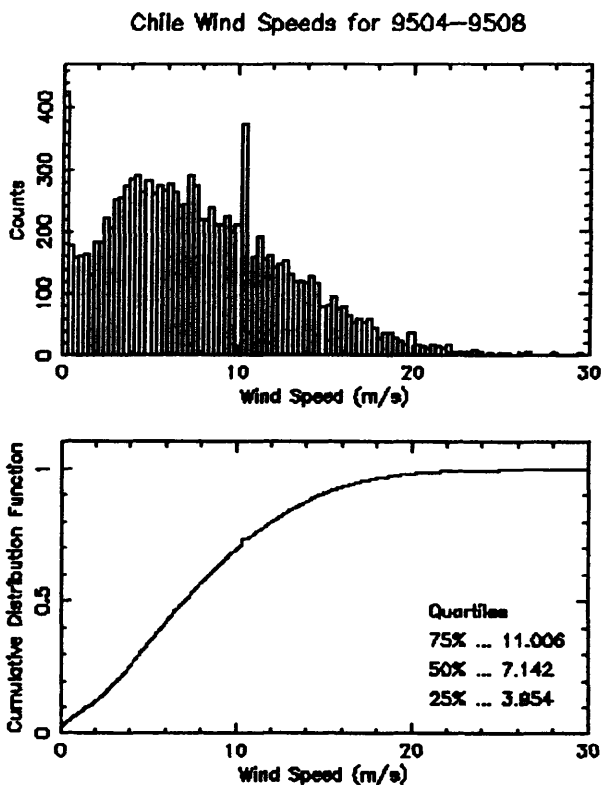


Figure 2. Distribution of wind speeds at Llano de Chajnantor, Chile, for April through August, 1995.

These antennas must facilitate observations of polarized radiation. Also, the aperture should have minimal blockage to maximize sensitivity and minimize spurious sidelobes. The optics design should support a 3x3 focal plane array at 230GHz. Mosaicking observations may require uniform aperture illumination, which can be implemented by moving a corrective lens in front of the feed.

### 3. Antenna Environment

The leading candidates for the MMA site are the shield area of the Mauna Kea volcano in Hawaii, that is, a gently sloping area to the northeast of the summit at an altitude of about 3,800m (12,500ft), and a flat region at 5,040m (16,500ft) on the Altiplano (high plateau) of the Andes mountain range 300km east of Antofagasta, Chile, and 50km east of the village of San Pedro de Atacama, Chile. The name of the Chilean site is Llano de Chajnantor. Both locations offer superb atmospheric transparency at millimeter wavelengths. At this writing, the Chilean site appears to have better atmospheric opacity, consistent with its greater altitude.

Figures 1 and 2 show the wind speeds for the Mauna Kea and Chilean sites, respectively. The median wind speed for Mauna Kea is approximately 5 m/s (11 mi/h) and for the Chilean site, approximately 7 m/s (16 mi/h). Being exposed, both sites experience high winds associated with storms, although the lower air densities of high elevation mean correspondingly lower air pressures upon the antenna structures. Figure 2 shows the Chilean site to have generally higher winds, as might be expected for a higher altitude site, and the wind speeds to have a broader range than those on Mauna Kea. Figures 3 and 4 show a range of air temperatures for these sites, measured over several months. The thin air provides little insulation against the influx of solar radiation, which will be the significant factor in the thermal response of the antenna structures.

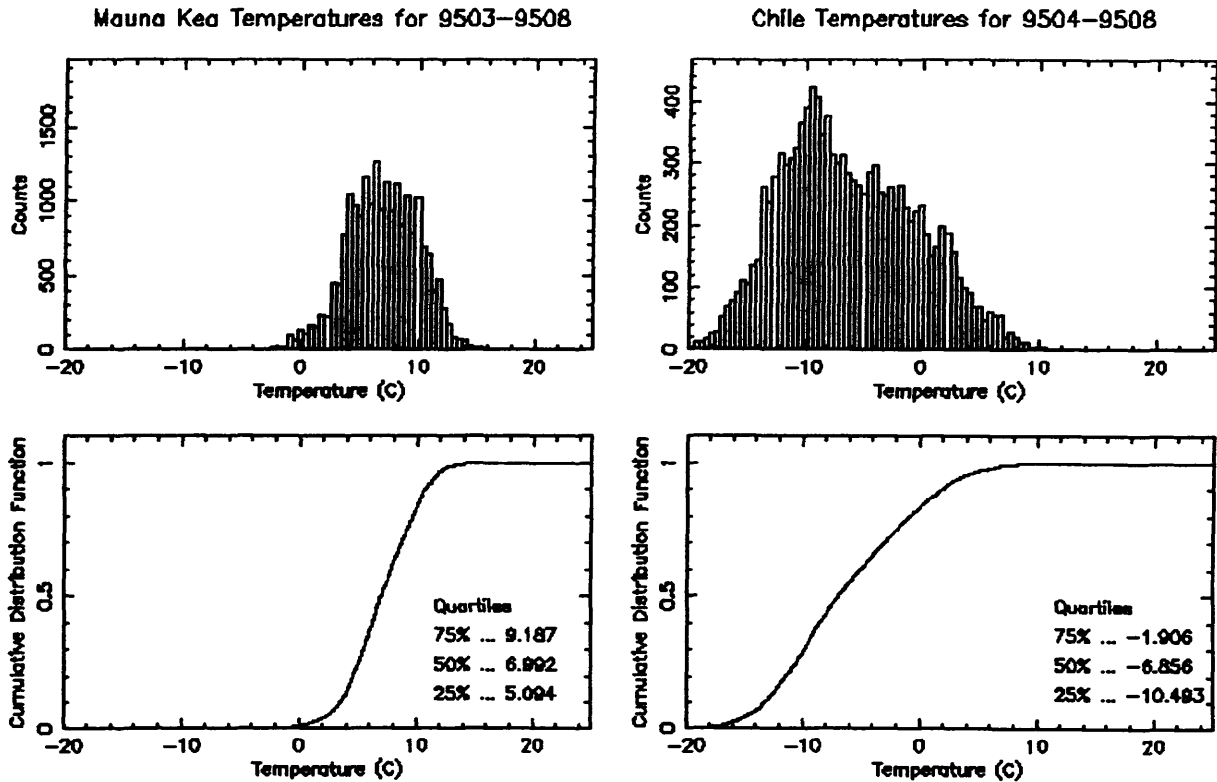


**Figure 4.** Distribution of air temperatures at the VLBA site on Mauna Kea, Hawaii, March through August, 1995. **Figure 3.** Distribution of air temperatures at Llano de Chajnantor, Chile, April through August 1995.

Perhaps most important for reliable operation of the MMA are the physiological effects of the thin air upon service personnel. Ideally, the antenna design should be as simple and robust as possible to minimize service requirements over the 30-year expected lifetime of the antennas. Also, initially as well as from time to time, it will be necessary to re-adjust the antenna surfaces at the site. The antenna design should make these re-adjustments easy to perform.

#### 4. Candidate Antenna Designs

The MMA antenna group has considered two designs, and Table 2 lists their principal structural elements. One is the conventional symmetric reflector on an "alt-azimuth" mount as shown in Fig. 5(a). The elevation and azimuth axes are orthogonal to one another. This design is based upon the proven 6m antennas used by the Berkeley-Illinois-Maryland Array (BIMA) in Hat Creek, California. Throughout this report we will refer to this design as the "conventional" design. The other design, shown in Fig. 5(b), is an offset reflector on a "slant axis" mount in which the "elevation" axis is not orthogonal to the azimuth axis, that is, slewing the upper support section alone changes the antenna position in *both* elevation and azimuth. In this report we will refer to this design as the "offset/slant-axis" design.

Both designs use cast aluminum panels whose surfaces have been cut with a numerically-controlled mill for the surface of the primary reflector. Both designs use steel for the pedestals. Both designs use carbon fiber re-enforced plastic (CFRP) for the support structures of the subreflector.

Unlike the conventional design, the offset/slant-axis design uses CFRP tubes instead of steel tubes for the back structure of the surface. It appears that CFRP is necessary for the offset/slant-axis design to meet the thermal performance specifications, whereas the conventional design is marginally able to meet the thermal requirements with steel tubes. At this writing, time prevents evaluation of both designs with identical materials. Where the material cause a significant difference in the performance or cost of the two designs, we have highlighted this difference so that the reader may judge its impact.

### A. Conventional Design

A salient feature of the conventional design is its low aperture blockage. The subreflector support legs are as thin as possible and extend to the edge of the primary reflector. This configuration eliminates the significant triangular shadowing that exists in configurations where the support legs pierce the primary reflector *inside* its edge, i.e., when the feed legs block part of the spherical wavefront reflecting from the area of the primary reflector *outside* the feed legs on its way to the subreflector. This design, together with its clean, circularly symmetric, optical path provides good electromagnetic performance. Because similar designs have often been used for radio telescopes, we can be confident of the performance of the conventional design for the MMA antennas.

This conventional design has some disadvantages relative to the offset/slant-axis alternative. One is its higher mass, which requires a stronger transporter and a better road system for reconfiguring the array. Also, the width of the yoke structure constrains the size of the receiver cabin, which must pass between the yoke arms. Most important, the yoke structure supporting the backstructure is inherently less stable than the rigid box structure of the offset/slant-axis design.

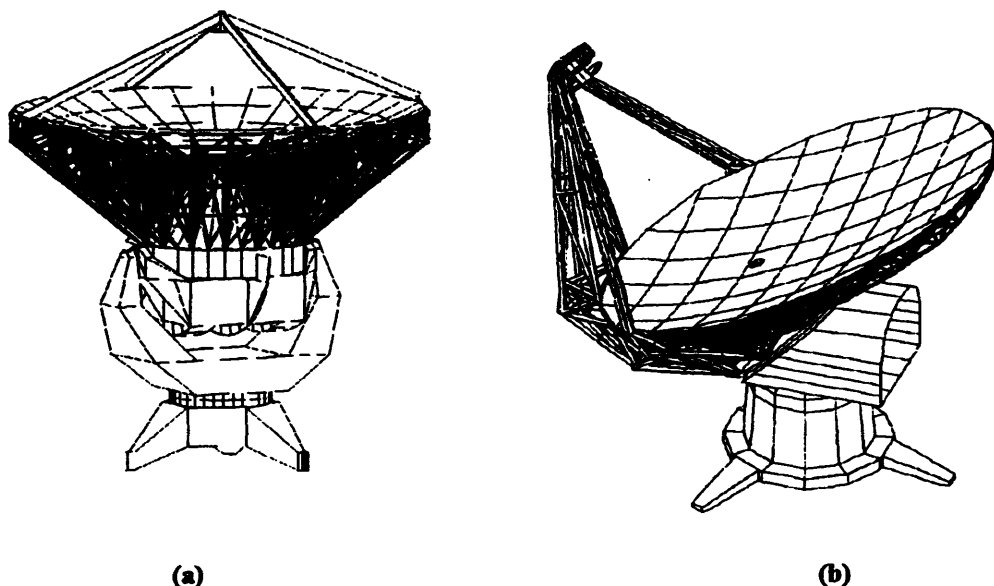


Figure 5. Two candidate antenna designs for the MMA: (a) the conventional design and (b) the offset/slant-axis design.

### B. Offset/slant-axis Design

In this design the primary reflector is an offset parabola, and the subreflector is supported by a braced monopod at the edge of the primary surface, as shown in Fig. 5b. The feeds and receivers are located in a cabin behind the center of the primary reflector. Because the subreflector and its support lie outside the aperture, the only blockage is a small hole in the middle of the primary reflector to allow the focussed beam to enter the receiver cabin. An optional optics design, which improves polarization and field-of-view performance (see section 5 below), uses two additional flat plate reflectors to bring the focussed beam down the monopod and into the receiver cabin along a path which lies behind the primary reflector, thereby eliminating the small hole in the primary reflector.

The salient features of the offset/slant-axis design are a lower aperture blockage and a lower overall mass than the conventional design. In part, the lower mass results from the absence of a counterweight. A primary structural advantage of the slant axis mount is the absence of a yoke structure, leading to a stiffer mount. The amount of space available for mounting receivers, and access to this space, is less constrained than it is in the conventional design.

A disadvantage of this design is that the asymmetry of the offset reflector degrades the polarization and field-of-view of the antenna. Furthermore, the off-axis monopod support for the secondary mirror is a cantilever structure which increases wind-induced pointing and phase errors. The bearing for the slant axis has to be large and, because the area in the middle of

the bearing is occupied by the receiver, an on-axis encoder cannot be used. A high precision off-axis encoder is very difficult to design and, hence, may contribute additional pointing errors. Because the offset/slant-axis antenna design is so different from anything previously used for radio astronomy, there is a greater risk of performance problems than for the conventional design.

**Table 2: Antenna Structural Elements**

<i>Element</i>	<i>Conventional</i>	<i>Offset/slant-axis</i>
Pedestal	Steel, 10 tonnes	Steel, 8 tonnes
Reflector mount	Steel (yoke), 13 tonnes	Steel (slant cabin), 8 tonnes
Backstructure	Steel, rectangular tubes	CFRP tubes
Primary reflector panels	Machined cast aluminum 120 triangular panels on 5 rings	Machined cast aluminum 70 rectangular panels
Feed support	High modulus CFRP tubes	CFRP box structure
Secondary reflector	Machined cast aluminum	Machined cast aluminum
Drive system Wind torque about azimuth axis Wind torque about second axis Moment about azimuth axis Moment about second axis	Friction 16x (wind pressure in Nm) 48x (wind pressure in Nm) 76 tonne-m <sup>2</sup> 58 tonne-m <sup>2</sup>	Friction 92x (wind pressure in Nm) 12x (wind pressure in Nm) 84 tonne-m <sup>2</sup> 47 tonne-m <sup>2</sup>
Thermal control	Sunshield & fans for dish Sunshield for dish ring Sunshield for yoke and pedestal	CFRP for dish and feed support Sunshield for cabin and pedestal
Encoder	Elevation - Inductosyn on axes Azimuth - Inductosyn on axis	Elevation - Off axis encoder (type unknown) Azimuth - Inductosyn on axis
Gravity loading on receivers	Varies with elevation angle	Rotates axially with cabin
Lowest natural frequency of structure	8 Hz	12 Hz

## 5. Electromagnetic Performance

Napier (1995) compares the electromagnetic performance of the two designs and Table 3 gives a summary of this comparison. The interpretation of the table entries is as follows:

### A. Relative Sensitivity

Rows 1 through 4 of Table 3 lists the relative sensitivity for the designs as a function of frequency. Column 2 gives a figure of merit that is a number proportional to the ratio (On Axis Gain)/(Total System Temperature) known as "G/T". This figure is normalized to the conventional design, whose entry is therefore set to 1.0. Row 1 indicates that at 86 GHz the offset/slant-axis design is 14% more sensitive than the conventional design. Rows 3 and 4 indicate the loss of sensitivity that occurs if 2 additional reflectors are added to the optical path of the offset/slant-axis design to improve its polarization and

field-of-view performance. To obtain these relative sensitivity results, one assumes very low values for atmospheric opacity ( $\tau=0.025$  nepers at 230 GHz) and for receiver temperature ( $T_{\alpha} = 2hf/k$  where  $h$  is Plank's constant,  $f$  is frequency and  $k$  is Boltzman's constant). Higher values of opacity and receiver temperature would reduce the sensitivity difference between the two antenna designs.

#### **B. Polarization Purity**

Row 5 shows the degradation in polarization performance caused by the asymmetry of the offset design. This degradation can be eliminated by adding two additional reflectors to reroute the optical path outside the monopod support and under the primary reflector.

#### **C. Field-of-view**

Field-of-view is a measure of how rapidly the beam deteriorates when the feed is moved in the focal plane away from the optical axis. The MMA needs a field-of-view sufficient to accommodate future focal plane array feeds, to allow off-axis feeds, if desired, in place of an on-axis rotating mirror for receiver selection, and to accommodate a nutating subreflector for total power stabilization.

Row 6 shows the degradation in field-of-view caused by the asymmetry of the offset/slant-axis design. The number given is the reduction in peak gain that results when the feed is translated in the focal plane by a distance which causes 4.2 beamwidths (BW) of beam scan. This amount of translation is appropriate for the corner elements of a 3x3 focal plane array in which the feed elements are separated by 3 BW.

#### **D. Sidelobe Asymmetry**

For either of the proposed mount designs, the antenna beam rotates on the sky as a radio source is tracked. If the beam and sidelobes are not sufficiently circularly symmetric, software corrections will be required to correct for the effect of beam rotation. The conventional design will have a small amount of sidelobe asymmetry due to the unsymmetric quadrupod blockage. Row 7 shows, for an aperture illumination taper of -10 dB, the difference in the level of the first sidelobe in the plane of the feed legs and in the 45 deg plane between the feed legs. The aperture illumination for the offset/slant-axis design will be slightly asymmetric, but the amount of asymmetry has yet to be calculated.

**Table 3: Electromagnetic Performance**

<i>Parameter</i>	<i>Conventional</i>	<i>Offset/slant-axis</i>
Relative Sensitivity (G/T) at 86 GHz	1.0	1.14
Relative Sensitivity (G/T) at 230 GHz	1.0	1.08
Relative Sensitivity (G/T) at 86 GHz with 2 tertiary reflectors added to correct polarization and FOV	Not required	0.91
Relative Sensitivity (G/T) at 230 GHz with 2 tertiary reflectors added to correct polarization and FOV	Not required	0.90
Polarization Purity	No degradation due to antenna. Limit imposed by feed and polarizer	Circular Pol.: 0.14 BW separation between LCP and RCP beams.  Linear Pol.: -22 dB cross polarized sidelobes.
Field of View: gain loss for 4.2 BW scan.	0 dB	-2.6 dB
Sidelobe asymmetry due to blockage	1 dB	0 dB

## 6. Surface Error

The "total surface error" for an antenna describes a hypothetical antenna with an imperfectly reflecting surface, that is, one assumes that all other components of the radiation path are perfect and that their contributions to the total surface error are negligibly small. Thus, total surface error is a figure of merit that one calculates by combining the errors contributed by parts of the actual antenna by the root of the sums of the squared errors (RSS). This arithmetical method weights the larger contributions heavily and has proved to give a reliable error estimate of an actual antenna.

Table 4 lists estimates for the contributions of individual components to the overall surface accuracy seen by incoming radiation to the antennas. John Lugten estimated the errors for the conventional design and Jingquan Cheng, the errors for the offset/slant-axis design.

### A. Backstructure

Row 1 of Table 4 discusses the error contributions due to the reflector backup structure. Gravity induced errors are larger for the conventional design because of the load of the quadrupod structure supported at the edge of the main reflector. Thermally induced deformations have been estimated using temperature gradients actually measured on the existing antennas of the BIMA array. It is likely that these temperature gradients could be reduced by improving the BIMA thermal control system, so these estimates should be regarded as conservative estimates. The steel backstructure of the conventional antenna has a larger coefficient of thermal expansion, correspondingly, larger errors induced by thermal gradients than the CFRP backstructure of the offset/slant-axis design. Thermal deformations of the conventional antenna could be reduced approximately to the same value as the offset/slant-axis if its backup structure were also made of CFRP.

### B. Panels

Row 2 of Table 4 estimates the contributions of the surface panels to the total surface error of the antennas. Both the BIMA and the Submillimeter Array (SMA) organizations have found that cast aluminum panels can be machined to an accuracy of  $\leq 8\mu\text{m}$  RMS. Typically, such panels are cast in the form of a thin surface supported by deep ribs to produce rigidity with minimum weight. This design also produces a large surface area for good coupling of the panel with the thermal

environment. Each panel is a section of a paraboloid and, therefore, has a curved surface. Isothermal changes in the panel temperature change the panel focal length without changing the RMS surface error of any given panel. However, if each panel of the surface has a different temperature, then each will assume a different curvature or focal length, and the RMS of the *entire* surface of the antenna will increase. Additional sources of surface errors contributed by the panels are deformations produced by wind pressure and gravity.

The differences in the error contributions of the panels between the conventional and offset/slant-axis designs are due principally to the larger size of the panels used in the latter design.

#### **C. Secondary Mirror**

Row 3 describes errors contributed by the secondary mirror. These are essentially the same for both designs. Manufacturing errors dominate this component.

#### **D. Holographic Setting**

This row presumes that final adjustment of the antenna surfaces will be made by comparing the phase of an incoming plane wavefront to that reflected from the primary mirror. Knowing the wavelength of the incoming waves, one converts the phase differences from angular to linear units. In radioastronomy this technique is called "holography" because it uses phase as well as amplitude information to make an image of the primary mirror. It has become the standard way to adjust the surfaces of antennas used for millimeter wavelengths. Presently, experience shows it's possible to measure the surface figure and set the surface panels within about  $8\mu\text{m}$ .

**Table 4: RMS Surface Errors ( $\mu\text{m}$ )**

<i>Error source</i>	<i>Conventional Design</i>	<i>Offset/slant-axis Design</i>	<i>Notes</i>
Backing structure gravity(ideal) gravity(non-ideal) absolute temp temp gradient wind total	12. 2. 1.5 18. * 1. 21.8	8. 4. 2. 10. 3. 13.8	*Daytime worst case error. Night time performance is significantly better. With CFRP backup structure, would be same as offset/slant-axis design
Panels manufacture absolute temp temp gradient gravity wind Panel mounting total	6. 2. 2. 1.5 1. 0.5 6.9	9. 4. 4. 6. 6. 1. 14.*	* Larger rectangular panels are proposed for offset design. Both designs use same type machined cast aluminum panels
Secondary mirror manufacture absolute temp temp gradient gravity wind aging* alignment total	6. 0.5 1. 1. 0.5 0.5 2. 6.3	6. 0.5 1. 1. 0.5 2. 2. 6.8	*Secondary mirror larger for offset/slant-axis design
Holographic setting total	8.	8.	
Grand total (RSS)	25.	22.	

## 7. Pointing Performance

The pointing errors for any antenna fall into two classes: repeatable and non-repeatable. Repeatable errors are those associated with physical effects that remain unchanged for long periods such as weeks or months or years. This category includes gravitational deformations, bearing irregularities, and foundation settling. Calibration at appropriate intervals can compensate for these errors. Repeatable errors are thus easily accommodated and are not considered further here.

Non-repeatable errors in a well-behaved structure stem from two main causes: temperature and wind. Errors from both sources can be reduced (but seldom eliminated) by instrumentation such as multiple temperature sensors, electronic levels, and lateral displacement sensors. The difficulty of installing, implementing and maintaining such instrumentation on the forty MMA antennas has persuaded us to avoid designs requiring such complex corrections. Nonetheless, provision must be made for the installation of such instrumentation so that it can be used to improve performance if required.

A major problem in analyzing pointing changes resulting from thermal effects is to define accurately the temperature distribution over the antenna structure. For this purpose we have made extensive use of a series of temperature measurements made on a BIMA antenna by Lamb and Forster (1993). Row 1 of Table 5 summarizes the thermal pointing errors for both the conventional and offset/slant-axis antenna designs. The temperature differences and rates of change of temperature are estimates based on the BIMA 6m measurements. These are typical summer daytime values at Hat Creek and each corresponds to an RMS temperature deviation across the antenna surface of 0.6C and a feedleg temperature difference of 1.5C. With the expected rate of change of thermal pointing error for the conventional antenna, an astronomical pointing calibration every 30 minutes will be sufficient to keep pointing errors below one arc second.

Row 2 of Table 5 summarizes the wind induced pointing errors. In contrast to the thermal effects, the wind-induced pointing errors are straightforward to calculate. The total wind induced error is the RSS of the component values and the errors vary as the square of the wind velocity.

**Table 5: Estimated Pointing Errors**

<i>Item</i>	<i>Conventional Design</i>	<i>Offset/slant-axis Design</i>	<i>Notes</i>
<b>Daytime Thermal Pointing Errors</b>			
Dish RMS Error	1.2 arcsec*	0.2 arcsec	* The conventional antenna with a CFRP backing structure will perform as well as the offset/slant-axis antenna. **A tilt meter, thermal insulation, and active temperature control will reduce these values
Feedleg RMS Error	0.2 arcsec	negligible	
Yoke RMS Error	0.9 arcsec**		
Total RSS Error	1.5 arc sec	0.2 arcsec	
Rate of Change of error	1.3 arcsec/hr	negligible	
<b>Typical Wind Pointing Errors</b>			
Secondary Mirror*	0.6 arcsec	1.0 arcsec	* Assumed 9m/s (20 mi/h) for wind speed
Yoke Structure*	0.9 arcsec	0.	
Other*	0.5 arcsec	0.1 arcsec	
Total Wind RSS Error	1.2 arcsec	1.0 arcsec	
<b>Scaled RSS Wind Pointing Errors*</b>			
12 m/s (27 mi/h)	2.1 arcsec	1.8 arcsec	* Wind-induced errors should scale as v <sup>2</sup>
6 m/s (13 mi/h)	0.6 arcsec	0.5 arcsec	
3 m/s (7 mi/h)	0.2 arcsec	0.1 arcsec	
<b>Total Wind and Thermal Pointing Errors, RSS</b>			
12 m/s (27 mi/h)	2.6 arcsec	1.8 arcsec	

**8. Phase Stability**

"Phase errors" is a term used to describe the errors in the detected phase of incoming wavefronts, that is, phase errors induced by the antenna system through variations in the wave pathlength. In an interferometer such errors degrade

sensitivity and image quality. As with pointing errors, phase errors fall into two classes: repeatable and non-repeatable. Repeatable errors result from structural variations from one antenna to another, from variations in cable or waveguide sections, etc. Such errors are long-term, can be easily compensated through calibration, and will not be further discussed here. In contrast, non-repeatable pathlength changes are primarily caused by thermal and wind deformations of the antenna and, as such, can vary on short time scales.

Table 6 lists the sizes of these pathlength errors for the two antenna designs. Data row 1 details the thermal phase errors. Again, as with pointing, the difficulty with the thermal analysis is to know what temperature distribution and rate of change of temperature to assume for the antenna structure. We use the same BIMA measurements described in section 7 above typically observed in about a 30 minute time period. Within this time interval the temperature changes for the mount and reflector backup structure are 1C and 1.5C during the day and 0.3C and 0.5C at night. The size of the RMS pathlength errors resulting from these temperature changes is shown in Table 6 as "phase error". In the column "after calibration" is the residual path length error if phase is calibrated astronomically every 3 minutes. The residual phase errors increase proportionately for calibration intervals longer than 3 minutes.

Data row 2 of Table 6 gives the RMS pathlength errors due to wind deformation of the antenna. The calculation assumes that wind phase errors will vary sufficiently rapidly so that they cannot be corrected with phase calibration on a 3-minute time scale.

Data row 3 provides a phase error budget for miscellaneous items such as bearings, panel adjusters, receiver position and other structural deformation.

**Table 6: Phase Errors**

Item	Conventional Design		Offset/slant-axis Design	
	Phase Error	After calibration every 3 min	Phase Error	After calibration every 3 min
Thermally-induced errors (peak value)				
Thermal gradient (daytime)	140 $\mu\text{m}$ *	14 $\mu\text{m}$	50 $\mu\text{m}$	5 $\mu\text{m}$
Thermal gradient (nighttime)	45 $\mu\text{m}$ *	5 $\mu\text{m}$	30 $\mu\text{m}$	3 $\mu\text{m}$
Wind-induced errors (peak value)				
12 m/s (27 mi/h) wind	26.7 $\mu\text{m}$	26.7 $\mu\text{m}$	17.8 $\mu\text{m}$	17.8 $\mu\text{m}$
9 m/s (20 mi/h) wind	15 $\mu\text{m}$	15 $\mu\text{m}$	10 $\mu\text{m}$	10 $\mu\text{m}$
6 m/s (13 mi/h) wind	6.7 $\mu\text{m}$	6.7 $\mu\text{m}$	4.5 $\mu\text{m}$	4.5 $\mu\text{m}$
3 m/s (7 mi/h) wind	1.7 $\mu\text{m}$	1.7 $\mu\text{m}$	1.1 $\mu\text{m}$	1.1 $\mu\text{m}$
Other errors (peak value)				
Miscellaneous sources	10 $\mu\text{m}$	10 $\mu\text{m}$	10 $\mu\text{m}$	10 $\mu\text{m}$
Total RMS errors				
Best condition		5 $\mu\text{m}$		2 $\mu\text{m}$
Average condition		7 $\mu\text{m}$		4 $\mu\text{m}$
Worst condition		10 $\mu\text{m}$		6 $\mu\text{m}$

\* These large values result from using different materials for the quadrupod (CFRP) and reflector backup structure (steel). Using CFRP for the back structure will reduce the errors of the conventional antenna to approximately the same values as the offset/slant-axis design.

## 9. Fast Switching

Phase errors caused by the atmosphere can quickly vary. To compensate for these errors, it is theoretically possible to move all the antennas rapidly to a nearby calibration source and then back to the astronomical source. This "fast-switching" calibration cycle would need to occur within six seconds to be effective. This calibration scheme requires antennas that can slew and settle extremely rapidly. Such slew rates can excite structural resonances, in particular those involving lateral movements of the subreflector. Woody (1995) has shown that slewing using carefully profiled trajectories can minimize the excitation of these resonances. The trajectories must be very smooth, probably requiring friction drives without gears.

Table 7 lists the antenna performance we might expect. The pointing errors listed are the RMS pointing errors remaining after initiating the fast switching cycle. We assume the amount of damping to be the natural damping provided by the construction materials. Even with the improved switching profile, the residual pointing errors are several times larger than needed. We expect that further work on a fully optimized switching profile can reduce the errors to meet specifications. However, the risk remains that our simplified computer models do not predict the actual dynamic performance adequately. If further improvement is needed, it may be possible to use active or passive damping on troublesome parts of the structure.

Our preliminary calculations as well as discussions with manufacturers of damping technology suggest that such damping techniques will work. These techniques are new and untried in antenna technology. They will require a development program which, like all such programs, may not be successful. Therefore, we believe it essential to construct and test a prototype antenna before commencing full production of the 40 MMA antennas.

**Table 7: Fast-Switching Performance**

<i>Time</i>	<i>Conventional (8 Hz resonance) Error after 1.5° step</i>	<i>Offset/slant-axis (12 Hz resonance) Error after 1.5° step</i>
<b>Normal Slew Trajectory</b>		
After 1 second time	50 arcsec	35 arcsec
After 2 seconds time	15 arcsec	10 arcsec
<b>Improved Slew Trajectory</b>		
After 1 second time	12.5 arcsec	8 arcsec
After 2 seconds time	5.0 arcsec	3.5 arcsec

## 10. Close Packing

Images of spatially extended objects require observations with the shortest possible interferometer baselines (Welch, 1995), a configuration known as "close packing" of the antennas. Specifically, close-packed configurations enable measurements of spectral components at small u-v coordinates, which contain significant information for spatially extended objects.

Table 8 lists the closest possible separations for the MMA array using the two antenna types. Row 1 gives the smallest separation between antenna centers for random orientations of the antennas. This case is the most conservative because it allows for inoperative antennas. Row 2 gives the smallest separation that can be allowed if all antennas are pointed in the same direction. This case is the most optimistic. It requires reliable anti-collision sensing equipment and shutdown switches on the array because, if antennas do not point in the same direction for any reason, they can collide.

When two antennas are close together, one antenna can block radiation from the one behind it when observing sources at low elevation. This condition, known as "shadowing", is a design consideration for multi-element interferometers. It appears that, for the MMA configurations, there is no significant difference between the two antenna designs with respect to the amount of shadowing providing the antennas are pointing in the same direction.

**Table 8: Close-Packing Performance**

<i>Case</i>	<i>Conventional Design</i>	<i>Offset/slant-axis Design</i>
Safe minimum packing distance between antennas. No protection required.	1.53×diameter = 12.2 m	1.36×diameter = 10.9 m
Minimum packing distance between antennas pointing in same direction. Collision protection required.	1.13×diameter = 9.04 m	1.20×diameter = 9.60 m

**11. Cost**

Table 6 compares the estimated cost of the two antenna designs. These estimates result from experience building antennas for the BIMA interferometer at Hat Creek, California, and the Submillimeter Array now being constructed on Mauna Kea, Hawaii. While we believe the accuracy of these estimates to be in the 10-20% range, additional studies will be necessary to confirm these costs.

**Table 9: Estimated Cost of the Antenna Designs in 1994\$**

<i>Element</i>	<i>Conventional Design</i>	<i>Offset/slant-axis Design</i>
Simple steel structure (\$1/pound)	\$110,000	\$60,000
Bearings	35,500	70,000
Panels	150,000	170,000
Drive system	100,000	100,000
Surface back structure		
Dish	100,000*	230,000
Sub-reflector support	80,000	150,000
Panel adjusters	40,000	30,000
Subtotal	220,000	410,000
Encoder	70,000	100,000
Thermal control	25,000	15,000
Sub-reflector mirror	30,000	40,000
Pointing instruments	60,000	60,000
Transportation and assembly	400,000	400,000
Other	100,000	100,000
Grand total	\$1,300,000	\$1,525,000

\*Increase by approximately \$150,000 for CFRP instead of steel structure

## 12. Conclusions

We divide the conclusions drawn from this initial work on the antenna design into three broad categories:

### A. Conclusions regarding performance

i. The conventional antenna design with CFRP feed support and steel backing structure gives excellent electromagnetic performance. This design meets the current specifications regarding pointing accuracy, surface accuracy and phase stability *if* phase calibration is performed every few minutes and pointing calibration, every 30 minutes. The mix of structural materials leads to a strong dependence of phase errors upon temperature. Using CFRP instead of steel for the surface back structure would greatly reduce these errors. The yoke structure is inherently less stable than the corresponding box structure of the offset/slant-axis design, but the instabilities appear to be manageable—especially if insulation and thermal control are used.

ii. The offset/slant-axis design also meets all current specifications. Although the simple asymmetric optics lead to poor polarization and field-of-view performance, the addition of two reflectors to the optical path can overcome these problems but at the cost of reduced G/T performance. These reflectors would reroute the optical path from the subreflector around the edge and under the primary surface rather than through a hole in the primary. The concomitant reduced G/T performance is significant only when the antennas are used at the very best site with the very best receivers, that is, at the extreme limit of the array capability.

iii. Each design falls slightly short of the fast switching and settling requirement. Additional work is needed to develop and refine the switching algorithms and to determine the feasibility and cost of active or passive damping to reduce the structural settling time.

### B. Questions for astronomers

i. Are the frequent phase and pointing calibrations required by the conventional antenna with a steel backstructure acceptable? This calibration procedure may not be adequate if the MMA performance is extended into sub-mm bands. Would the increased cost (approximately \$150k per antenna, or \$6M for 40 antennas) of a CFRP backstructure be justified by the improved performance of the conventional antenna?

ii. Are the relatively poor polarization and off-axis performance of the offset/slant-axis design serious problems? Although additional mirrors can overcome these specific problems, is the accompanying degradation in G/T acceptable?

iii. Is the wind speed adopted for the pointing specification reasonable? This leads to an RMS pointing error of 1 arcsec 50% of the time.

iv. Is subreflector nutation necessary? While subreflector nutation is possible with either antenna design, it increases costs by approximately \$800K for 40 antennas and increases complexity. If necessary, is nutation only in the azimuth direction adequate?

### C. Recommendations

i. Based upon the analysis available now, the AWG would choose the conventional design for the MMA antennas although either design would be acceptable, each with different shortcomings. For both designs, more design work is required to meet the stringent specifications for fast switching and settling. Additionally, the AWG believes it would be prudent to investigate a combination of the two designs discussed here: a conventional reflector with a CFRP back structure on a slant-axis mount. If frequent calibration for phase and pointing errors is not possible, then the combination structure would be a better design.

ii. The AWG believes that the stringent performance specifications (particularly the fast switching) make it prudent to build and test a prototype antenna before committing funds for the remaining 40 antennas.

## **References**

Lamb, J. and Forster, R, "Temperature Measurements on BIMA 6-m Antennas—Part I: Backing Structure", MMA Memo No 100, 1993.

Napier, P. J., "Electromagnetic Performance Comparison of an Offset and a Conventional MMA Antenna Design", MMA Memo No 135, Sept., 1995.

Welch, W. J., "Some Comments on Sampling, Antenna Spacings, and Uniform Aperture Illumination", MMA Memo No 134, 1995.

Woody, D. P., "Optimized Trajectory for Fast Position Switching", in preparation, 1995.

# MMA Memo 190: A System Design for the MMA

A. R. Thompson

November 6, 1997

This report is concerned with the MMA receiving system and is based upon discussions of the MMA systems group. The part of the system considered here includes the signal paths from the outputs of the front ends to the digital samplers, and the local oscillator (LO) system, but does not include details of the front ends, the digital delays or the correlator. The system shown is designed to work with optical fiber transmission of IF signals in *analog* form from the antennas to the Electronics building at the site. Some discussion on the choice of analog or digital transmission can be found in MMA Memo.142. The digital alternative is not ruled out. It remains under study and will be discussed in a later memorandum. With digital transmission practically all of the system discussed here would remain, but some of it would be relocated to the antennas and some further hardware would be required. It is clear that digital transmission would result in a more expensive and complicated system. Measurements with the two-element prototype system should be used to help verify the final choice of analog or digital transmission.

At this point in the project development the intention is to provide a broad outline of the proposed system. The diagrams indicate the signal flow through the system by showing mainly filters, mixers and switches. Amplifiers, attenuators, isolators, etc. will be added as design details are developed, and precise frequencies of filters, LOs, etc. may require minor adjustments. A simplified block diagram of the overall system is shown in Fig. 1. Components at the left-hand side of the optical fibers in the IF and LO paths are located at the antennas and those at the right-hand side are in the Electronics building which also contains the delay system and correlator. Signals from the Cassegrain feeds are converted to IFs in the front ends. There are approximately ten front ends covering the total observing range of the MMA. The IF signals from the front end that is selected at any time are transmitted to the Electronics building in the form of two 8 GHz-wide analog bands. At the Electronics building the signals are split into eight baseband channels and filtered, digitized, delayed and correlated. A frequency standard provides the reference frequencies for various local oscillators and for timing of the digital units. For the LOs at the antennas, frequencies are generated at the Electronics building and are transmitted to the antennas on optical fibers. Another fiber may be provided for measurement of the round-trip phase. Appropriate phase switching and fringe-frequency phase rotation are inserted through to LO system. A monitor and control system interacts with all parts of the electronics.

### Signal Paths at the Antennas

Figure 2 shows the system at the antennas. The front ends for frequencies above approximately 115 GHz will use SIS mixers and those below 90 GHz will use HFET amplifiers. The choice for the 90-115 GHz has not yet been made. The SIS mixers will have separate outputs

for the upper and lower sidebands. Thus there will be four IF outputs from each SIS front end, to provide signals for two polarizations and two sidebands. Each output goes to one of four 1x10 switches. An IF band spanning 4 to 12 GHz (i.e. a bandwidth of 8 GHz) for each of the two polarizations can be accommodated. SIS mixers used by NRAO currently have IF bandwidths no greater than 2 GHz, but a mixer with a 4 GHz IF bandwidth and good noise temperature has been demonstrated by Padin et al. (1996) using an IF stage integrated with the mixer. It is felt that 8 GHz bandwidth is an achievable goal within the construction period of the MMA. However, in the shorter term the noise temperature of SIS front ends matched to a 4 GHz bandwidth may be better than those matched to the full 8 GHz bandwidth. Thus, instead of two 8-GHz-wide bands it may be preferable to use four 4-GHz-wide bands from each SIS front end (i.e. both polarizations for upper and lower sidebands) in order to maximize the sensitivity. By means of the four 1x2 and two 1x3 switches shown in Fig. 2, the input to each optical transmitter can be selected to come from either one 4-12 GHz front end output or two 4-8 GHz front end outputs, one of the latter being converted to 8-12 GHz for transmission on the fiber. Note that a rearrangement of the components shown plus the addition of two optical transmitters would allow the signals to be transmitted as to the building as four bands of width 4 GHz, although it is not expected that there will be any difficulty in transmitting 8 GHz bandwidths over fiber lengths up to 20 km.

The HFET-amplifier front ends have separate outputs for the two polarizations. The maximum bandwidth of any of the HFET front end is approximately 26 GHz. The first IF for the HFET front ends is 14 to 22 GHz, so there is a frequency space of 28 GHz between the upper and lower sideband responses at the mixer that converts to the first IF. Thus for most HFET front ends it should be possible to avoid an image response if a filter is included to confine the amplifier response to the nominal band. If necessary the LO can be on the low side when the required IF band is in the lower half of the HFET band and on the high side when the required band is in the upper half of the HFET band, to keep the image response further away from the amplifier passband. Note that the IF band 14-22 GHz is about as low in frequency as is possible to use while avoiding direct feed through to the 4-12 GHz band. For reasons of cost it is preferable to keep intermediate frequencies as low as possible, but the IF bandwidths required place lower limits on the frequencies because of the need to avoid image responses, etc.

The arrangement of switches shown in Fig. 2 is one of several possibilities and the final system design will have to take into account the availability and cost of different types of switches. Some modes of operation of the array may require continuous switching between two front ends at intervals of  $\sim 10$  sec. Specified lifetimes of some mechanical switches are  $\sim 10^6$  cycles, which could be reached after about 100 days of such operation. Thus solid state switches may be necessary.

### **IF Signal Processing at the Electronics Building**

Each of the 4-12 GHz IF bands is demultiplexed into four 2 GHz-wide bands when received at the Electronics building. Figure 3 shows the circuitry for the signal from one optical fiber. Two such Demultiplexer units are required for each antenna. The basic reason for this frequency demultiplexing is that the maximum clock frequency of the samplers is 4 GHz. All four 2 GHz-wide bands are converted to the same frequency (2-4 GHz) so that in the next stage of signal processing they can be handled by identical baseband units. The 2-4 GHz filters at the outputs of this unit require a sharp response at the 4 GHz edge, since when using the full bandwidth the

signals are converted to baseband with the 3.2-5.2 GHz LO (see Fig. 4) tuned to 4 GHz in the Baseband Converters. The switching network allows the four outputs to be connected to four Baseband Converter inputs in any manner desired. For example, all four Baseband Converters may be connected to one 2 GHz-wide IF band if one wishes to study four narrow lines that all lie within the same 2 GHz-wide band. The switching network could be implemented by a combination of four 4-way power dividers and four single-pole, 1x4 switches.

In the Baseband Converter unit in Fig. 4, the input signal at 2-4 GHz is converted to the baseband range and filters are provided for selection of bandwidths from 2 GHz down to 31.25 MHz in steps of a factor of two. The 3.2-5.2 GHz LO at the first frequency conversion is tunable to allow the response of the Baseband Converter to be set at any part of the 2-GHz-wide IF input band. In designing the Baseband Converter, it was decided to use a system involving a number of frequency conversions with filters chosen to reject the unwanted sideband responses, rather than using a sideband-separating mixer scheme because the latter, although simpler, does not provide sufficient rejection of unwanted sidebands. The widest bandwidth, 0.1-2.0 GHz, may contain a small unwanted component which arises from conversion of residual frequencies in the 4 GHz skirt of the 2-4 GHz filters. This component consists of frequencies that are folded into the low frequency end of the baseband by the conversion process, and the filter response rejects frequencies below 0.1 GHz to minimize such unwanted signals. (The 0.1 GHz filter edge is a nominal value at this time and may require adjustment when the response of the 2-4 GHz filters in the demultiplexing unit (Fig. 3) is specified in detail.) The 1-2 and 1-1.5 GHz filters are far enough away from the low end of the 0-2 GHz baseband to be free from such unwanted components. Similarly the two frequency bands following each of the 1.5 GHz and 375 MHz LOs are well above zero frequency and will not include unwanted components from spectrum fold-over at an LO frequency. Listed below are the bandwidth of each filter, the frequency range of the passband as seen at the output of the first mixer (the one with the 3.2-5.2 GHz LO), and the tuning range of the LO which just covers the 2-4 GHz input band in each case. Images fall above 4 GHz in all cases.

Bandwidth	Filter response as seen at output of first mixer	LO tuning range
1.9 GHz	0.1-2.0 GHz	4.0 GHz
1.0 GHz	1.0-2.0 GHz	4.0-5.0 GHz
500 MHz	1.0-1.5 GHz	3.5-5.0 GHz
250 MHz	1.0-1.25 GHz	3.25-5.0 GHz
125 MHz	1.125-1.25 GHz	3.25-5.125 GHz
62.5 MHz	1.1875-1.250 GHz	3.25-5.1875 GHz
31.25 MHz	1.1875- 1.21875 GHz	3.2187-5.1875 GHz

The fractional bandwidths of the filters, other than the two widest ones, are in the range 0.4 to 0.67. Note that if the chosen output band comes from one of the three widest filters, the input of the 1.5 GHz LO signal to the module should, if necessary, be turned off to prevent pickup of this LO frequency in the earlier filters. Similarly, unless one of the two narrowest bandwidths is being used the 375 MHz signal should be switched. The filtered outputs are sampled at a 4 GHz clock rate and digitized. The digital data go to the delay and correlator systems and redundant samples for the bandwidths of 1 GHz and less are removed as necessary at an appropriate stage. Eight Baseband Converter units are required for each antenna.

## Total Power Observations and Signal Level Control

In the IF system at the antennas (Fig. 2) detectors are shown which measure the IF signal level in the 4-GHz-wide and 8-GHz-wide bands at the inputs to the optical transmitters. In the Baseband Converter (Fig. 4) a detector is shown which measures the level of the signal going to the digital sampler. These detectors perform two functions. First, they can be used for total power measurements. Those at the antenna would be used for wide-band continuum measurements. For total power measurements in spectral line mode the autocorrelation outputs of the correlators are required. Note that at the antennas it is possible to make total power measurements on all four 4-12 GHz outputs of an SIS front end simultaneously, thus making use of twice the bandwidth that is available in interferometer mode.

The second use of the detectors is to check the IF level at two points where the level is critical. One of these is the inputs to the optical transmitters in which nonlinearity can occur if the level is too high, and loss of SNR can occur if the level is too low. The other point is the sampler input where it is necessary to know the reference levels in terms of the rms input noise level. In either case some range of level variation is acceptable, and it is considered that use of an ALC loop may be undesirable. However, a variable attenuator or a variable-gain amplifier (not shown in the figures) will be included in the signal path ahead of each detector. These gain controls and the detector outputs will be accessed through the monitor and control (M/C) system. Thus various control schemes including adjustment in discrete steps, full ALC, sample-and-hold, etc. can be implemented through a control computer. If on-the-fly mapping or subreflector nutation are used in observing, then it may be necessary to measure the gain for a particular reference direction of the beam.

As a means of calibrating the system noise and gain, it is proposed to inject a controlled level of noise into the front ends in a switched sequence including zero additional noise and two levels chosen to increase the system noise by a few percent. An arrangement involving thermal sources radiated from a small aperture in the antenna subreflector is being investigated at Berkeley.

## Phase Switching and Fringe Rotation

Although SIS mixers incorporating sideband separation are being developed for the MMA, it is expected that it will be possible to achieve only 10-15 dB of isolation between the sidebands. This is sufficient to eliminate the noise from the unwanted sideband to a satisfactory degree. However, spectral dynamic range at least as high as 40 dB is desirable, so it is also necessary to include sideband separation either by 90 deg phase switching or by a frequency offset scheme suggested by B. Clark. Either of these schemes must be applied to the first LO. It is also generally useful to incorporate 180 deg phase switching to reduce effects such as unsymmetrical offsets in the sampler reference levels and spurious responses from unwanted signals that infiltrate the IF stages.

A complication in the use of phase switching with the MMA occurs because of the requirement for integration times as short as 10 ms. For the longest baselines which we take to be 10 km, and for a source at a low elevation angle, the difference in the times at which an incident wavefront reaches different antennas can be as much as  $33\mu\text{s}$ . Now to preserve the orthogonality of the Walsh functions the switching transitions must be coincident at the correlator input, i.e. after the compensating delay. Thus, at the points where the Walsh function switching is introduced, it is necessary to introduce time offsets of up to  $33\mu\text{s}$  into the transitions. These offsets depend upon the position of the antenna concerned within the array, and the position

of the source on the sky. (In the VLA the corresponding timing differences all fall within the 1 ms intervals of the waveguide cycle in which the IF signals are switched off, and can thus be ignored.) For the MMA, if the shortest switching interval of the Walsh functions is much longer than  $33\mu\text{s}$ , say 33ms, then the timing offsets of the Walsh functions could probably be ignored. For a number of antennas between 64 and 128 the duration of a complete Walsh cycle is 128 times the shortest switching interval, and it is necessary to integrate for integral numbers of Walsh cycles if the phase switching is to work efficiently. Thus the requirement for ignoring the timing offsets of the Walsh functions would be integration times longer than  $\sim 4$  sec. So the conclusion is that if Walsh function phase switching is used on the MMA, time offsets of the transitions are required. This is not a big problem, but it results in a complication of the software that one would prefer to avoid.

For the sideband separation the 90 phase switching can be avoided by using the frequency offset scheme mentioned above. To explain this scheme, consider first just two elements of the array. Let the natural fringe frequencies (i.e. fringe frequencies with no fringe rotation applied) be  $f_{nl}$  and  $f_{nu}$  for the lower and upper sidebands respectively. At the first LO of one of the antennas an offset  $f_1$  is applied so that the two fringe frequencies become  $(f_{nl} + f_1)$  and  $(f_{nu} + f_1)$ . The frequency  $f_1$  is chosen such that  $f_1 + (f_{nl} + f_{nu})/2 = n/(2t)$ , where  $n$  is an integer and  $t$  is the integration time between correlator data dumps. (Note that the natural fringe frequencies for the MMA vary from zero to about 600 kHz, so  $f_1$  may have to be positive or be negative, i.e. the natural frequency may have to be increased or reduced.) Then at a later LO, which in the present plan is the LO at the first mixer of the Baseband Converter, we introduce a second frequency offset to convert to zero frequency the fringes of the sideband that we want to use. For example, if we want to keep the upper sideband then this second LO offset is  $-(f_{nu} + f_1)$ . The effect on the lower sideband is to offset its frequency in the opposite direction, that is, the frequency of the lower sideband fringes becomes  $(f_{nl} + f_1) + (f_{nu} + f_1) = n/t$ . The lower sideband fringes then integrate to zero in time  $t$ . To apply this scheme to the full array the value of  $n$  must be different for each antenna, and can run from 0 to  $(N_a - 1)$ , where  $N_a$  is the number of antennas. For  $t \sim 10$  ms and  $t \sim N_a$  100 the fringe frequencies of the unwanted sideband at the correlator output are of order 1 kHz and no constraint is placed on the rate of correlator data dumps.

The fringe-offset scheme for removing the unwanted sideband has other advantages over the process of fringe separation by 90 phase switching. It can be implemented by using the fringe rotators that are required in any case to bring the fringe frequency of the wanted sideband to zero, so no extra hardware is required. Also, the variation with time of the differential path lengths to the antennas, which in the case of Walsh function switching requires timing offsets, is in this scheme taken care of by the fringe rotation. The unwanted sideband is lost in the integration, but this is not a problem since we are planning to use sideband-separating SIS mixers so any IF signal contains only one sideband at full sensitivity, the other being reduced by at least 10 dB.

Unfortunately there does not appear to be any frequency-offset method of implementing the 180 phase switching, so Walsh-function switching with timing offsets to compensate for the different path lengths of the incoming wavefront remains the complete solution. If the phase switching is necessary only to correct for non-symmetrical quantization thresholds, then it would be possible to replace it by automatic control of the threshold levels. For four-level sampling the dc level of the sampled waveform would be adjusted to equalize the total numbers of positive and negative samples, and the quantization levels would be adjusted to equalize the numbers

of positive and negative high-level counts. Counters for the four sampling levels would provide inputs to digital-to-analog converters to provide the dc levels. Such a scheme may be examined as part of the two-element prototype testing. Removal of the phase switching would occur just after the digital samplers by sign reversal of the appropriate samples as controlled by the phase-switching Walsh function, and is shown in Fig. 4.

The fringe rotators may also be used for fine adjustment of the Doppler correction, the magnitude of which may be as large as 100 MHz at 800 GHz. Thus the range of the offsets from the fringe rotator should be as wide as the narrowest tuning interval provided by any other LO, to provide complete frequency flexibility. Alternatively, Doppler shifts can be removed by interpolation of the spectra at the correlator output.

### The Local Oscillator System

Two version of the LO system are shown in Figs. 5 and 6. Figure 5 shows the system with a conventional multiplier scheme for the first LO, and Fig. 6 shows the photonic system for the first LO which will offer significant advantages if it proves successful. In both figures a frequency standard provides inputs for various synthesizers and other units. The double line indicates multiple signal paths carrying several frequencies, such as 1 Hz, 1 MHz, 1 GHz, and 10 GHz. The final values for these reference frequencies will be chosen to take account of the design details of the synthesizer units for which they are required. The synthesizers at the top left of the figures provide the two fixed frequencies (375 MHz and 1.5 GHz) required by the Baseband Converters (Fig. 4). The four synthesizers immediately below them provide the four LO signals required by the Demultiplexer units in Fig. 3. In the lower left part of the figures there are units designated as "3.2-5.2 GHz PLO". These are phase-locked oscillators that produce the 3.2-5.2 GHz LO signals with fringe rotation that are used in the Baseband Converters in Fig. 4. Each PLO unit receives a signal from a fringe generator which uses a number-controlled oscillator or similar device to produce a signal at some convenient low frequency, such as 1 MHz, with the required fringe frequency offset,  $-(f_{nu} + f_1)$  or  $-(f_{nl} + f_1)$ . Each PLO unit also receives a signal from a synthesizer tuned such that the sum of the fringe generator and synthesizer frequencies is equal to the required LO frequency, including the fringe frequency offset.

The other part of the local oscillator system in Figs. 5 and 6 is concerned with the LOs required at the antenna. In the lower right area, fixed-frequency synthesizers at the antenna produce 26 GHz for the second LO for the HFET front ends and 16 GHz to convert 4-8 GHz IF bands to 8-12 GHz. The 10 GHz reference frequency can be returned to the Electronics building on a separated fiber to provide a round-trip phase measurement. It is assumed here that all fibers going to an antenna will be in a similar environment and suffer similar thermal expansion.

In Fig. 5 the first LO system is in the upper right area. The unit labeled "10-15 GHz YIG oscillator and multipliers" (in the Driver-Multiplier unit) produces the 6<sup>th</sup> or 8<sup>th</sup> harmonics of a 10-15 GHz YIG oscillator (60-90 or 80-120 GHz), and this is suitably amplified to a level of no less than 50 mW. This frequency is locked to the corresponding harmonic of a synthesizer that uses a fixed reference frequency that has been filtered by means of a phase-locked loop with a crystal oscillator (VCXO). The phase-locked loop for the YIG oscillator uses a phase reference that contains the required frequency offsets and phase changes for the fringe rotation and phase switching. The 60-90 GHz and 80-120 GHz signals are sufficient to drive multipliers that can supply the first LO for any of the front ends above 60 GHz. For lower frequency front ends an LO signal can be brought out from an earlier stage of the multiplier chains. Note that the

frequencies in the multiplier chains are too high for switches other than waveguide type and these are deemed undesirable because of expense and because experience shows that they do not always reset with sufficient mechanical precision, resulting in reflections and phase errors. Thus a separate Driver-Multiplier unit is required for each front end band at each antenna (i.e. approximately ten at each antenna). However, the output of the fringe and phase switch synthesizer, shown in the Driver-Multiplier unit, can be switched and shared between the Driver-Multiplier units at an antenna. It is expected that the multiplier scheme will be used for the two-antenna test array to be constructed as the first phase of the project.

The upper part of Fig. 6 shows the photonic LO system that is being investigated for the first LO. Two optical signals that differ in frequency by the first LO frequency are transmitted to the antenna on a single fiber. These are then combined in a photo-diode which should result in enough power to drive an SIS mixer. For the HFET-amplifier front ends the photo diode output can be used to lock a Gunn oscillator, or a YIG oscillator driving a frequency multiplier, to provide the increased power required for a conventional mixer. A separate photo-diode may be required for each band. The two lasers that generate the optical signals for each antenna are located at the Electronics building. One of them could, in principle, be common to all antennas, but the available optical power would probably not be enough to supply more than a few antennas. For each antenna a second laser is phase-locked to the first one with a frequency offset equal to the required first LO, including fringe rotation and phase switching. In the phase-lock scheme, the difference frequency of the two masers is produced in a photo-diode at the Electronics building, and this is mixed with the  $n$ -th harmonic of a signal from a synthesizer at frequency  $f_1$ . The difference frequency, at the loop IF, is amplified and then compared in a phase detector with a frequency from a second synthesizer which produces a frequency  $f_2$  that contains the required fringe-frequency offset and phase switching. The frequency difference between the lasers is locked to  $nf_1 \pm f_2$ . Here  $f_1$  would be of order tens of GHz and  $f_2$  of order 100 MHz: the choice of the values of will depend upon the range of  $n$  for which satisfactory operation of a harmonic multiplier can be obtained. If the photonic scheme proves practicable, it would greatly simplify the electronics since the requirement for frequency multipliers producing power levels sufficient to drive the mixers would be eliminated. Switching the LO signal to different front ends could be done using an optical fiber switch, and would eliminate the requirement of a separate Driver-Multiplier unit (Fig. 5) for each frequency band at an antenna.

### Dispersion in the Optical Fiber

The optical transmitters should use external modulators to avoid causing frequency modulation of the laser. The optical frequency of the laser at 1300 nm wavelength is  $2.3 \times 10^{14}$  Hz, and a 2 GHz-wide IF signal spans 0.011 nm in wavelength. Assume that we are using standard fiber for which the zero dispersion point is 1300 nm. Assume also that the laser wavelength is within 20 nm the zero-dispersion point, so that the dispersion is no more than 2 ps/nm.km. Then for 25 km of fiber the time difference for frequencies at the edges of a 2 GHz-wide band is no more than 5.5ps, which corresponds to 4 deg of phase at 2 GHz. This is the effect of the dispersion on the intrinsic bandwidth of the IF signal. Thus any loss in coherence between an IF band that has traversed 25 km of fiber and one that has not is entirely negligible. Now consider the effect of variation of the laser wavelength which is a function of temperature. If the laser wavelength changes by 1 nm, and again the dispersion is about 2 ps/nm.km, then the time for traversal of 25 km of fiber changes by 50 ps. This should be compared with the minimum increment in the

compensating delay in the system which we will take to be  $1/32$  or the reciprocal bandwidth at the sampler, which is 16 ps. Delay errors smaller than, say, 5 ps, which would result from a change in the laser wavelength of about 0.1 nm, should be small enough to be ignored. However, since the correlator is a spectral type, larger delay errors, which would result mainly in a linear variation of phase with frequency, would be corrected by observation of a phase-calibrator source.

The effects of variation in the effective length of the fiber on the LO signals must also be considered. A change in delay of 5 ps corresponds to a phase error of 4 cycles at 800 GHz. The effect of a slow variation of this magnitude over several hours would be removed by frequent switching to a calibrator source, which is required in any case to correct for atmospheric effects. Faster variations could be monitored by a round-trip phase measuring system. Round-trip phase systems have been satisfactorily demonstrated in fiber optic transmission, using either the same fiber as the outgoing signal (Primes, et al.), or a separate fiber, for the returned signal (Webber and Thacker 1990). If the optical carrier for the returned signal is generated in a different laser from the carrier for the outgoing signal, the effects of the wavelength stability of the lasers and the dispersion in the fiber on the overall accuracy should be considered. At this time there appears to be no serious problem in implementing round-trip phase on the LO signals, but details of design will depend on data such as the wavelength stability of masers that remain to be investigated when MMA development is started.

Members of the MMA Systems group include, D. Bagri, J. Carlstrom, B. Clark, L. R. D'Addario, D. Emerson, R. Escoffier, P. Napier, F. Owen, S. Padin, J. Romney, R. Sramek, D. Thornton, J. Webber, and J. Welch.

### References

Padin, S., D. P. Woody, J. A. Stern, H. G. Leduc, R. Blundell, C.-Y. E. Tong, and M. W. Pospieszalski, An Integrated SIS Mixer and HEMT Amplifier, IEEE Trans. Microwave Theory Tech., 44,987-990, 1996.

Primes, L. E., G. F. Lutes and R. L. Snyder, Stabilized Fiber Optic Frequency Distribution System, JPL Report (my copy is undated).

Webber, J. C. and D. L. Thacker, Phase Distribution on Fiber Optic Cable, Report prepared by Interferometrics, Inc. for Naval Research Lab., May 3, 1990.

Figure 1: Overall block diagram of the MMA System

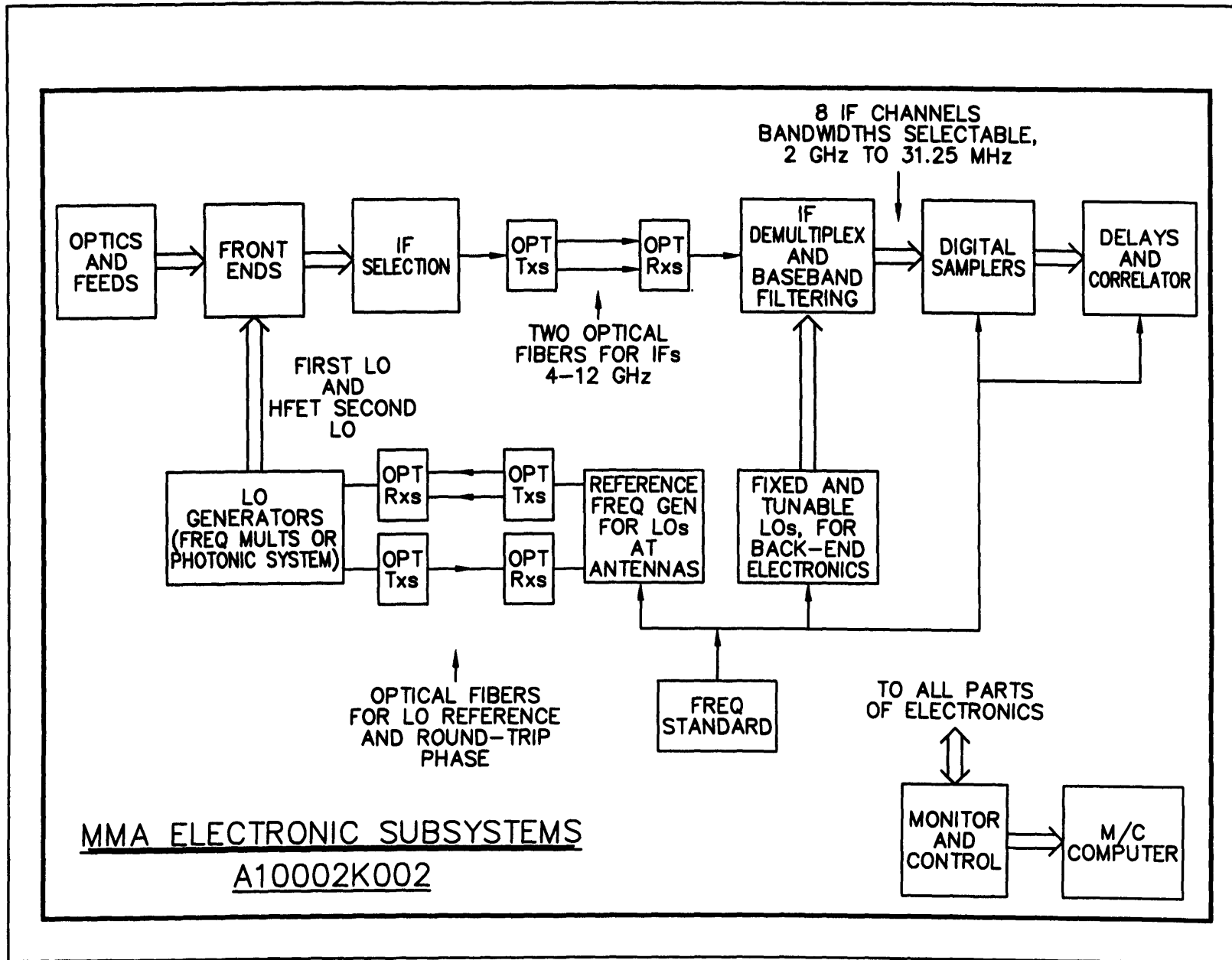


Figure 2: IF System at an Antenna

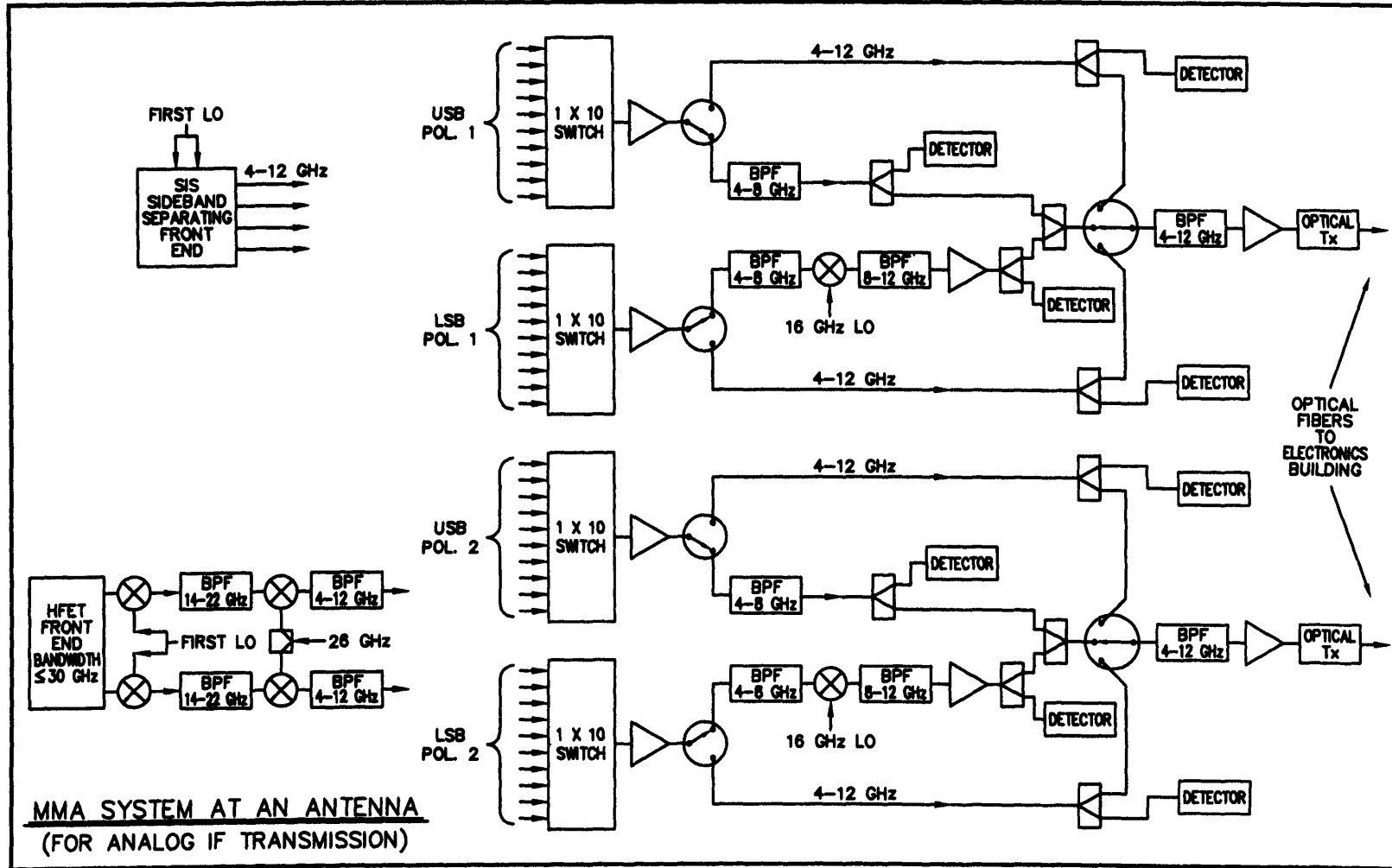


Figure 3: IF Demultiplexing Unit

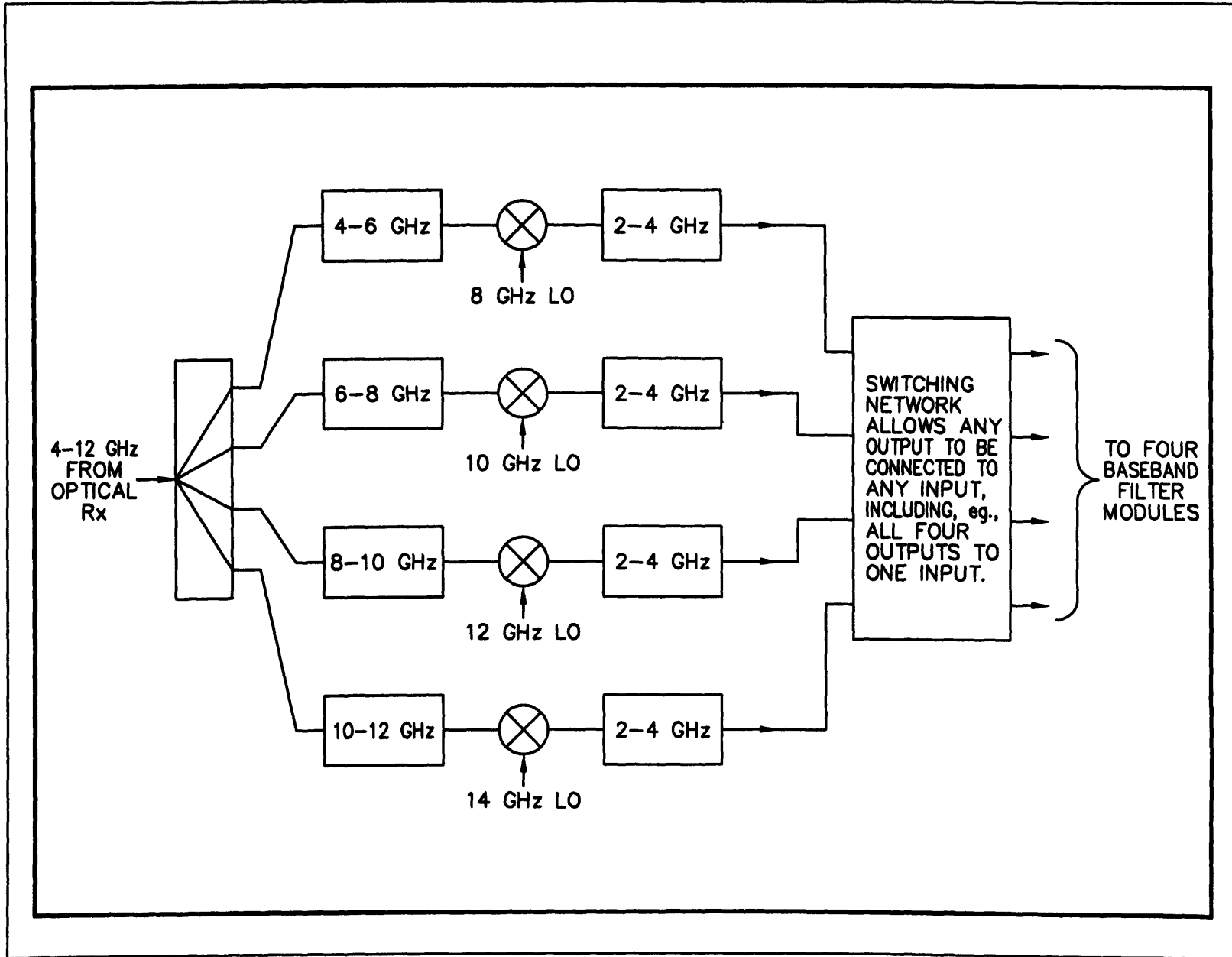
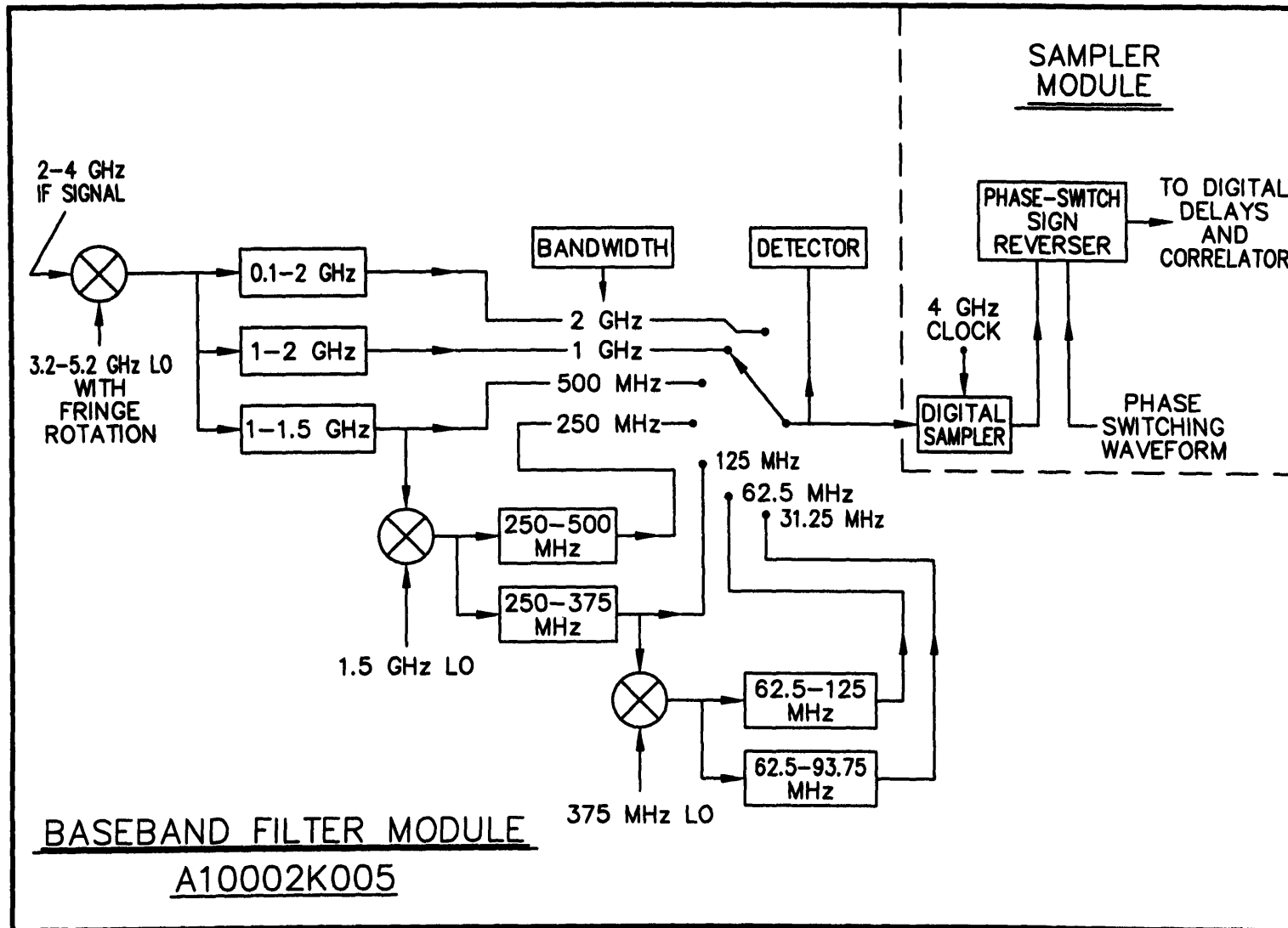


Figure 4: Baseband Converter and Digital Sampler



A10002K005

Figure 5: LO System with  $1\frac{3}{4}$  Multipliers for First LO

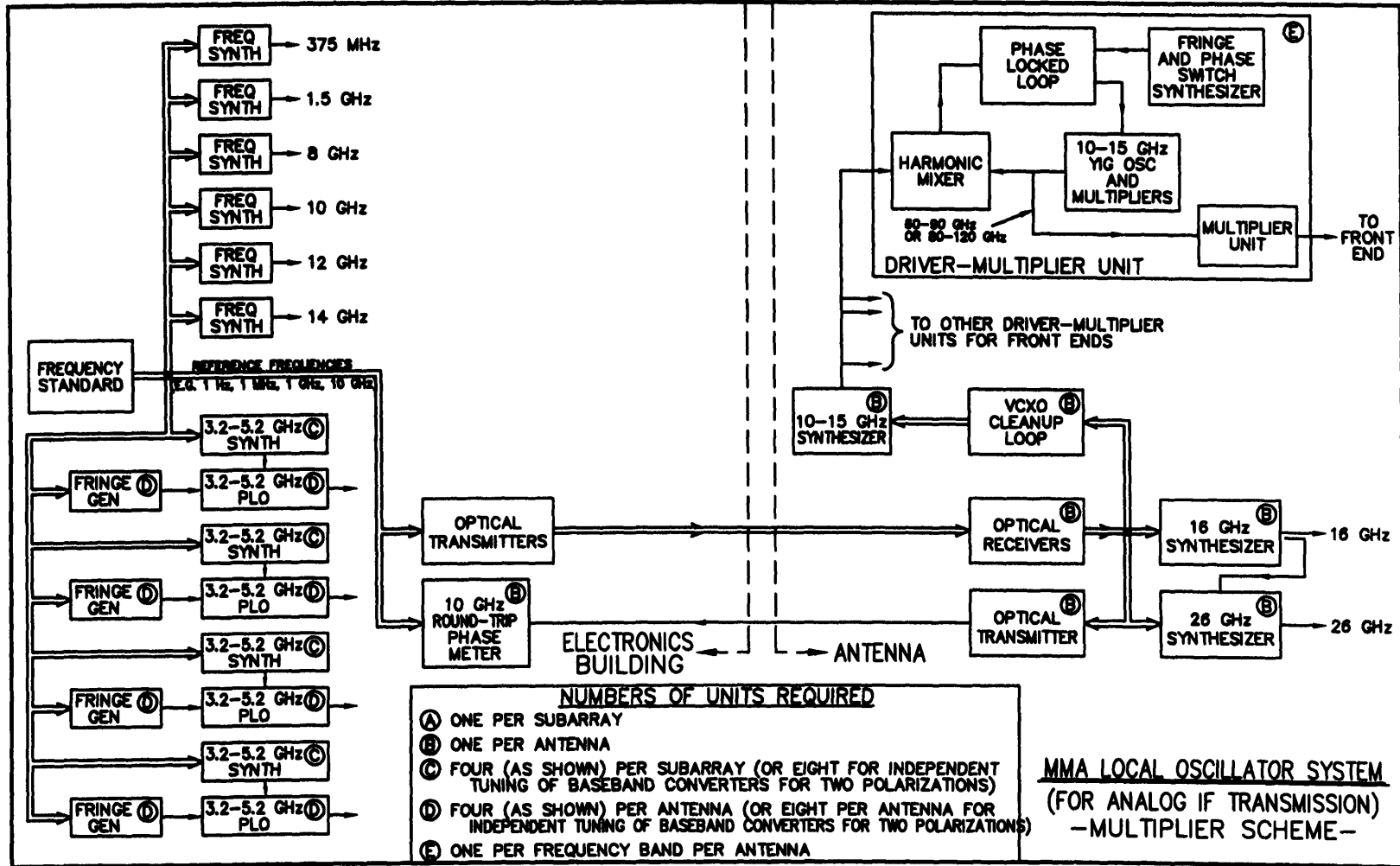
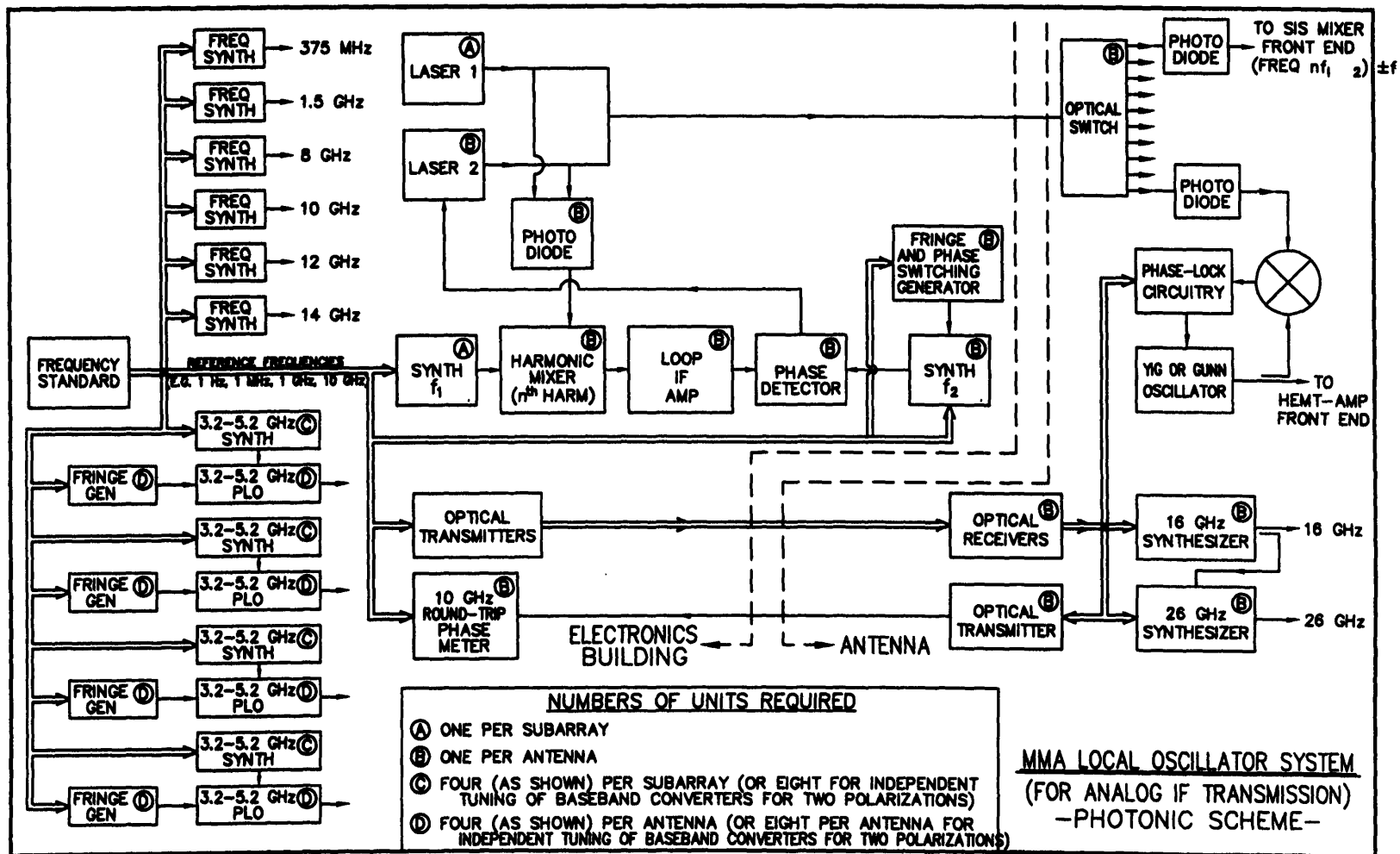


Figure 6: LO System with Photonic First LO



## DESIGN OF PLANAR IMAGE SEPARATING AND BALANCED SIS MIXERS

A. R. Kerr and S.-K. Pan

National Radio Astronomy Observatory\*  
Charlottesville, VA 22903

### Abstract

With noise temperatures of SIS receivers now in the range 2-4 times the photon temperature ( $hf/k$ ), the overall sensitivity of radio astronomy measurements can be seriously degraded by atmospheric noise, and sometimes by noise from the local oscillator source. In spectral line measurements, atmospheric noise in the unwanted (image) sideband can be eliminated by using an image separating scheme. To reduce local oscillator noise, balanced mixers can be used.

It is possible to realize image separating and balanced mixers using quasioptical or waveguide RF circuits, but they are difficult to fabricate and bulky. We believe it is now practical to include the necessary signal and LO power dividers, couplers, and cold loads with the SIS mixer on the same quartz substrate. The complete image separating or balanced mixer can be fabricated using a standard niobium SIS mixer fabrication process with one or two additional layers.

We describe the design of single-chip balanced and image separating mixers for 200-300 GHz. The circuits are designed using a modified form of coplanar transmission line which has a convenient range of characteristic impedances while minimizing coupling to adjacent circuit elements. It is hoped ultimately to combine the image separating and balanced designs to make a balanced image separating mixer on a single chip.

---

\*The National Radio Astronomy Observatory is a facility of the National Science Foundation operated under cooperative agreement by Associated Universities, Inc.

## The Virtues of Image Separating Mixers

While most mixer receivers respond to both upper and lower sidebands, the majority of applications require only a single sideband response. Signals and noise received in the unwanted (image) sideband degrade the overall system sensitivity. At the NRAO 12-m telescope at Kitt Peak in Arizona, the antenna temperature at the zenith is typically 60 K at 230 GHz. In spectral line measurements with a double-sideband SIS receiver, the image noise contributes ~30% of the overall system noise, thereby doubling the integration time required to attain a given sensitivity.

There are three ways to eliminate the image response of a broadband mixer receiver: (i) A filter can be inserted in front of the mixer, which terminates the mixer reactively at the image frequency. This is difficult in widely tunable receivers. (ii) A tunable four-port diplexer with a cold image termination can be used. This can be done quasioptically, e.g., using a Martin-Puplett interferometer as a sideband diplexer, but has a limited IF fractional bandwidth and is cumbersome at millimeter wavelengths. (iii) A phasing type of image separation mixer can be used, as will be discussed below.

## Types of Image Separating Mixer

At microwave frequencies, the usual realization of an image separating mixer, shown in Fig. 1, uses a quadrature hybrid to couple the LO to two identical (balanced) mixers with a  $\pi/2$  phase difference. The signal power is divided equally between the mixers with zero phase difference, and the IF outputs of the two mixers are connected to an IF quadrature hybrid. The down-converted upper and lower sideband signals appear separately at the two output ports of the IF hybrid. The in-phase and  $\pi/2$  couplers in the signal and LO paths can be interchanged without losing image separation.

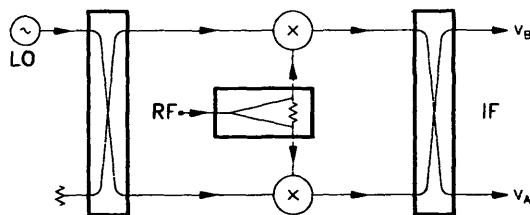


**Fig. 1. A common configuration for an image separating mixer, consisting of LO and IF quadrature hybrids, and an RF in-phase power splitter.**

A 100 GHz image separating mixer, using a waveguide magic-T and an adjustable phase shifter in the LO path to one mixer, has been described in [1], see Fig. 2. At shorter wavelengths, the signal and LO phasing can be done quasi-optically, as described in [1] and [2]. A quasi-optical image separating scheme is shown in Fig. 3, in which a crossed-grid power splitter [3] acts as an in-phase beam-splitter for the input signal, and splits the circularly polarized LO beam into two linearly polarized beams with  $\pi/2$  phase difference. Inclined-grid couplers couple typically 1% of the LO power into each mixer, with 99% of the signal. Even at 250 GHz, such a quasi-optical scheme is physically cumbersome, and requires a large cryostat if several receivers are to be attached to the same refrigerator.

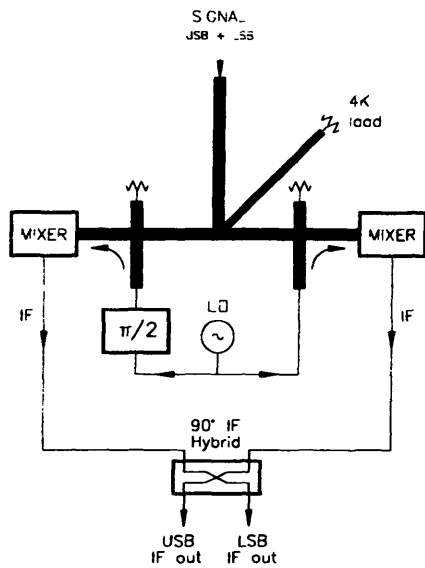


**Fig. 2. The 100 GHz image separating mixer of [1] based on a waveguide magic-T.**

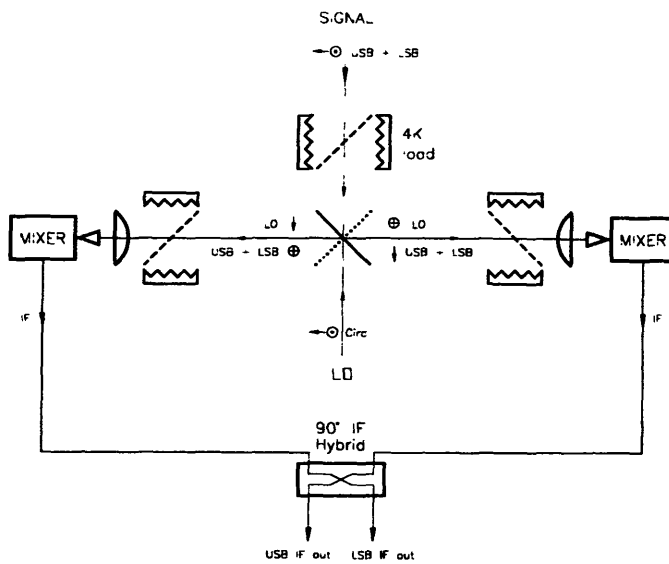


**Fig.3 A possible quasi-optical image separating mixer using a 45° signal polarization selector, a crossed-grid signal and LO splitter, and inclined-grid LO couplers.**

It is important to note that, in all image separating mixers, noise from the termination on the fourth port of the signal input coupler is down-converted and appears at the IF output ports.

In the present work, a scheme similar to that of Fig. 1 is used, but with the signal and LO ports interchanged, so the signal enters through a quadrature hybrid, and the LO through an in-phase power splitter. The RF quadrature hybrid, LO power divider, LO couplers, and SIS mixers are all fabricated on the same quartz substrate.

### Choice of Transmission Line Medium

To avoid the need for very thin quartz substrates, the circuit is designed with thin-film ground plane, dielectric layer, and wiring-layer conductors all on the same side of a thick quartz substrate. The dimensions of coplanar transmission lines are kept substantially smaller than the substrate thickness to prevent the fields penetrating appreciably through the substrate.

The external RF source and IF load impedances are near 50 ohms. The characteristic impedances required in the RF quadrature hybrid and the matching circuit of the SIS mixer range from 3 to 116 ohms. The lower values are readily obtained with superconducting microstrip lines, while coplanar waveguide (CPW) can be used for the higher impedances. In the range from about 10 to 60 ohms, microstrip lines with thin-film dielectrics are too narrow to use, while CPW requires very narrow gaps between center conductor and ground plane. We therefore lower the characteristic impedance of CPW by using periodic capacitive loading.

A capacitively loaded coplanar waveguide (CLCPW) can be regarded as a standard CPW with periodic capacitors to ground. The equivalent circuit of a section of CLCPW is shown in Fig. 4; with 570 nm SiO<sub>2</sub>, the characteristic impedance of this CLCPW is 63 ohms. For the CLCPW's used in this work, simulation using Sonnet *em* [4] indicates that the inductors L<sub>1</sub> and L<sub>2</sub> can be ignored if the reference plane is chosen at the center of the bridge, as shown.

Additional important advantages of CLCPW over standard CPW are that the periodic capacitors act as ground bridges, and: (i) greatly reduce coupling between adjacent components, and (ii), prevent odd-mode gap resonances in long CPW lines.

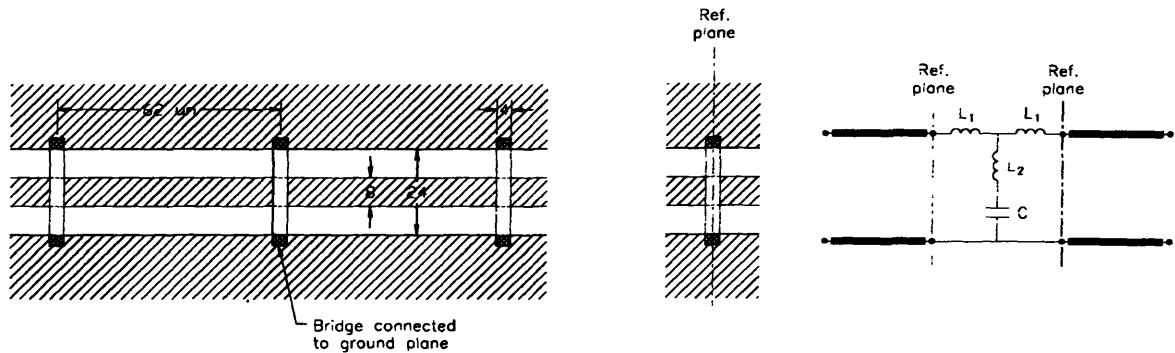


**Fig. 4. A length of capacitively loaded coplanar waveguide (CLCPW), and equivalent circuit. Dimensions are in microns.**

#### An Integrated Image Separating SIS Mixer for 200-300 GHz

The mixer is on a 2 x 1 mm quartz substrate, mounted in a block with separate waveguide inputs for the signal and LO, as shown in Fig. 5. Coupling from the waveguide to the mixer substrate is by broadband probes and suspended-stripline on smaller quartz substrates. Connections between the probes and the main substrate are by thin Au ribbon. IF and bias connections are by short wire bonds.

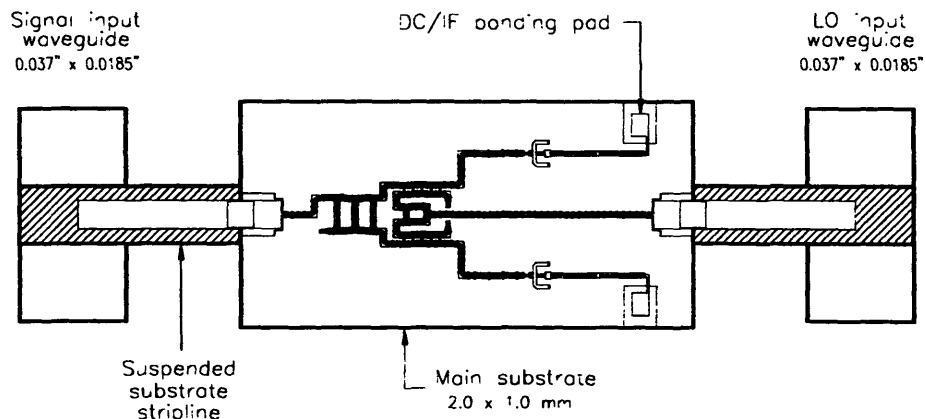


**Fig. 5. The image separating mixer, showing the signal and LO waveguides, suspended stripline coupling probes, and the main substrate.**

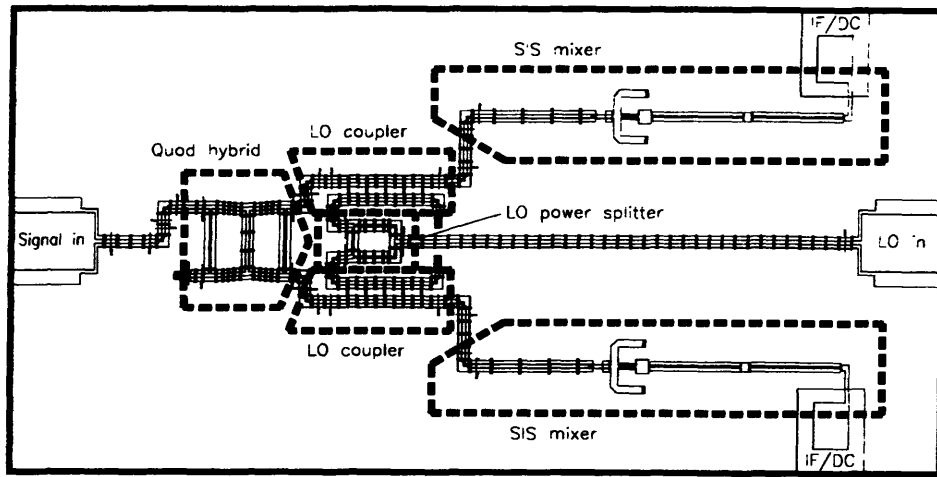


**Fig. 6. Main substrate of the image separating mixer, showing the main components.**

An enlarged view of the substrate is shown in Fig. 6. The main components are: (i) a 3 dB quadrature hybrid at the signal input, (ii) a 17 dB LO injection coupler in front of each mixer, (iii) an in-phase power splitter in the LO path, and (iv) two SIS mixers. Noise from the resistive termination on the fourth port of the input hybrid is downconverted to appear at the IF output ports of the mixer.

**Amplitude & Phase Requirements**

The image rejection obtainable in the image separating mixer depends on the amplitude and phase balance of the two quadrature hybrids and the mixers. The signal flow through the circuit is depicted in Fig. 7. The quantities  $c_1$ ,  $c_2$ , and  $t_1$ ,  $t_2$ , are the coupled port and through port scattering parameters ( $s_{21}$  and  $s_{31}$ ) of the input hybrid ( $c_1$ ,  $t_1$ ) and IF output hybrid ( $c_2$ ,  $t_2$ ). Using the notation in the figure, the amplitudes at IF ports A and B are:

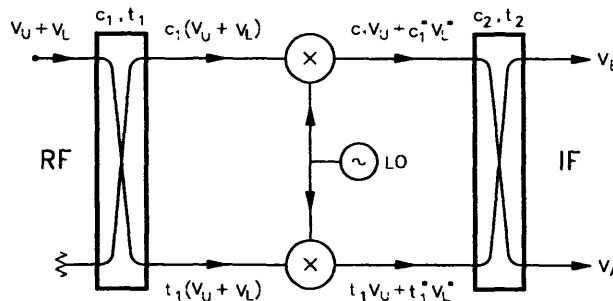


**Fig. 7. Signal flow through the image separating mixer. For simplicity, the mixers are assumed to have unit conversion gain.  $V_U$  and  $V_L$  are the complex amplitudes of the incident USB and LSB signals.**

$$V_A = V_U t_1 t_2 \left[ \frac{c_2}{t_2} + \frac{c_1}{t_1} \right] + V_L t_1^* t_2 \left[ \frac{c_2}{t_2} + \frac{c_1^*}{t_1^*} \right],$$

and

$$V_B = V_U t_1 t_2 \left[ 1 + \frac{c_1}{t_1} \frac{c_2}{t_2} \right] + V_L t_1^* t_2 \left[ 1 + \frac{c_1^*}{t_1^*} \frac{c_2}{t_2} \right].$$

At IF port A, the sideband amplitude ratio(LSB/USB) is  $\frac{\frac{c_2}{t_2} + \frac{c_1^*}{t_1^*}}{\frac{c_2}{t_2} + \frac{c_1}{t_1}}$ , and

at IF port B, the sideband amplitude ratio(USB/LSB) is  $\frac{1 + \frac{c_1}{t_1} \frac{c_2}{t_2}}{1 + \frac{c_1^*}{t_1^*} \frac{c_2}{t_2}}$ . It is clear

that the image rejection depends on the deviation of  $|c/t|$  from unity, and the deviation of  $\arg(c/t)$  from  $-\pi/2$ , in the two hybrids. (If the mixers have unequal conversion loss, the difference can be included in  $c_1$  and  $t_1$ .)

In the ideal case,  $t_1 = t_2 = \frac{1}{\sqrt{2}}$ , and  $c_1 = c_2 = \frac{1}{\sqrt{2}} e^{-j\frac{\pi}{2}}$ , and perfect image rejection

results, with  $V_A = V_U e^{-j\frac{\pi}{2}}$  and  $V_B = V_L$ . With non-ideal hybrids, the worst-case image rejection is plotted in Fig. 8 as a function of amplitude imbalance and phase imbalance. The amplitude and phase imbalance are the combined quantities (sum of magnitudes) for the two couplers and mixers. From the figure it is clear that to ensure 20 dB image rejection, the amplitude imbalance (for the whole circuit) must be  $< 1.7$  dB or the phase imbalance  $< 12^\circ$ . For 10 dB image rejection, the amplitude imbalance must be  $< 5.7$  dB or the phase imbalance  $< 35^\circ$ . The surprisingly large allowable asymmetry is a result of dealing with sums and differences of complex amplitudes, rather than powers.

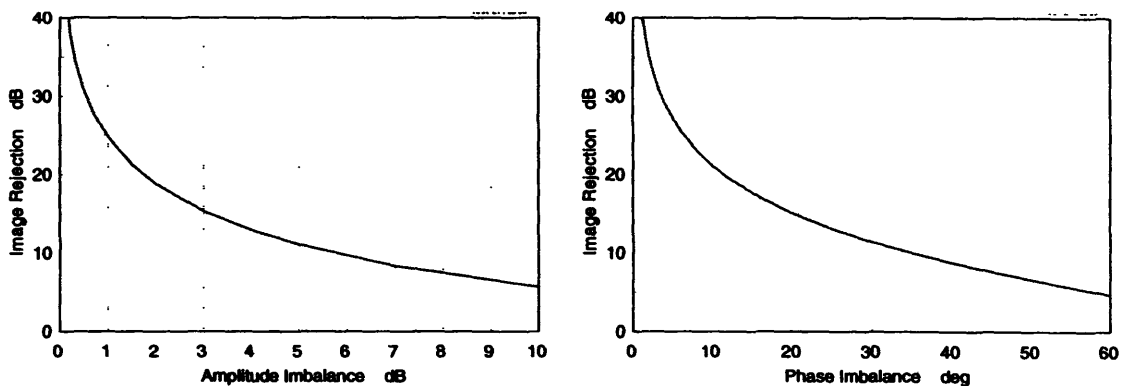


Fig. 8. Image rejection as functions of amplitude and phase imbalance for an image separating mixer.

## Description of the Components

### Input Quadrature Hybrid

Branchline directional couplers have been used for many years in stripline, microstrip, and waveguide circuits, and their design is well documented [5]. Within the design frequency band, the amplitude and phase variation decrease as the number of branches in the coupler increases, but the branch characteristic impedances increase. To keep the characteristic impedances in a suitable range, a three branch design was used, which for a 50-ohm nominal impedance requires sections with impedances 39, 47, and 116 ohms. For the frequency range 200-300 GHz, it is theoretically possible to obtain amplitude tracking within 1.2 dB, and phase tracking within  $1.2^\circ$  from  $90^\circ$ .

To realize a branchline coupler in CLCPW, Sonnet *em* was used to characterize the individual components (CPW sections, CLCPW bridges, and T-junctions), then MMICAD [6] was used to optimize the design. Finally *em* was used to analyse the whole coupler. The hybrid is shown in Fig. 9. A 1000 x scale model was built and measured with a vector network analyser. Fig. 10 shows the predicted performance of the optimized MMICAD design. Fig. 11 shows the results of the *em* analysis of the complete hybrid, and Fig. 12 shows the results measured on the 1000 x scale model.

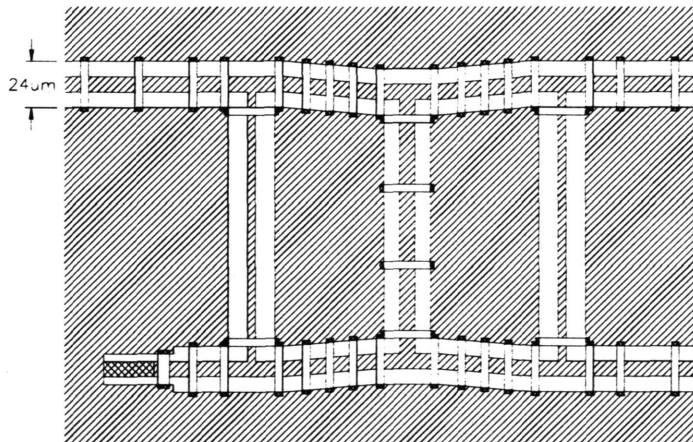


**Fig. 9. Quadrature hybrid, including a matched termination in the lower left corner.**

The obvious differences between the MMICAD and Sonnet *em* simulations are attributed to coupling beyond adjacent components of the circuit. Very close agreement is seen between the Sonnet *em* simulations and the results measured on the scale model.

### LO Couplers

The LO couplers use two parallel CLCPW's with periodic capacitive coupling strips between the lines, as shown in Fig. 13. Again, equivalent circuits for individual sections of the coupler were deduced using Sonnet *em* and MMICAD. The

design was optimized using MMICAD, and the final design checked using *em*. Fig. 14 shows the *em* results for the the final design. The coupling varies from 19-15 dB over the 200-300 GHz band, while the input return loss  $\geq 28$  dB and the directivity  $> 9$  dB.

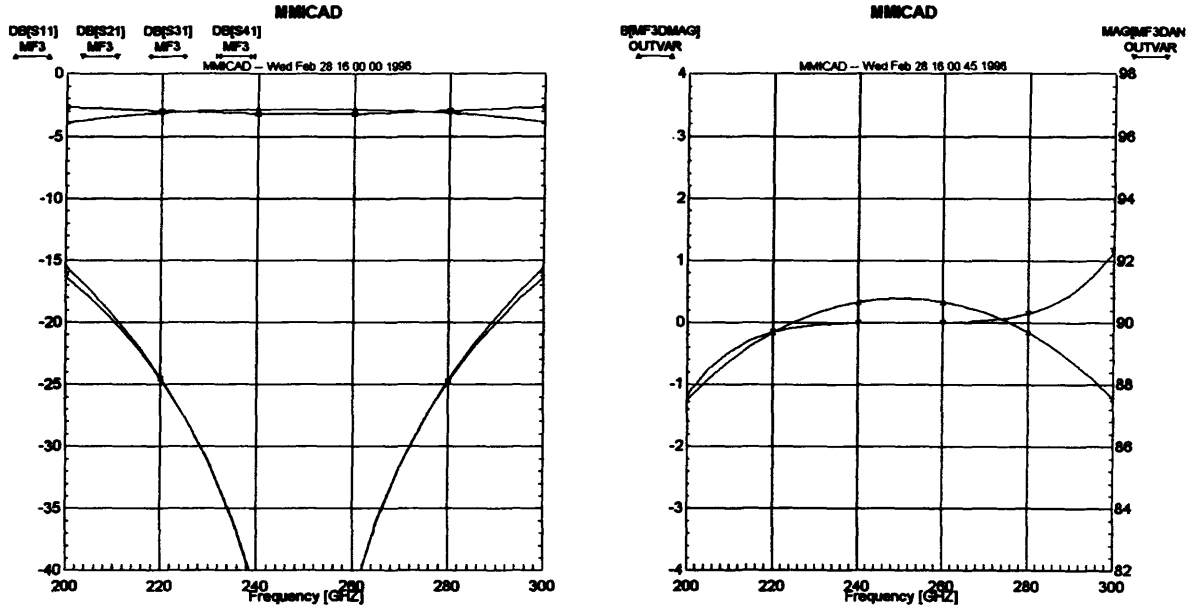


Fig. 10. S-parameters of the quadrature hybrid after optimization of the circuit model.

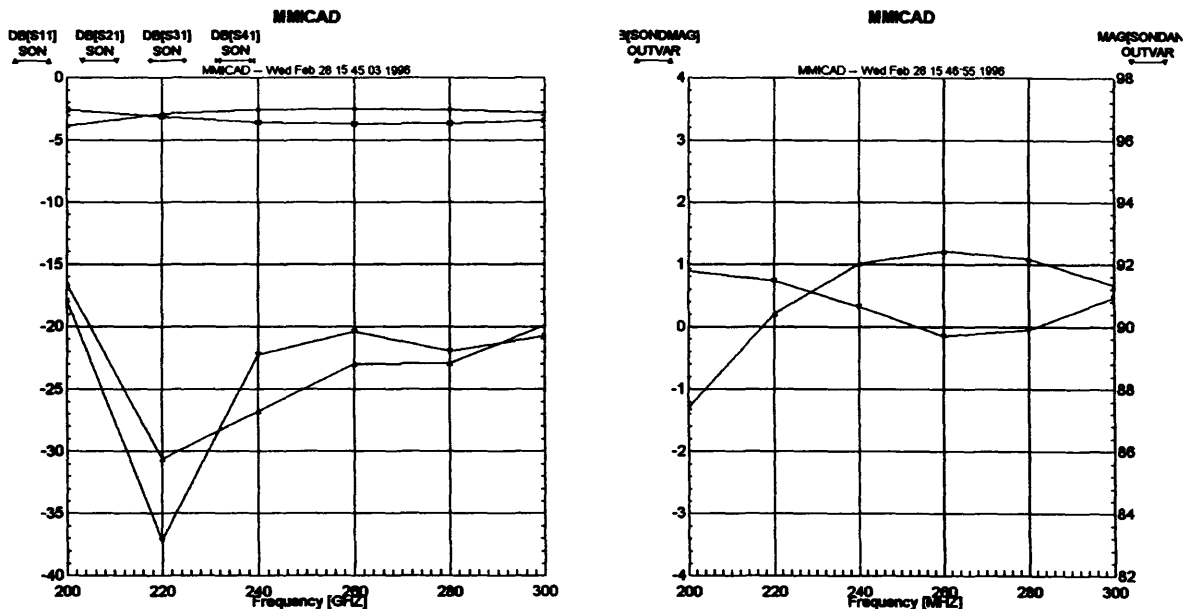


Fig. 11. S-parameters of the quadrature hybrid from Sonnet *em* simulation.

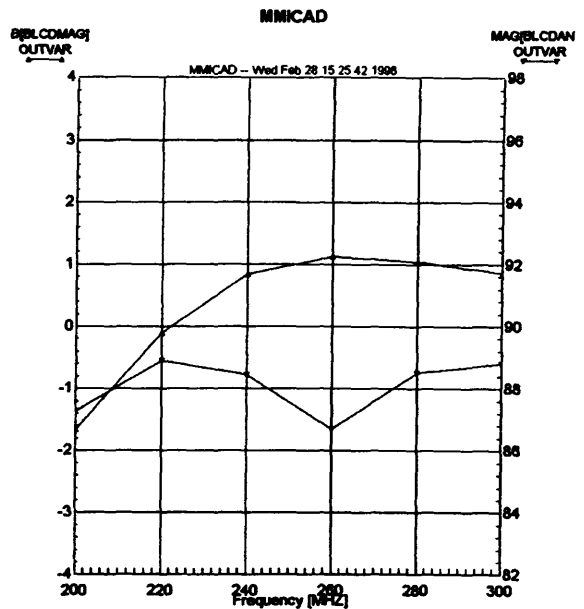
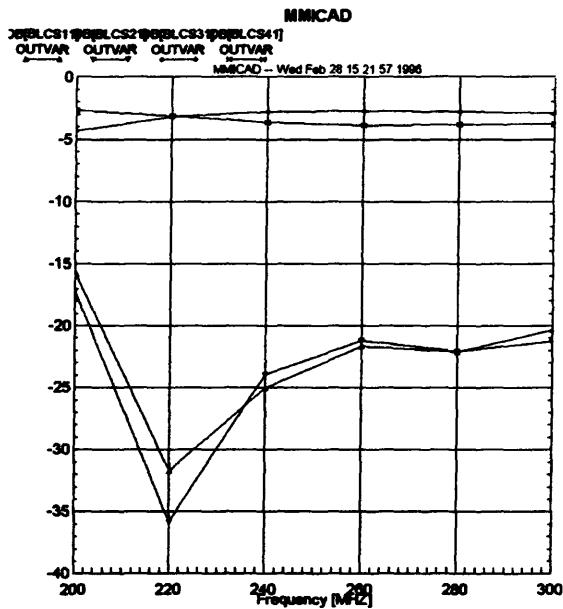


Fig. 12. S-parameters of the 1000 x scale model of the quadrature hybrid.

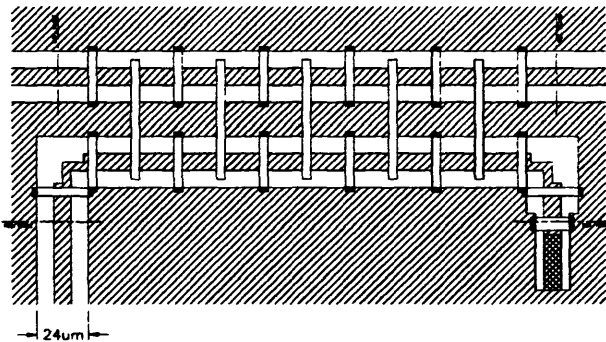


Fig. 13. The LO coupler. The five long vertical strips couple capacitively between the two CLCPW's.

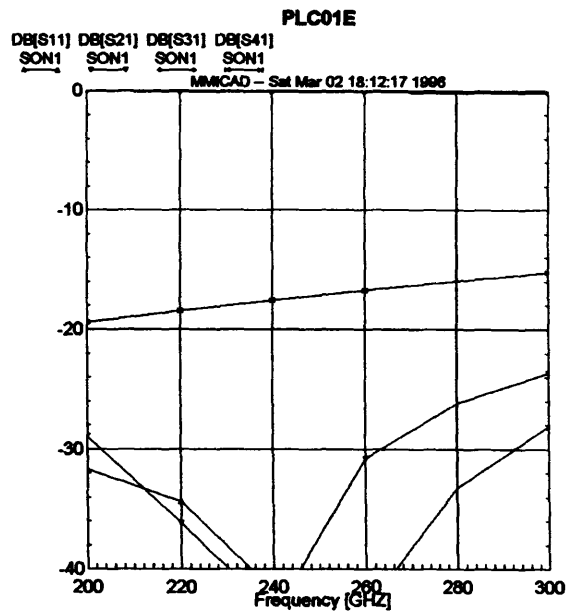


Fig.14. S-parameters of the LO coupler from Sonnet *em* simulation.

## LO Power Splitter

The LO power-splitter, shown in Fig. 15, is based on the standard Wilkinson configuration, and was also designed using Sonnet *em* and MMICAD. Ideally this type of circuit requires a lumped resistor connected between the output ports to absorb the difference signals between those ports. The 100-ohm resistor in the present design is not electrically short, which accounts for the relatively poor output match and isolation, shown in Fig. 16. The input return loss and isolation are  $\geq 16$  dB, while the output return loss  $\geq 13$  dB from 200-300 GHz. The critical parameters, equal phase and amplitude at the output ports, are assured by the symmetry of the circuit.

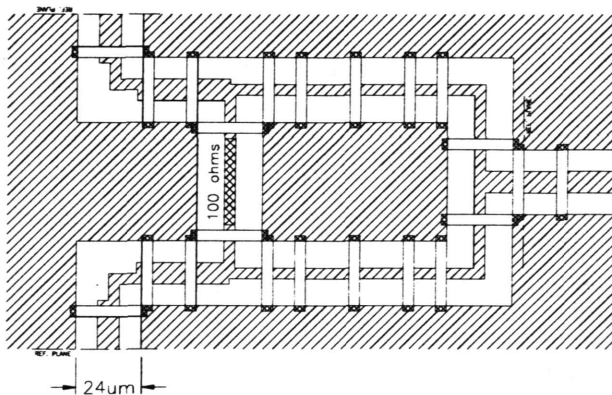


Fig. 15. The LO power splitter.

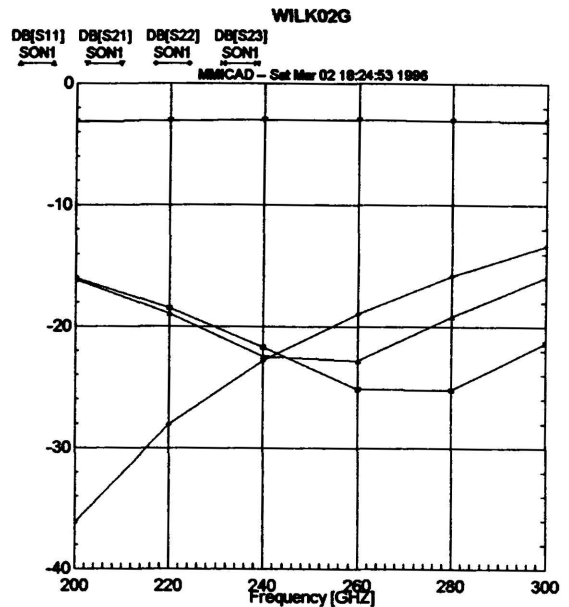


Fig.16. S-parameters of the power splitter from Sonnet *em* simulation.

## The Case for Balanced Mixers

The LO power is usually coupled into a millimeter-wave SIS mixer using a directional coupler or beam splitter. If the signal path loss through the LO coupler is to be kept small, the LO loss must be substantial, and is typically 15-20 dB. In addition to wasting most of the LO power, noise from the LO source in the signal and image bands is coupled into the mixer. Depending on the nature of the LO source, its (sideband) noise temperature may be room temperature or higher. If the LO source has an effective noise temperature of 300 K at the sideband frequencies, then a 15-20 dB beam splitter will contribute 10-3 K in each sideband at the input of the mixer, which may be comparable with the intrinsic noise temperature of the receiver itself. We have observed with some LO sources a considerably higher excess sideband noise; some frequency multipliers in the 200-300 GHz range have been observed to contribute as much as 50 K of sideband noise at the input of the mixer.

A balanced mixer eliminates both these shortcomings. It has a separate LO port with efficient coupling (but two mixers to drive), so the required LO power is

reduced by 12-17 dB relative to the simple single-ended mixer. Sideband noise is reduced by an amount dependent on the accuracy of the 180° phase shift and amplitude balance through the mixer.

### Types of Balanced Mixer

Many types of balanced mixer exist. The most common at radio frequencies is the transformer type. In waveguide, the magic-T balanced mixer, was once common, although it has now largely been replaced by the planar hybrid-ring and quadrature hybrid types. The circuit of the quadrature hybrid type is shown in Fig. 17. The signal and LO are coupled to the individual mixers through the quadrature hybrid. A 180° IF hybrid combines IF output of the two mixers so that all the down-converted signal appears at one output port, and all the LO sideband noise appears at the other (a convenient scheme for measuring LO sideband noise).

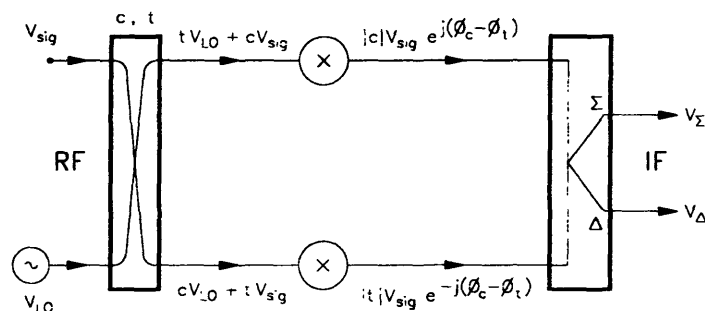


**Fig. 17. Circuit of a balanced mixer consisting of a quadrature hybrid, an identical pair of simple mixers, and a 180° IF hybrid.**

### Amplitude and Phase Requirements

The isolation of a balanced mixer depends on the amplitude and phase balance of the components. The signal flow through the mixer is indicated in Fig. 17, where the mixers are assumed for convenience to have unit conversion gain. Using an analysis similar to that used above in the case of the image separating mixer, it is possible to calculate the worst-case isolation for given amplitude and phase uncertainties in the components. The results are approximately the same as shown in Fig. 8 for the image rejection of the image separating mixer. In the case of the balanced mixer, the vertical axes in Fig. 8 give the isolation in dB, the amplitude imbalance is the signal path imbalance, and the phase imbalance is (twice the phase imbalance of the quadrature hybrid) + (the phase imbalance of the isolated port of the 180° hybrid). If the mixers have unequal conversion loss, the difference can be included in  $c$  and  $t$ . From Fig. 8 it is clear that to ensure 20 dB image rejection, the amplitude imbalance must be < 1.7 dB or the phase imbalance < 12°. For 10 dB image rejection, the amplitude imbalance must be < 5.7 dB or the phase imbalance < 35°. Again, the surprisingly large allowable asymmetry is a result of dealing with sums and differences of complex amplitudes rather than powers.

### A Balanced Mixer for 200-300 GHz

A balanced mixer is considerably simpler than an image separating mixer, and can be designed using the same quadrature hybrid and SIS mixers. As no resistive terminations are required on the substrate, fabrication is also less complex. Fig. 18 shows a balanced mixer which uses the components described earlier in this paper.

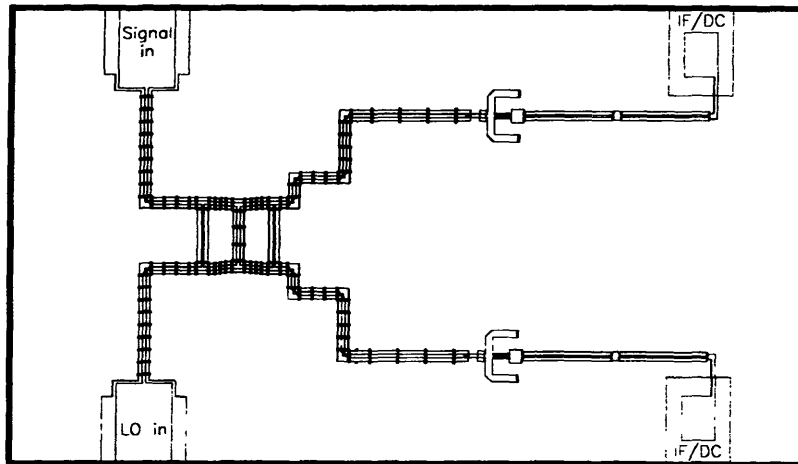


**Fig. 18. Main substrate of the balanced mixer, showing the quadrature hybrid and two SIS mixers.**

### Discussion

It is apparent that construction of single-chip image separating and balanced SIS mixers is now practical. There has been some concern that the tolerances on critical parameters in today's Nb foundries may not be good enough for circuits of this complexity. However, by far the most critical components in these circuits are the SIS junctions and their immediate matching circuits; if these can be made sufficiently reproducibly, which appears now to be the case, then we can expect an acceptable yield of the more complex circuits. It is not known yet whether the relatively large area of each circuit will increase the probability of a significant fabrication defect in any given mixer to an unacceptable level. Considering the phenomenally low defect rate in the Si microcircuit industry, this should not be a fundamental limitation.

If the image separating mixer turns out to be practical, it is only a small additional step to use balanced mixers within the image separating mixer — a balanced image separating mixer. This will be relatively immune to LO noise, and will require a LO power level 14 dB lower than a single simple SIS mixer using a 20 dB LO coupler.

## Acknowledgments

The authors wish to acknowledge: N. Bailey for making measurements on the scale model and IF quadrature hybrids, R. Bradley for simulation of an image separating mixer to verify signal phase calculations, and D. Boyd for constructing the 1000 x model of the quadrature hybrid.

## References

- [1] R. L. Akeson, J. E. Carlstrom, D. P. Woody, J. Kawamura, A. R. Kerr, S.-K. Pan, and K. Wan, "Development of a sideband separation receiver at 100 GHz," Proceedings of the Fourth International Symposium on Space Terahertz Technology, pp. 12-17, March 1993.
- [2] C.-Y. E. Tong and R. Blundell, "A Quasi-Optical Image Separation Scheme for Millimeter and Submillimeter Waves," *IEEE Trans. Microwave Theory Tech.*, vol. MTT-42, no. 11, pp. 2174-2177, Nov. 1994.
- [3] J. M. Payne, J. W. Lamb, J. G. Cochran and N. Bailey, "A New Generation of SIS Receivers for Millimeter-Wave Radio Astronomy," *Proc. IEEE*, vol. 82, no. 5, pp. 811-823, May 1994.
- [4] Sonnet Software Inc., Liverpool, NY 13090.
- [5] G. L. Matthaei, L. Young, E. M. T. Jones, "Microwave Filters, Impedance-Matching Networks, and Coupling Structures," New York: McGraw-Hill, 1964.
- [6] MMICAD is a microwave integrated circuit analysis and optimization program, and is a product of Optotek, Ltd., Ontario, Canada K2K-2A9.



# MMA Memo 166: The MMA Correlator

R. Escoffier

April 1, 1997

## 1) INTRODUCTION

This memo will describe the design of a correlator for the MMA. The MMA project will likely begin in earnest in a few months, and the time has come to start definite considerations for this large and expensive subsystem of the array.

The design described here is for a lag correlator and justification for this approach will be given. A system clock rate of 125 MHz is also chosen and also justified. The decisions of system architecture and clock rate are the most important to be made in selecting a correlator design and much caution must be used before adopting the final approach.

At this time, no consideration will be given to the Atacama array (the combined MMA and Japanese LMSA), and the design described will be a correlator for the MMA alone. As plans and specifications for the Atacama array develop, the MMA correlator design will be reconsidered.

## 2) CORRELATOR SPECIFICATIONS

This section gives a summary of the MMA correlator specifications. Detailed system specifications will be developed over the next few months, and this section will provide a starting point for this effort. The basic starting specs for the correlator are:

- 40 antennas
- 8 IFs per antenna (maximum bandwidth/antenna = 16 GHz)
- 4 GHz maximum sampling rate per IF
- 2 bit, 4 level sampling
- 1024 lags per baseline with a 2-GHz bandwidth, minimum
- 4 product pairs (RR, RL, LR, LL) possible for polarization
- 30 KM maximum baseline delay range

## 3) JUSTIFICATION OF THE LAG ARCHITECTURE

Up to this point in considering designs for the MMA correlator, both lag and FX architectures have been studied. NRAO has experience in both types of systems for large arrays, having previously built the VLA with its lag correlator and the VLBA with its FX correlator. The text below attempts to justify the selection of the lag approach for the MMA correlator.

The MMA correlator will be a very large and expensive system as correlators for astronomical instruments go. Conventional wisdom has it that for small systems a lag correlator is most economical,

but as an array acquires more antennas, the FX approach will eventually become less expensive. This is because, for a lag correlator, much of the hardware required varies as the square of the number of antennas, whereas for the FX approach, much of the logic (specifically, the FFT engines) increases linearly with the number of antennas. This consideration, however, applies only to the silicon component of the hardware and other requirements must be studied.

The table below compares the lag and FX correlator designs for the MMA application. This table assumes:

1. a system clock rate of 125 MHz (see Section 4).
2. a custom lag correlator chip with a 4 X 4 X 2 matrix of correlators (4 ant. by 4 ant. by 2 polarizations, see Figure 4).
3. a custom FX chip that will do one radix 8 FFT butterfly.
4. a custom FX cross multiply chip with a 4 X 4 matrix of multipliers.
5. FFT-to-cross multiply interface of 12 wires (4-bit real, 4-bit imaginary, and a 4-bit exponent) at 1/2 the clock rate.

parameter	lag correlator	FX correlator
custom chip designs	1	2
number of custom chips (station)	0	30,720 [1]
number of custom chips (cross mult)	12,800 [2]	12,480 [3]
number of signal cables [*]	0	20,480 [4]
number of signal cables [+]	20,480 [4]	61,440 [5]

[\*] between the delay lines and the FFT engines.

[+] between the FFT engines or delay lines and the cross multipliers.

[1] 40 ant. X 8 IFs X 32 parallel paths X 3 chips per FFT.

[2] (40 X 40) X 8 IFs X 32 parallel paths / 16 corr per chip / 2 polz per chip.

[3] (40 X 39)/2 X 8 IFs X 32 parallel paths / 16 circuits per chip.

[4] 40 ant. X 8 IFs X 2 bits per sample X 32 parallel paths.

[5] 40 ant. X 8 IFs X 12 bits per point X 32 parallel paths / 2 (1/2 clock rate).

The advantages of the lag correlator are clear from this table:

1. The FX correlator would require 2 custom chip designs, one for the FFT and one for a matrix of cross multipliers, whereas the lag design requires only one chip.
2. The FFT butterfly chip would be very complex (at least 16-bit arithmetic at 125 MHz is required) and would probably take at least one year longer to develop than would the much simpler (but probably larger) lag correlator chip.
3. The amount of 125 MHz inter-stage wiring is much higher for the FX design than for the lag correlator. The FX design will require over 80,000 cables whereas the lag system requires only a little over 20,000 (to put this in perspective, 80,000 125 MHz signal cables is a factor of 380 times the VLA correlator requirement). In addition, the number of signal cables given in the table above represents a minimum. In order to achieve this minimum number of signal wires, the cross

multiplier matrix must be built in such a compact fashion that no output of the station logic is required to drive more than one cable. As will be seen in Section 5, this requirement can probably be met with the lag design. However, the FFT output of the FX design requires many more signals to drive the cross multipliers and, because of the limitations of I/O pins in the cross multiplier cards, a minimum wire interconnect will probably not be possible for the FX. If this minimum condition is not met, the FX cable requirements becomes more than 140,000 cables.

The number of signal cables is by far the most important factor in determining the practicability of the MMA correlator. The number of wires can be controlled by increasing the interface clock rate but at the cost of requiring more expensive cables and larger, more expensive, connectors. Section 4 will argue that a 125 MHz system clock rate is optimum for the MMA correlator.

Neither custom chip postulated for the FX design would be very large. If not for the large I/O requirements, higher levels of integration could be considered to make the FX approach more attractive (at least from the silicon standpoint). Still, the silicon utilization efficiency of the FX custom chips would not be as high as for a large lag correlator chip. The simple and regular nature of the lag correlator layout allows more efficient use of the surface area of the chip.

Additional disadvantages of the FX system include the much more complicated control logic requirements (for supplying the trig tables and timing signals, etc. for hundreds of FFT cards). This additional complexity will result in a longer development schedule and in a longer time to bring the system to operational status (as was experienced with the VLBA correlator).

#### **4) SYSTEM CLOCK RATE**

The MMA correlator will be a very large system by any standards. Based on just the bandwidth and number of baselines, it will have 178 times the capacity of the VLA correlator. The maximum sample rate to be used in the system will be 4 GHz. Since there is no practical way to handle this high clock rate in such a large system, a lower clock rate parallel design must be considered. The selection of the system clock rate is of extreme importance. This decision will determine the final cost, size, reliability and operation power requirements of the system, and it is important to select a design that will optimize all of these considerations to the extent possible at the onset.

The table below gives a list of several possible selections for the system clock rate, the number of resulting signal wires between the samplers and the delay lines, and other considerations (the lag correlator design is now assumed):

system clock	wires from samplers	possible interface medium	possible logic family	comment
4 GHz	640	individual coax	-	impractical
2 GHz	1,280	individual coax	-	impractical
1 GHz	2,560	individual coax	-	impractical
500 MHz	5,120	individual coax	GaAs?	-
250 MHz	10,240	multi-signal coax	ECL 100K	-
125 MHz	20,480	multi-signal cable	ECL 10K	VLA technology
62 MHz	40,960	multi-signal cable	ECL 10K	-
31 MHz	81,920	twisted pair	TTL 74F	VLBA technology

In this table, the term multi-signal cable refers to a medium such as the Gore flat cable used in the VLA correlator. This cable can fit eight 50 ohm transmission lines in a flat cable about 0.5 inches wide and costs about \$10 for a 5-foot terminated 8-signal cable. The multi-coax cable term refers to a medium such as AMP coaxial ribbon cable (AMP p/n 226581-9). This cable fits eight 50 ohm coax lines into a flat cable about 0.8 inches wide and costs about \$40 for a 5-foot terminated cable.

In addition to the wiring technology, applicable logic families for each design are given in the table above.

To minimize the cost and size of the correlator, one wants to select from the table above the highest system clock rate which retains a convenient IC logic family, inexpensive and compact interconnect cables and straight forward printed circuit card technology.

A low clock rate, such as 31 MHz, would use very inexpensive interconnect cable (twisted pair), but it has the disadvantage of requiring many parallel paths. Also, the 74F TTL logic family is not good at driving terminated transmission lines. This inability to drive low impedances makes the rack-to-rack signal drive difficult and also makes printed circuit card design more difficult because long unterminated lines on a card must be avoided.

Higher clock rates, such as 250 MHz, require expensive and bulky signal cables. Expensive and poorly supported logic families, like the ECL 100K family, as well as more critical pc card design would also be required.

Based on previous NRAO correlator design experience, the highest clock frequency in the table above for which a convenient logic family, inexpensive interconnect cables, and simple pc card technology exists is at 125 MHz. Hence, this clock rate is chosen for the MMA correlator design.

## 5) SYSTEM BLOCK DIAGRAM

A simplified block diagram for the MMA correlator is given in Figure 1. This diagram presents a fairly

conventional lag correlator.

The analog outputs of the IF system drive sampler inputs where 2-bit, 4-level sampling is done at 4 GS/S. A block diagram of a sampler is seen in Figure 2. Some cost saving can be realized by making dual samplers that share parts of the circuitry such as the phase lock loop and the sample clock phase shift. This configuration means that a small residual delay error between two IFs of the same antenna would have to be removed in software.

Logic in the mode selection block routes the sampler outputs into the delay system. When fewer than 8 samplers per antenna are being used, this stage will assure high system efficiency by replicating active sampler outputs into unused delay lines and, hence, into otherwise unused correlators where additional lags can be generated. In this way, maximum performance will be obtained for the observational mode desired.

Next, delay lines are provided to phase the signals. The delay will be provided in very efficient high density RAMs. For a 30 KM delay range, 524,288 RAM bits per sampler output bit is required.

The data format conversion block seen in Figure 1 will take the 32 parallel outputs of each sampler and, using RAMs, re-sort the samples. Thus, the 32 parallel outputs of a high-speed sampler would be converted from each carrying every 32nd sample to each carrying short (about 1 msec) bursts of contiguous samples. If the N-wide parallel (2-bit) output of a high-speed sampler (each output carrying every Nth sample) were to drive the correlators directly, an N-by-N matrix of correlators would be required so that every sample gets correlated with every other sample. For  $N = 32$ , this would mean a matrix of 1024 small correlators to correlate the output of every IF of every baseline (each 8-lags in length).

By using the proposed format conversion scheme, the 32-wide parallel output from a high-speed sampler will be transformed into 32 parallel signals each carrying 1 msec segments of time contiguous samples that need only drive an N-by-1 array of correlators. This simplification in the correlator requirements is obtained at the cost of an inefficiency of about 0.2% which results because the end bits in adjacent 1 msec time segments of samples will never be correlated with each other.

Block diagrams (not shown) for the delay line and a data format conversion card are almost identical, and it is possible that these two cards can be of a single design. This design would have re-programmable logic such as field programmable logic arrays that would be configured at power up for one or the other function.

The cross correlator matrix of Figure 1 is used to correlate the sampler outputs of each antenna with those of every other antenna. At the intersection of any antenna X with another antenna Y in this matrix, there will be a 256-lag correlator. This correlator will compute lag products for the XY baseline, while the antenna Y and antenna X intersection of the matrix will compute the baseline lead products. Auto correlation products for each antenna are obtained from correlators on the matrix diagonal.

Figure 3 gives a possible layout for the correlator card. (The two axes of the correlator matrix in Figure 3 are described as the "prompt" and "delayed" inputs.) In order to minimize the delay line-to-cross multiplier cable interconnect, a very compact cross correlator matrix is essential. The design of Figure 3 places an entire 40 X 40 cross correlator matrix for two IFs of opposite polarization on a single printed circuit card. This PC card in addition is configured such that no signal drives more than one load.

Each chip passes along its input signals to adjacent chips in a matrix fashion. Column drive signals pass up through each column from the card input pins and row drive signals come up a column to the diagonal of the matrix and then drive in each direction to the entire row. Small programmable delay lines will be required at the input to each internal correlator to insure that all signals are phased to the correct bit regardless of the length of the path required to reach the correlator.

The correlator card layout of Figure 3 has one serious problem. The 125 MHz clock for two adjacent chip columns must be kept properly phased so that two chips high up in the column can exchange signals. It is possible that a very fast chip design will accommodate this requirement. Otherwise, a slightly more complicated clock distribution will be required.

Figure 4 shows a block diagram of the proposed custom lag correlator chip. This chip has a dual 4-by-4 array of correlators (one for each of 2 polarizations). The chip can be programmed via a microprocessor supplied program word for its position in the matrix and to select one of three correlator configurations:

- 1) four short correlators to compute the lags of all 4 polarization products (RR, RL, LR, and LL).
- 2) two longer correlators to compute just the lags for the two polarization components (RR and LL).
- 3) a single long correlator to compute lags for only one the two IFs.

In observations where fewer than 8 IFs are being used, more lags can be produced by dedicating more than one correlator array to process the outputs of active IFs. When this happens, cards in the data format conversion stage will be used to effectively connect two or more correlator arrays in series. The delayed input to the correlator chips that are to compute the higher level lags will be displaced in time the appropriate number of bits by offset RAM addressing in the data format conversion cards.

The data format conversion stage will also do the sample decimation for observations in which sample rates less than 4 GS/S are needed. Again, offset RAM addressing in this stage will generate offset delays for the computation of additional lags.

The long-term accumulation block seen in Figure 1 integrates the correlator outputs for the desired duration. The correlator chips will produce a total of 52,428,800 lag results to be accumulated. The parallelism factor, 32, allows the reduction of this number to 1,638,400, which when double buffered and spread across 32 long-term accumulator cards will require integration storage of 102,400 results per card.

## **6) SIZE AND POWER REQUIREMENT ESTIMATE**

The table below gives a preliminary count of the module and printed circuit card requirements for the MMA correlator:

Item	# req'd	size	power req'd	racks
4 GS/S dual sampler	160	2-wide VLBA module	20 w	4 racks
mode card	40	6U euro card	20 w	with samples
delay line	320	6U euro card	80 w	10 racks
memory card	320	6U euro card	80 w	with delay lines
correlator card	128	9U euro card	300 w	8 racks
control cards	32	-	40 w	with other cards
long term accumulator	32	-	60 w	with correlators
<b>totals</b>			100 kw	22 racks

The power estimates given in the table above are based on the experience gained in the development of the GBT spectrometer. The biggest unknown at this time is the dissipation to be expected in the custom correlator chip, 12,800 of which will be required in the system. The GBT correlator chip dissipates about 5 watts with a clock rate of 125 MHz. Such a high chip dissipation in the MMA correlator would mean both high system power requirements and lower reliability because of the difficulty in removing the heat from the system at the high altitude site.

By using low voltage chip technology, it is hoped that the custom correlator chip described in this document can be built with about a 2 or 3 watt power requirement. The chip represents about a factor 2 increase in the level of integration when compared to the GBT correlator chip (twice the number of transistors). By using a more modern process, with finer component features and low voltage technology, a smaller chip with lower power requirements should be possible. The smaller silicon size should also mean a higher yield in the manufacturing process.

## 7) COST ESTIMATE

It is difficult to estimate the cost of the MMA correlator at this time. There are a number of items which will require more experience and study before accurate estimates can be made. The table below is a first attempt at a cost estimate (it is probably on the low side):

Item	NRE	no. required	cost per item	total
custom sampler chip	\$100,000	400	\$ 250	\$ 200,000
custom corr chip	\$400,000	15,000	\$ 250	\$4,150,000
EMI racks		22	\$2,500	\$ 55,000
power supplies		100KW	\$ 2/W	\$ 200,000
pc card development		10	\$2,500	\$ 25,000
samplers		160	\$2,500 [*]	\$ 400,000
mode card		40	\$ 500	\$ 20,000
delay line		320	\$1,000	\$ 320,000

memory card	320	\$1,000	\$ 320,000
correlator card	128	\$ 500 [*]	\$ 64,000
control cards	32	\$1,500	\$ 48,000
long-term accumulators	32	\$2,500	\$ 80,000
backplanes	100	\$ 500	\$ 50,000
8-conductor signal cables	5,000!	\$ 10	\$ 50,000
sampler bins	16	\$ 300	\$ 5,000
card bins	75	\$ 1000	\$ 75,000
metal work			\$ 100,000
contingency			\$ 750,000
test equipment			\$ 75,000
computer hardware			?
computer software			?
<b>total</b>			<b>~\$7,000,000+</b>

[\*] does not include custom chips

---

FIGURE 1) MMA CORRELATOR BLOCK DIAGRAM

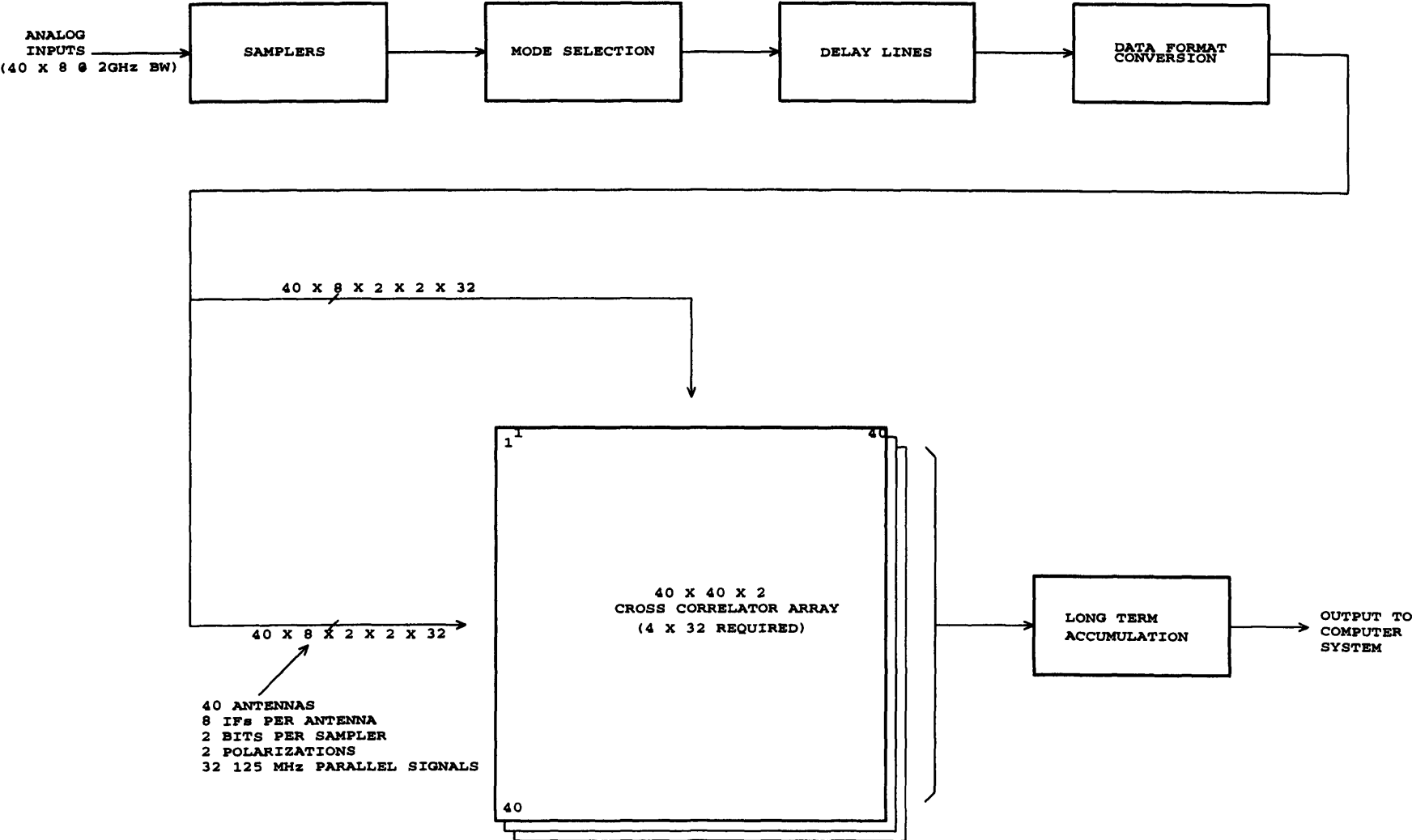


FIGURE 2) 4 GHz DUAL SAMPLER

2-BIT, 4-LEVEL SAMPLES ARE TAKEN AT 4 GS/S AND DEMULTIPLEXED BY A FACTOR OF 4 IN A GALLIUM ARSENIDE CUSTOM CHIP. THE OUTPUT IS IN 4 PARALLEL 2-BIT SIGNALS AT ECL LOGIC LEVELS.

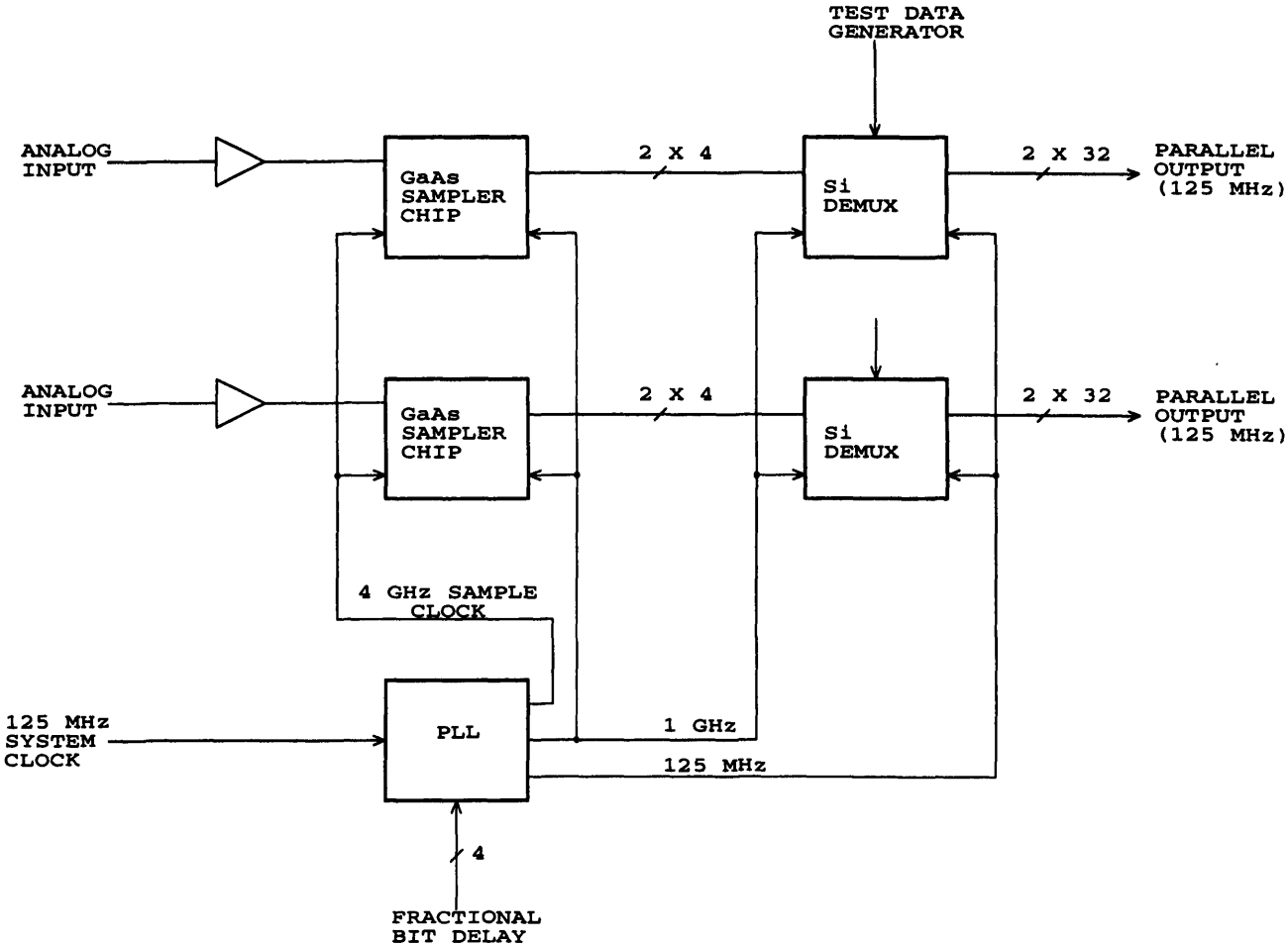
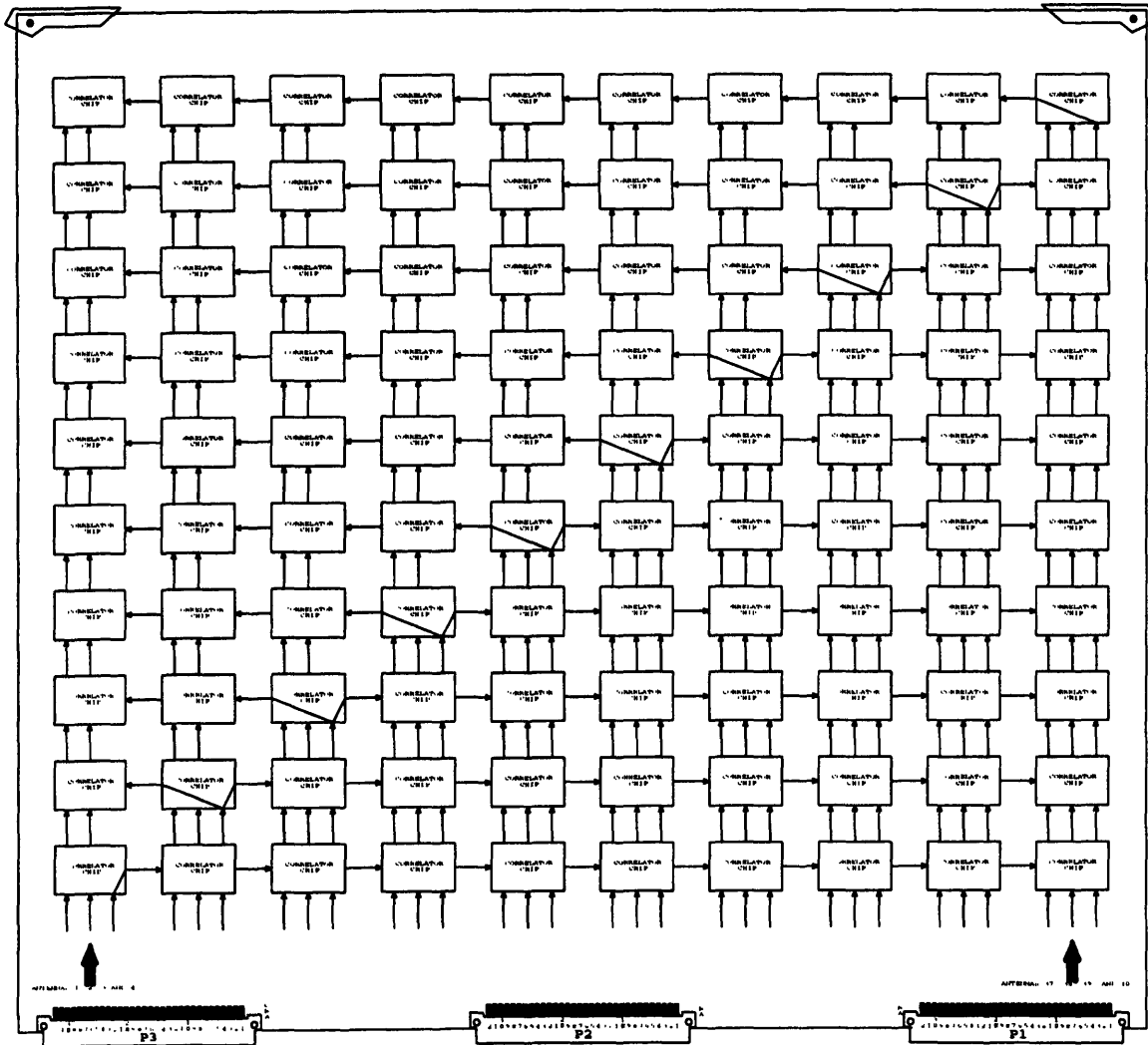


FIGURE 3) MMA CORRELATOR CARD.



NOTE: CORRELATOR CHIPS ARE IDENTIFIED BY THE NUMBERING ON THE CORRELATOR CHIP.  
 CORRELATOR CHIPS ARE IDENTIFIED BY THE NUMBERING ON THE CORRELATOR CHIP.  
 THESE ALL THE SAME AND ALL THE SAME THE SAME.  
 ALL THE SAME AND ALL THE SAME THE SAME.  
 ALL THE SAME AND ALL THE SAME THE SAME.  
 ALL THE SAME AND ALL THE SAME THE SAME.

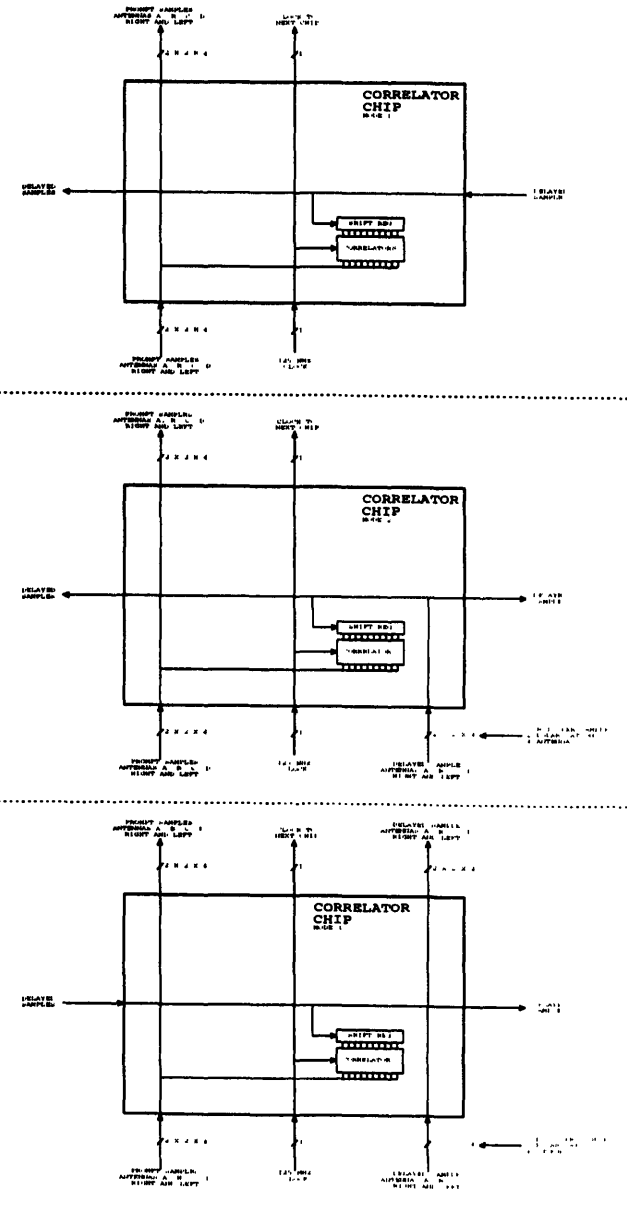
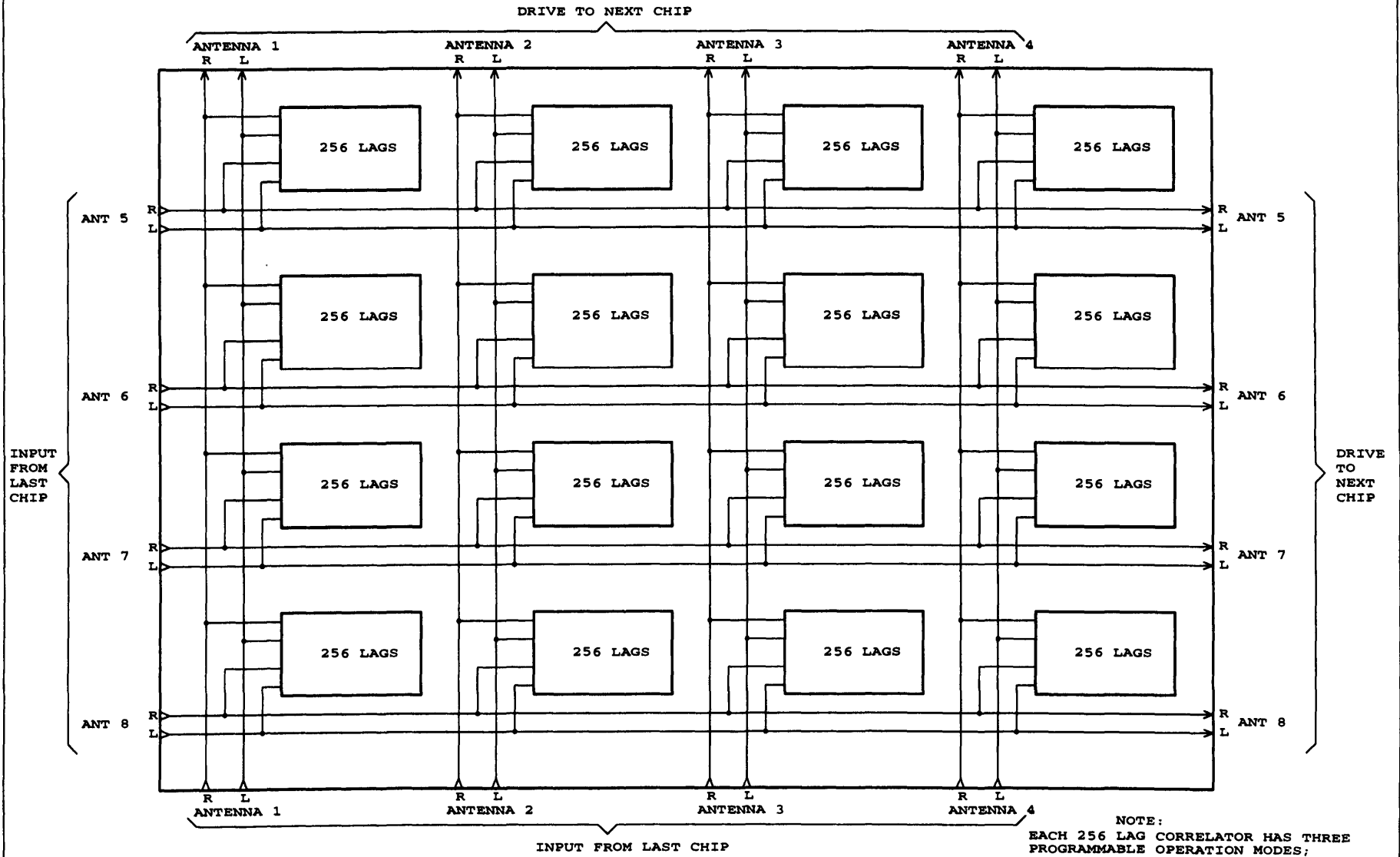


FIGURE 4) CORRELATOR CHIP



- NOTE:
- 1) EACH 256 LAG CORRELATOR HAS THREE PROGRAMMABLE OPERATION MODES;
  - 2) FOUR 64 LAG CORRELATOR BLOCKS FOR RR, RL, LR, AND LL.
  - 3) TWO 128 LAG BLOCKS FOR RR AND LL.
  - 4) ONE 256 LAG BLOCK FOR EITHER RR OR LL.

# **MMA Memo 164: MMA Computing Working Group Report**

11 Nov, 96

Steve Scott, Darrel Emerson, Rick Fisher, Mark Holdaway, Jill Knapp, Lee Mundy, Remo Tilanus, Mel Wright

## **1.0 Overview**

The variability of both calibrators and the atmosphere at millimeter and sub-millimeter wavelengths and the potential complexity of the MMA require that the computer control system for the MMA be much more sophisticated than present day instruments. We propose an instrument where the astronomer will interact with the instrument by specifying scientific goals rather than instrumental parameters and the system will intelligently select appropriate parameters. The instrument will typically produce images rather than visibilities.

A system with a state-side control center and wide bandwidth link to the operations support base near the array is optimal for remote access to the instrument by astronomers and engineers. The center will serve as the central hub for interaction with the instrument and the archival database. Almost all observing will be done remotely through the center. The overall computer system architecture will be a distributed hierarchical system, similar to many modern telescope systems (GBT, Gemini, VLT). This design would utilize both embedded microprocessors and more general purpose machines to produce an integrated system. It should be possible to present any aspect of the hardware remotely to allow full fault diagnosis and trouble shooting.

The MMA has the capability to produce data at a rate that would exceed data reduction capabilities. This potential problem has been addressed with data rate limitations, data condensation, and an imaging pipeline. Archive space and data processing resources are treated as finite resources, much like present VLBI tapes. Integration times of around 10 seconds will be the norm, but higher time resolution will be available at the expense of channels and baselines. The 10 second integration time will provide the capability for data editing, self-calibration, and other calibration procedures with reasonable time resolution. The data will flow from the realtime system into a calibration and condensation routine that will apply some calibration and will average the data into frequency bins that match the science requirements. Some of these operations are irreversible. Visibility data will then be written to a database and, in parallel, put into a pipeline to produce images. Dirty images from a subset of the data will be sent to the control center in realtime to aid in data evaluation. The MMA will differ from other previous synthesis imaging instruments in that a concerted effort will be made to automatically produce images that satisfy the scientific requirements for as many of the projects as possible. This will increase the scientific output of the instrument and contribute toward ease of use.

The proposed instrumental specifications that affect computing follow. See Appendix I for details of assumptions and their implications.

1. Minimum interferometric (phase-switched) integration time: 70 msec
2. Minimum single dish (non phase-switched) integration time: 3 msec

3. Maximum data rate: 10 MBytes/sec
4. Average data rate: 1 MByte/sec
5. Setup time: 50 msec

## **2.0 System Architecture**

The basic access model assumed for the instrument involves parallel data streams to operators, observers, engineers and support staff with few restrictions placed on their locations. This model will greatly increase the number of experts available to the array because they can be virtually anywhere, free of the burden of travel. Remote observing, sometimes in a cooperative manner between several astronomers, is viewed as a common way of observing. To support this access model, a wideband data link from somewhere in the U.S. to the operations support base near the array is essential for support of remote observing. Judging from a single quote from AT&T of \$750K/year for T1 bandwidth to Chile, the cost of bandwidth to the array is high enough that data sent over the link will have to be carefully chosen to minimize size and then redistributed from a state-side control center over less expensive networks to satisfy the requirements for parallel access. The link itself must be fast enough to provide images for monitoring observations and for other diagnostics. It appears to be prohibitively expensive to move all the UV data and images over a data link, so CDROMs or tapes will be made on site and sent to the control center for archiving.

The state-side control center serves as the terminus for the data link, the location of the archival database and as the hub for access to the array. The only technical requirement to access the array or the archival database will be an adequate bandwidth link to this center. The links to the center may be the Internet or perhaps an intranet between NRAO and some universities and research centers. Dial-up digital links to the control center with adequate bandwidth will certainly be an option at some point in the operation of the MMA.

Time critical processor intensive chores will be handled by embedded microprocessors closely integrated with the hardware. Higher level tasks of coordination, integration, data reduction and human interface will be handled by workstation style technology. Parallel processing will be used to handle requirements of spatial diversity and raw processing power (see the pipeline requirements). Communication and interfacing in a distributed system can be an important design decision that must be made early.

Maintaining high efficiency from the array will require continuous monitoring of the hardware and evaluation of fault conditions. Diagnosis of problems can be aided by software that understands the interconnections and flow of signals within the instrument, including reconfiguration.

## **3.0 Observing Modes and Configurability**

There will be 6 different modes of observing, or data integration, supported by the software. The phased array mode will only be implemented if the hardware component is included in the instrument. The number of phased arrays may be constrained by the hardware but not by the software.

1. Array synthesis imaging
2. Array On The Fly synthesis mosaicing
3. Single dish On The Fly mapping (continuum and spectral line)
4. Single dish position switched integration

5. Single dish frequency switched (with optional position switching) integration
6. Phased arrays

The ability to configure different portions of the array into sub-arrays that can use different observing modes is useful for several types of experiments and essential for testing. An extreme possibility is using the array as 40 independent single-dish telescopes, so there should be no restrictions on sub-arrays from the standpoint of the software. Any sub-array can be used for any of the 6 different modes of observing. Another configuration concept is a telescope cluster which is defined as a group of telescopes where no correlation products are formed within the cluster. There will be no limits imposed on the number of clusters. Clustering is only valid for the two synthesis observing modes.

## **4.0 Data Collection**

Data collection and processing estimates require that some assumptions be made about progress in future computing capabilities. We have conservatively estimated that technological progress will increase processing speeds and storage densities by the year 2005 by a factor of approximately 20 over resources commonly in use today (assumed to be of 1995 vintage).

The minimum interferometric integration time of 70 msec is driven by solar and flare star observations but constrained by the need to have a full Walsh phase switch cycle and to do the FFT's on every integration. At short integration times, the number of channels available is greatly reduced to stay within the maximum data rate. It is possible to fine tune this number if necessary, as phase switching details are not yet complete.

The minimum single dish integration time of 3 msec is driven by on-the-fly (OTF) continuum mapping. The goal is to Nyquist sample the beam at the targeted mapping rate of a degree per second. At 300 GHz this will be satisfied by samples every 3 msec. Spectral line OTF experience at Kitt Peak shows that there are still gains to be made by sampling faster than 100 msec. Therefore OTF mapping can be done in either spectral line and/or total power allowing a trade off to be made of the sample rate for channels to stay within the maximum data rate of the instrument.

The peak data rate was chosen to satisfy the science requirements specified at Tucson. This rate of 10MB/sec (36GB/hr, 0.9TB/day) will pose no problem at the data recording stage as it can be done with today's technology. The observer must again trade off time resolution for channels and baselines to stay within this limit. This limit is soft and can be increased if warranted. Parallel techniques can be used for the FFTs, calibration and recording if necessary.

The average data rate specification of 1MB/sec was chosen to provide average data sets of a size that have a reasonable chance of being reduced. For example, this rate would be met by experiments with a 10 second integration time and 3200 channels. A 4 hour project collecting data at the average rate would produce a 14GB data set which is equivalent to a 700MB data set using today's technology. Administrative implementation of the average data rate may require that data rate be considered in the proposal evaluation stage. The software will have to enforce the awarded data rate as an integral part of the approved project specification. The limitations imposed by this average rate will encourage wise use of the correlator, conserve archive space, and are consistent with the goal of having the array produce a stack of usable images. Increasing this instrumental specification will have a strong effect on the already difficult problem of the pipeline and data reduction.

A large reduction in data volume can be achieved if the data are channel averaged from the raw correlator resolution to match the proposed science. Several of the calibration steps (some irreversible) must first be performed on the data. This requires treating the software errors as if they were hardware errors - if they seriously compromise the data then the observations must be repeated. The calibrations to be applied are:

1. Atmospheric phase correction
2. Passband
3. Elimination of "end" channels from the spectrum
4. Channel averaging

Work on the atmospheric phase correction is still in progress, but it is possible that corrections will be needed in realtime on timescales of 1 second. These may be applied to the LO or alternately to the baseline visibilities as they are being integrated. It may be necessary to consider recording both the atmospheric corrected data and the uncorrected data and allow the observer to choose from the two data sets on a per baseline basis in the reduction. This would potentially double the data rate specification.

Phase calibration from the phase reference source will be applied to the data before recording and the correction recorded; this is a reversible step. Fast phase calibration cycles can be done faster than the data recording integration time, if necessary, with the constraint that there be an integral number of cycles per recorded integration.

The minimum setup time required is driven by the fast phase calibration scheme, band changes, single dish frequency switching, and wideband frequency synthesis within a band. Both fast calibration and band changes require slewing the telescope and are therefore limited to a fraction of a second. Frequency switching is desired at rates of several Hz so reasonable efficiency requires a setup time of around 50 msec. The wideband synthesis (stepping the LO by many GHz on successive integrations to cover the entire receiver band) is useful for solar work and could benefit from running as fast as possible. A 50 msec setup time gives a 60% duty cycle at the fastest sample rate.

## **5.0 Near Real-Time Astronomical Feedback**

While observing, the observer or array operator requires some near real-time feedback on the observations to verify that the array is operating correctly, that the observational parameters have been chosen wisely, and to ensure that the scientific objectives specified in the proposal (i.e. noise level) are being met. This feedback is essential for modifying the observing schedule by either human intervention or an automated procedure. The near real-time feedback should be fast, should be able to overcome the low signal to noise inherent in short integrations, and should result in compact data products which can be quickly transmitted to distant observers. Near real-time feedback might include:

- time series or spatial distributions of monitor or calibration data (for example, the atmospheric phase or bandpass solutions).
- preliminary astronomical images that are produced quickly with enhanced SNR by averaging selected spectral channels and tapering in the Fourier plane (no deconvolution).
- preliminary astronomical images that are updated with time to show the improved signal to noise obtained from longer integration.
- in mosaicing, total power images of a few selected spectral channels.
- spectra at a single point in a dirty image.

All of these "quick look" examples of near real-time feedback represent computing and data transmission requirements which are small compared to that of the production imaging system designed to produce final images from the data. A single workstation can probably meet the near real-time demands.

## 6.0 Imaging Pipeline Requirements

It is clear from the volume of data produced by the MMA that an automated imaging pipeline which would provide final or near final images for the majority of the scientific projects is desirable to optimize both computing and astronomer efficiency. As the majority of spectral line projects will probably be limited by noise rather than systematic errors, many projects are well suited to the automated pipeline described here. There is an additional need for off-line computing to produce images for projects that are too demanding for the pipeline.

The magnitude of the pipeline requirements has been estimated by benchmarking the pipeline tasks on simulated single channel MMA data. The benchmarking machine was a mid-level workstation, a 60 MHz Sparc 20. To scale the benchmarks to the full MMA pipeline, processor power has been scaled using the 20 fold increase previously mentioned and the number of channels and integration times chosen based on data rate limitations and on the brightness sensitivity of the array. The results are given in Appendix II and show that the pipeline will require approximately 40 workstations or their multiprocessor equivalents. The total pipeline cost of about \$800k is obtained by scaling the \$20k cost of the benchmarking machine. The overall computing demand is very high largely because of multiple spectral channels. Imaging algorithms operate on a single channel at a time, and the single channel imaging problems are quite modest and well suited to individual processors. Hence, the pipeline requires a data server that makes the appropriate spectral channels' data available to each processor.

The pipeline specifications are quite preliminary and are likely to change. The performance-to-cost ratio may improve more than the conservative assumption of 20 before the MMA is operational, and mosaicing and deconvolution algorithms may become more efficient. At this time, the computing requirements placed on the pipeline do not seem to be too extreme, and the entire pipeline will likely cost under one million dollars.

## 7.0 Observational Scheduling

There are three different methods proposed for scheduling observing time that span the range from those conventionally used today to some new methods that are particularly well suited to the MMA. Atmospheric conditions will almost certainly play an important role in efficiently scheduling the array and is the area explored by the proposed new methods. Phase correction techniques may make a major impact on the ability of the instrument to adapt to the atmosphere but these techniques are still under development.

The most traditional method of single dish mm observing, **interactive**, will give control of the array to an observer for a fixed time interval. The observer uses feedback from the observations to determine the next observation. The second scheduling method is **fixed queue** observing which simply steps through a set of pre-planned observations. These may be fixed in sequence or fixed in absolute or sidereal time. In the context of the MMA, this mode would be used when observing must be done at specified times (solar system events, VLBI, etc.) or when a specific set of observations needs to be done independent of

other factors. It is also the simplest form of automated observing and will therefore play a role as the array is brought online. The scheduling method that can take maximal advantage of changing weather conditions is **flexible scheduling**. It uses the current atmospheric monitors (seeing and opacity) and instrument status information to select from the queue the project which makes the best use of telescope time under these conditions.

Remote observing (either from a state-side control center or local 2500m operations center) is a requirement for any of the scheduling modes as it will reduce travel and is essential for flexible scheduling. The transition from the flex mode into interactive will require that interactive projects be elevated into a "standby" state while awaiting appropriate atmospheric conditions and that the observer be notified to be prepared to observe.

There are innovative yet simple ways to extend the flexible queue that will provide all of the features of the traditional mode as well as some interesting advantages. On most occasions the interactive user simply requires one or more 'checkpoints' during the observations to enable a decision on the further direction of the project. Such requirements for feedback can be incorporated into the flexible queue so that it will stop a project at a predetermined point, continue with the rest of the queue, and make the project ineligible for rescheduling until there is feedback from the observer. This allows indefinite time (minutes, hours, or even days) for head scratching and reflection without pressure. A simple yet powerful example of the use of checkpoints occurs while trying to integrate down to an adequate S/N. After spending only half of the projected integration time, a checkpoint can be scheduled, and spectral or spatial smoothing will allow a decent evaluation of the data. Cases in which either the science target has already been met or which will never achieve their science goal within the allotted time should be obvious. This thus argues for a system of 'mid-way checkpoints' for a whole class of observations, with the potential of greatly enhancing the efficiency of the telescope. The exact mixture of classical interactive and the enhanced flex queue will depend on the success of the implementations and will probably vary over time.

A number of the points raised above may seem fairly unconventional, but most of these techniques (flexible scheduling, remote observing, checkpoints) are in use, being planned or in the process of being implemented at telescopes such as the JCMT, BIMA, OVRO, and the SMA. By the time the MMA begins operation, remote observing using flexible queues should be common for mm telescopes.

## **8.0 Smart Observing Algorithms and Tools**

The variability of the atmosphere and of the calibrators requires the use of sophisticated "smart" algorithms to make observing easier and more efficient. Some of these algorithms will be capable of figuring out optimal observing parameters on the fly and adjusting them accordingly. The goal is to let the experiment be specified in terms of the science instead of instrumental parameters. In all cases it will be possible to override smart parameter settings and run in manual mode. Some suggested concepts, algorithms and tools are:

### **1. Proposal preparation tool**

The user should be able to specify source(s), catalogs, frequencies, spectral resolution, pointing centers; i.e. the astronomically desired parameters. The tool will generate an expert observing file that can then be edited by hand if desired. This file can subsequently be checked and optionally used to generate model beams and images with expected noise levels for several classes of weather conditions. The checking operation will include validation of syntax, evaluation of integration time

on sources and calibrations, and scanning for potential problems such as long slew times or erroneous spectrometer configurations. This output can be used to evaluate weather dependent factors filled in on the proposal form.

## 2. Science goal comparison operators

Many traditional interactive observations are implicitly doing tests such as "if SNR in channel 20 is greater than 3 then" or "if integrated flux over channels 6 to 120 is less than 50mj then" to determine the flow of the observations. To support this decision making in an automated way, it must be possible to extract the following from the pipeline data so that it can be used by the scheduling system:

- Flux - integrated, average, max or min
- Signal to noise - average, max or min
- Noise in map

The above quantities are specified over sets of boxes in the image cube as selected by the observer.

## 3. Calibration interval adjuster

Uses the atmospheric seeing monitor to select how often phase calibration needs to be done.

## 4. Calibrator selector

At the start of a new source, measures flux of adjacent potential calibrators using the array as 40 separate single dishes at lower frequencies or interferometrically at high frequencies where SNR is a limiting factor.

## 5. Pointing peak-up routine

Integrates coherently until adequate SNR is achieved and then moves on to the next measurement point. Does multiple points to statistically measure the accuracy of the offsets and automatically quits when the offsets are measured to sufficient accuracy.

## 9.0 Archival Database

The data will be shipped on tape or CDROM from the array to the control center where the database will be located and then become accessible from there. Items to be stored in an archival database include instrumental parameters, weather, and pointing as well as the headers for the data. The actual visibilities and images may be stored in another file system but pointers to it would be part of the headers stored in the database. The database will be used to provide general access to the data when the proprietary period has expired. To promote this data mining, it must support general queries via a structured interface plus some higher level constructs for ease of use.

## 10.0 Design and Implementation Issues

The complexity of the MMA and heavy reliance on flexible remote operation create a very challenging software design problem for control and monitoring. A long and iterative design analysis period must be anticipated and begun as early as possible. Ideally, the MMA project will assemble a design team with full-time participation of people from the several most recent telescope control software projects.

Experience is the most transferable software product, and the best experience is that which has used modern software design and management techniques on closely related projects. The result will draw heavily on industry standards and incorporate the best features of existing systems and packages such as CORBA, EPICS, and glish. However, each instrument and its requirements are different and new enough to require a fresh design. This must be recognized in the project cost.

One lesson learned from other projects is the importance of a thorough analysis of the data flow from the outset of the project. This will ensure a smooth interface between major components of the system. The

VLT is a good example of the use of this technique. The flow should begin at proposal submission and include proposal review, observing schedules, actual observing logs, data products, and archival data. Implementation should be done with a single database to maintain a consistent view of the data as it moves through different stages in its life cycle.

---

## Appendix I

### Data Rate Assumptions and Implications

To evaluate the data rate assumptions a clear definition of a "channel" and the correlator capabilities is needed. A "channel" here is one spectral channel (real & imag from a single sideband - 2 numbers total) on one baseline. There is one channel per sideband from every lag. The per baseline correlator is 1K lags at full clock and 32K lags at the slowest clock. These lags may be split over multiple windows but this will only cause a modest increase in header, not data.

At the Tucson meeting in Oct, '96 the science groups presented their requirements which are now summarized.

- Solar flares and flare stars require temporal resolution of 50-100 msec but with a reduced number of channels.
- Single dish spectral line on-the-fly mapping requires sample rates of 100 Hz.
- On-the-fly interferometric mosaicing at sample rates of 1 sec but restricted to a few thousand channels.
- Fast switching (~10 sec cycle) between source and phase calibrator will be required if a realtime phase correction for atmospheric water vapor is not possible. The system should support integration times of 10 seconds for the full correlator output (the phase calibrator will be wideband only). If shorter cycles are required then multiple cycles can be integrated together to form one recorded integration.

Assuming the data are stored using scaled integers so that each number takes 2 bytes, all of the above requirements can be met with a maximum data rate of 10MBytes/second. If all 780 baselines (or 40 telescopes in the single dish case) are used then the following table holds:

	Min int time	Channels	Data Rate
<b>Solar flares &amp; Flare stars</b>	70msec	224	10MB/sec
<b>Single dish OTF mapping</b>	3msec	420	10MB/sec
<b>OTF mosaicing</b>	1sec	3200	10MB/sec
<b>Fast phase calibration</b>	10sec	32000	10MB/sec

---

## Appendix II

## **Imaging Pipeline Requirements**

The basis for the assessment of the imaging pipeline computing requirements is a series of benchmarks of the reduction time for simulated single channel MMA data. The benchmark platform was a 60 MHz Sparc 20 purchased in 1995. Three problems were considered:

- one hour single pointing observations including imaging and deconvolution
- compact array linear mosaicing for moderate dynamic range observations
- compact array nonlinear mosaicing for high dynamic range observations

Phase and bandpass calibration require much less computing than imaging, and will not be considered further. The extrapolations from the benchmarks to typical MMA projects involve an estimation of the number of channels and integration times for different configurations. The 3200 channels used for the 2 compact MMA arrays are consistent with the average data rate with 10 second integrations. For the larger arrays, the brightness sensitivity of the MMA decreases and wider bandwidths are required in order to detect typical astronomical lines. Hence, we assume the B array will typically image 1600 or fewer channels, and the A array will image 400 or fewer channels. This will partially offset the increased computing requirements of the larger arrays caused by the larger number of pixels across the primary beam.

More detailed justification for these estimates and for the pipeline will be given in an upcoming MMA memo "Computing Requirements of an MMA Imaging Pipeline" (Holdaway, 1996).

### **A. Single Pointing Observations**

The single pointing observations consisted of one hour spectral line observations with the number of channels given above. The timing results for imaging without deconvolution are summarized in Table 1. At 10 s integration times, gridding dominates the compact array imaging. Averaging the data can result in a significant reduction in processing time as is shown in the lower half of the table with 240 s integration times. In the extended arrays, the FFT gains relative importance and is clearly dominant in the A array. The UV cell crossing time will restrict integration times to about 120 s in B array and 30 s in A array but these should not prove to be practical limitations because the gridding is less important than in the compact arrays. Deconvolution requirements are more difficult to estimate due to the strong dependencies on noise level, array configuration, source structure, the fraction of the field which is filled with emission, and the deconvolution algorithm. However, the interplay of these factors will be addressed in detail in the future MMA memo. For the time being, it is assumed that deconvolution will take about 10 times longer than generating the dirty images. With the factor of 10 for deconvolution, the future MMA pipeline of 40 processors can keep up with the data as long as the dirty imaging cpu time c. 2005 for all channels is less than about 4 hours. For D and C array, this will require integrations of about 30 s, B array will require about 20 s, while A array can use 10 s.

**Table 1. Imaging 1 hour of data without deconvolution**

Array	FFT Size	CPU Time c.1995 for 1 Channel	Number of Channels (N)	CPU Time c.2005 for N channels
<b>10 s int time: dominated by reweighting and gridding</b>				
D (80m)	64x64	226 s	3200	10.0 h
C (200m)	256x256	237 s	3200	10.5 h
B (800m)	512x512	257 s	1600	5.7 h
A (3000m)	2048x2048	558 s	400	3.0 h
<b>240 s int time: dominated by FFT</b>				
D (80m)	64x64	10.3 s	3200	0.46 h
C (200m)	256x256	16.6 s	3200	0.74 h
B (800m)	512x512	33.4 s	1600	0.75 h
A (3000m)	2048x2048	389 s	400	2.2 h

## B. Linear Mosaicing Observations

The brightness sensitivity of the MMA in its most compact array permits integrations as short as a few seconds per mosaic pointing. The linear mosaic algorithm, which assumes that each pointing has the same point spread function, can efficiently mosaic MMA data with dynamic range up to about 500:1. With 2 s integrations per pointing and 3200 channels, the pipeline can keep pace with the MMA using 32 of its future processors.

## C. Nonlinear Mosaicing Observations

Nonlinear mosaicing will usually only be required for very high dynamic range (greater than about 500:1) observations. At 60 s integration times and 400 channels per pointing (or 1 s and 6 channels per pointing), the pipeline could image as fast as the MMA produces data. This is probably sufficient for the very limited use of the nonlinear mosaic algorithm.

---

*Steve Scott (scott@ovro.caltech.edu)*



